No. 58 INTERPRETATION OF RANGER VII RECORDS*

by GERARD P. KUIPER

The pictorial records obtained by *Ranger VII* have provided the first close-up views of our satellite. They have led to important advances in our factual knowledge of the lunar surface.

This report is an attempt to interpret the *Ranger VII* photographs and to assess their impact on lunar science. The principal assets of the *Ranger* photographs are (1) the truly remarkable quality of the TV records, transmitted over a distance of 60 Earth radii; (2) their high resolution, exceeding the best Earth-based photography by factors up to 2000; and (3) their adequate redundancy, giving confidence in the reality of the image content. Their limitations, though obvious, must also be borne in mind: (1) the records covered a limited area, and image resolutions of better than 0.1 arc sec, as seen from the Earth are confined to about 10,000 km^2 or $\frac{1}{1000}$ of an orthogonally projected hemisphere; (2) the Sun was 23 deg above the horizon at the impact point (selected for reasons that have been described elsewhere), whereas Earth-based photography can extend to 1 deg or less, giving a relative gain in vertical resolution of some 20 times. For extended terrain features, therefore, the vertical resolution of Earth-based photography competes favorably with the *Ranger* records; and it is available over the entire visible disk.

It follows that the interpretation of the *Ranger VII* records is best made in the context of all available data. This at the same time allows an assessment of the question as to whether the results on Mare Cognitum are representative of lunar maria in general, and what is indicated for future missions.

The program of this report follows the above considerations. It starts with a classification of the *lunar maria,* based on their gross structure as found from Earth-based photography (resolution about 1 km). Mare Cognitum is seen to be an impact mare, its basin having been formed well before that of Mare Imbrium. Most of the surrounding mountain walls were destroyed before the basin was flooded. Then follows a study of the vertical structure of

*Reprinted with slight revisions from *Ranger VII, Part II: Experimenters' Analyses and Interpretations,* Jet Propulsion Laboratory Technical Report No. 32-700, pp. 9-73, Feb. 10, 1965, with permission. Figs. 5, 8, 11, 12, 14, 15, 16a, 17b, 18, 19b, 24, 32, 36, 37, 38, 39, 40, and 42 have been replaced by improved versions, and some supplementary material has been added in two appendixes. The second *Ranger* report (JPL Tech. Report No. 32-800, March 1966, pp. 35-248), based largely on the *Ranger VIII* and *IX* material, will not be reprinted in these *Communications* as no important improvements are available at this time. This second report deals, among others, with certain topics relevant to the *Ranger VII* records also: thermal anomalies ("hot spots"), sputtering by the solar wind, lunar white mountains and their terrestrial analogs (sublimate deposits), dimple craters, and caves, with terrestrial analogs. The bearing strength of the lunar maria, first derived in this report, has since been confirmed as to order of magnitude in the *Ranger VIII-IX* report, and by *Surveyor I.*

maria in general at the intermediate scale (vertical resolution about 10 m), based on Earth-based photography at very low Sun angles and on color photography with a wide baseline (3800–8000Å). Two of the maria (Imbrium and Serenitatis) appear to consist of a *succession of flows*, each flow being roughly 30–200 m thick and having a characteristic color. Successive flows may differ in color, with the most recent (top-level) tending to be the bluest. While no direct similar evidence exists for the other maria, partly because the data are less precise, it seems reasonable to assume that all maria have essentially similar structure.

Next are presented the results concerning the presence or absence of a *cosmic dust layer*. From high-resolution color photography it is concluded that no such layer covers the Moon, although the uppermost meter or more has undoubtedly been contaminated with cosmic debris. From the sharpness of the color boundaries it is further found that, since the formation of the maria, a general horizontal migration of dust by electrostatic forces, if it has occurred at all, was limited to subtelescopic dimensions. That some material has been widely scattered over the surface during major impacts is shown by the many scars and crater rays having distant sources. The existence of the color provinces in the maria indicates, however, that far from the large craters, with their swarms of secondaries extending to several crater diameters (and outside visible crater rays, secondaries, and scars), the scattering process has been inappreciable—not enough to erase the sharp color contrasts. This observation is of decisive importance in all that follows.

The *Ranger* records have yielded abundant data on lunar *craters* and *crater rays*, and these data are reviewed in this report. They have raised the question of the relationship between the swarms of secondary craters known to surround all major post-mare primary craters and the newly discovered clusters of secondary craters accompanied by short ray elements. The *Ranger* photographs demonstrated the existence of these clusters, but re-examination of Earth-based photography indicated that this basic structure of lunar rays is general. One is led to assume that the swarms of individual secondaries (having no rays) are due to lunar surface materials ejected during major impacts, but that the clusters of secondaries and their associated ray elements have a different cause, presumably fragments blown away from the impacting body itself. This explanation requires the impacting body to be of a different composition than the Moon. It may be postulated that it was a comet, as suggested by H. C. Urey and E. A. Whitaker. This assumption would also explain the nature of the crater rays, as is shown by E. A. Whitaker in *Comm. LPL* No. 59. The hypothesis is examined quantitatively and found satisfactory.

The *Ranger* records have also provided a clue to the morphology of the *ridges* in the maria. These ridges appear to belong to two classes: (1) those showing local or mare-wide patterns and (2) those that are part of the "grid system," a global pattern of structural lines that seems connected with the dynamics of the lunar globe as a whole. In either case, the hypothesis can be made that ridges follow a pattern of fractures in the lunar crust along which up-welling magmas caused dikes to erupt sporadically through the lunar surface. This hypothesis can be tested on the *Ranger* photographs, notably some of the last B and P frames (especially B196), through the fortunate circumstance that one ridge was dissected by a crater that has laid bare the ridge substructure. It is found that the ridges are basically strips of the lunar mare surface pushed up by dike-forming intrusive magmas which locally spread out horizontally between crustal layers and widened the overlying ridges. The *Ranger* photographs may be regarded as having clarified the morphology of the ridges; but the interesting dynamical problems of fissure formation and the related clues to the tidal history of the Moon remain unsolved.

The third major problem with respect to which the *Ranger* photographs supply decisive information is the physical and mechanical structure of the *upper layers* of the mare floor. Of particular interest is the average thickness of the layer of lunar debris scattered between observable craters within 1–2 km from its source (within the sharpness of the observed color boundaries). Regardless of whether or not this debris has subsequently been consolidated into metamorphic rock as a result of vacuum welding or other processes, the layer will not possess the tectonic properties and the fine structure of the original flows at the time of mare deposition. Two approaches lead to an estimated thickness of this disturbed layer. One is based on the study of lineaments, the other on the morphology of craters and crustal depressions. A study of the *lineaments*, made by R. Strom using standard geological methods, is included in this report. It is found that Mare Cognitum possesses three main lineament directions, down to the smallest scale observable on the *Ranger* records. Two of these are identical to the directions found in adjacent test areas and belong to the global lunar grid system. The third direction is composite in nature, and its interpretation is complex. On the basis of these lineament studies, it is concluded that the average thickness of the disturbed layer between observable craters is less than 2 m.

The interpretation of the craters and depressions observed on the *Ranger* photographs is incomplete. A basic question in the analysis is the initial state of the mare floor. Recent experiments by Dobar *et al.* (Ref. 1) and at this Laboratory have confirmed occasional speculations that the upper layers of a lunar lava flow may be composed of a *low-density rock froth*, whose thickness might attain several meters or possibly tens of meters. This conclusion would not be important if the maria were not lava but dust. With the maria apparently consisting of a succession of flows, the physical processes of a lava deposit in a vacuum on a body with a low surface gravity are relevant. With the bulk density of the upper layers of the mare floors estimated at 0.1–0.3, the impact mechanics of secondary craters will be quite different from impacts in rock, alluvium, or sand. The properties of both primary and secondary craters are likely to reflect this unfamiliar medium. The bearing strength found for such material (roughly 3–8 kg/cm^2) further accounts for the virtual absence on the Moon of loose blocks and fragments tossed out of primary craters. Rocks of 1-m size and larger could have remained on the surface only if they originated in the immediate vicinity ($D < 100$–200 m); otherwise, they would have penetrated the rock-froth surface. Finally, the observed infrequency of very small ray craters might thus be accounted for, rays having been formed only when the deeper and more compact layers were struck.

In addition to objects that are clearly craters, the *Ranger* records have shown a new class of objects—*shallow depressions* and *dimple craters*. These have no rims, and the outer portions are identical in that their shape approximates an inverted Gaussian curve, rotated around its vertical axis. The depressions continue on the Gaussian profile and thus have a roundish, nearly level bottom; whereas the dimple craters are pointed at their centers or end in a short horizontal line. These depressions closely resemble the collapse depressions, usually perfectly circular, abundant on the Earth. The latter are partial cave-ins (sinkholes) in nearly horizontal pahoehoe flows usually of considerable thickness. On the Moon, withdrawal of magma, cave-ins of deeper frothy layers by the new flow, shrinkage in volume upon solidification and subsequent cooling, and possibly venting of subsurface gases are held responsible. The apparent absence of a conical section on the slopes of the dimple craters indicates that the thickness of loose material on the maria capable of forming talus slopes is inappreciable.

Two additional sources of information about the lunar crust exist: (1) the rate of particle influx on the Moon and (2) the structure of the upper meter or two as derived from radio emission and radar reflections, supplemented by the emission of the upper few millimeters observed at shorter wavelengths. There is still some numerical uncertainty about the rate of particle influx on the Moon. A recent summary by McCracken and Dubin (Ref. 2) fixes the rate as 1 g/cm^2/4.5 $\times$ 10^9 years for particles of mass less than 10^4 g, a value supported by more recent work by W. G. Elford and G. S. Hawkins. Particles larger than 10^4 g would cause primary craters well visible on the *Ranger* photographs ($D > 5$ m), and very large impacting masses would also produce numerous secondaries. If these secondaries are excluded as much as possible, by considering areas outside crater rays and outside the concentrations of secondaries around primaries, the quoted primary impact rate of roughly 1 g/cm^2 during the history of the lunar maria appears appropriate; Dr. Dubin regards the numerical value uncertain by a factor of nearly 10. The 1964–65 *Mariner* mission to Mars is accumulating data that will make the value more precise.

One might assume that the initial post-mare impact rate was much larger than it is at present, both because the Moon was probably closer to the Earth and because the post-mare period came at the close of a period of very active lunar bombardment. However, the cosmic component for the entire post-mare period has been too small to have obliterated the sharply defined color differences on the lunar maria; further, most of the impacting mass below 10^4 g, at least now, consists of submillimeter particles (Ref. 2) which cannot penetrate the lunar crust to great depth. It therefore appears that the McCracken–Dubin primary impact rate, when applied to the entire post-mare period, is not grossly underestimated. The color differences also indicate that the secondary spray from distant impact craters is not important either except where visible as craters or scars.

The photometric results show that the top layer of the Moon (a few millimeters or centimeters thick) is a very open structure, only some 10% of the volume being occupied (Ref. 3). This is consistent with the thermal measurements at 10 μ made during eclipses, which require the presence of a loosely open or dust-like layer at least a few millimeters thick. Ray craters such as Tycho appear only thinly covered (< 1 mm) with such a layer (Ref. 4). For deeper layers, the radar reflections at $\lambda = 68$ cm indicate a bulk density of 0.4–0.5 of solid rock (Ref. 5); or less, according to other authors.

The high-resolution *Ranger* records are limited to a region in and near a weak Tycho crater ray. On the last P frames, this region is partly resolved into a remarkable continuing pattern not unlike a tree bark (e.g., Ponderosa

pine). This *tree-bark* pattern probably represents the surface structure of a lava flow, modified by partial collapse, which may have added surface cracks. The raised elements are typically of the order of 20–30 m long, 10 m wide, and 1–2 m high. Among them is the boat-like structure illustrated in Section F (Figs. 37 and 38), and several structures like it, less well covered by the *Ranger* records. The tree-bark structure appears soft and rounded off, with a scale of 0.5–1 m. The rounding off is presumably due to erosion.

A linear mountain range (Bonpland γ) occurs near 21°E, 10°S, situated in one of the most prominent ridges of Mare Cognitum. It and similar mountain ridges on the south shore of the mare (one at 21°E, 13°30'S) show by the calderas on their crests that they are of *igneous* origin. This observation has important implications for the origin of many such linear mountains in the Carpathians and elsewhere, also situated along structural lines (in the case of the Carpathians, radial to Mare Imbrium).

The highest resolution obtained by *Ranger VII* occurs on two photographs of the last P frame (190), namely 0.25 and 0.4 m. The hope that high-resolution photography would yield basic new evidence on lunar crustal structure and, thus, on lunar history and development, has been fulfilled. The *Ranger* results have further stimulated an intensive re-examination of the Earth-based photographs, which, in turn, has decisively assisted in the evaluation of the *Ranger* data. Since high-resolution photography will, for some time to come, necessarily be limited to selected regions of the lunar surface, Earth-based photography pushed to the highest attainable resolution (about 0.1 arc sec) has become a prime requisite.

Continued studies of terrestrial impact and explosion craters will also be needed. There are two classes of such craters, those that occur naturally near volcanoes and those produced by artificial surface or subsurface explosions in desert terrain. The first class is represented by the extraordinary crater field produced in 1960 on the slopes of Laimana Crater, Hawaii. We discovered this field in the course of the preparation of this report, and some photographs taken there are reproduced in a later section. In addition to hundreds of "secondary" impact craters, we found some craters and crater chains, somewhat resembling features on the Moon, that were due to drainage. The dimple craters, however, are different in shape from drainage craters. Artificial secondaries have recently been described by W. A. Roberts* and others.

*Roberts, W. A., "Secondary Craters," *Icarus*, Vol. 3 (1964), p. 348, and references given there.

Attention is called to the excellent maps of the area covered by *Ranger VII* published by the Air Force Aeronautical Chart and Information Center, at scales of 1:1,000,000; 1:500,000; 1:100,000; 1:10,000; 1:1,000; and 1:350. These maps portray, in condensed form, the essential information contained on the more than 4300 *Ranger VII* photographs, on coordinates, nomenclature, and qualitative relief, as well as the dimensions and orientation of the numerous features included. The maps were produced in record time and will be an indispensable aid in the further reduction and evaluation of the data.

AF-ACIC has also called attention to the treasure of information contained in the stereo coverage of the Ptolemaeus to Mare Nubium area, obtained by combining Earth-based photography with the B series of *Ranger VII* photographs.

The studies of Mare Cognitum refer to one of the older impact maria on the Moon. It has a rather yellow surface, almost certainly antedating bluer maria such as Mare Tranquillitatis. Studies of one of the bluer maria will be needed before general conclusions can be drawn. The impact area on Mare Cognitum was selected to avoid prominent lunar landscape features such as faults, rilles, graben, mountain chains, large craters, or intense crater rays. The *Ranger* pictures therefore are less spectacular than they would have been had such major structural features been chosen instead. The choice was made in part in support of future landing operations, unmanned and manned, which require the type of terrain actually encountered. Continued scientific exploration of the Moon will benefit if close-up photography of such major structural elements can be included.

A. The Gross Structure of Lunar Maria

Since the impact of *Ranger VII* occurred in one of the lunar maria, the *Ranger* data of highest resolution pertain to a mare surface. Since, additionally, the impact occurred in a minor crater ray, with other minor rays in the vicinity, the data also provide information on the fine structure of lunar crater rays. In order that the specific conclusions derived from the *Ranger* records may be related to the problems of lunar maria and crater rays in general, these problems are reviewed first.

The lunar maria are of two main types: (1) those that are nearly circular and are surrounded by near-circular mountain arcs or fault scarps; these maria also show some circular symmetry in the peripheral rille systems and in the ridge systems of the mare floors, and (2) those that are

irregular. Examples of class 1 are Mare Crisium (Figs. 1, 2), Mare Nectaris (Fig. 3), and Mare Orientale (Fig. 4). Mare Crisium is surrounded by one prominent mountain wall (D=450 km) and fragments of two weaker walls (D=670 and 1060 km); Mare Nectaris is surrounded by three rings (D=400, 600, and 840 km); and Mare Orientale is surrounded by at least five rings (D=320, 480, 620, 930, and 1300 km). Examples of class 2 (irregular maria) are Mare Nubium (part of which is shown in Fig. 5) and Mare Tranquillitatis (Figs. 6–8). Here the ridge systems show patterns of a regional nature, with several such systems covering the entire mare. The outlines of these maria are irregular, probably the result of flooding onto terrain with irregular contours and complex tectonic origin; and no peripheral mountain walls or scarps are observed.

Among the various hypotheses that have been advanced to account for the existence and general appearance of the maria, the following are of interest:

1. The maria are lava fields, though not necessarily identical in composition or fine structure to terrestrial lava beds. It is usually assumed that the nearly circular maria were caused by impact and subsequent flooding; the irregular maria, without surrounding walls and associated rille systems, by flooding only. The source of the lava requires a separate explanation, which is discussed below.

2. The same classification of maria is made, but the explanation for the dark mare material is not lava but dust, or lava and dust. It is assumed that this dust resulted from the impacts that formed the mare basins.

3. The mare basins were filled with dust that accumulated in those low-lying areas during the long lunar history, the source of the dust being erosional and the transportation to the basins by electrical forces.

4. The maria are the oldest regions on the Moon, with the dark surfaces caused by solar radiation effects.

Hypothesis 4 may be ruled out if it is assumed, as is done on excellent grounds (Section G), that the great majority of the lunar craters are caused by impacts. It then follows, from the crater densities in the maria and on the terrae, that the maria do not constitute the oldest parts of the lunar surface but the most recent. Hypothesis 3 would require that the floors of the oldest lunar craters be covered with the largest amount of dark material and those of the most recent craters with the smallest amount. This is contrary to fact. The craters with dark floors, such as those in Fig. 2, appear to be of intermediate age, with both the oldest and the most recent craters having light-colored floors. Also, the mare basins would be expected to be essentially featureless. In reality, structural details related to the general basin geometry may be found all over the maria when observed under favorable conditions of illumination and resolution (cf. Figs. 5–12), and these structural units show the nature of the lunar maria to be basically plutonic.

A compelling argument against a general migration of dust across the surface of the Moon is based on the sharp boundaries observed for the different color provinces, shown in Figs. 13–15. These boundaries often coincide with structural units such as flows (discussed in Section B) and are so sharp that any migration must be within subtelescopic dimensions.

The plates selected for reproduction here emphasize structural features especially relevant to the interpretation of the *Ranger VII* photographs, with the object of determining the nature of a typical mare surface. They were taken in part from the *Consolidated Lunar Atlas* now in preparation, which includes the results of new Earth-based lunar photography carried out under federal sponsorship. For a more general description and systematic photographic coverage of the lunar maria, reference is made to a paper by Hartmann and Kuiper, entitled *Concentric Structures Surrounding the Lunar Basins* (Ref. 6). This paper contains 77 photographic reproductions, many of them rectified, with a summary for each of the maria on the ridge and rille systems, indicating the presence or absence of concentric surrounding mountain walls or faults. A sequel to this study is contained in two papers by Hartmann on *Radial Structures Surrounding Lunar Basins* (Ref. 7), which, incidentally provide much additional photographic coverage. Earlier systematic lunar photography is reproduced in the *Photographic Lunar Atlas* and the *Rectified Lunar Atlas.*

Figure 5 shows the southeastern corner of Mare Nubium, including the region of the Straight Wall, about 20 deg from Mare Cognitum. It is noted that the mare floor exhibits a complex system of ridges, unlike Mare Crisium (Fig. 1), Mare Nectaris (Fig. 3), and other near-circular maria such as Mare Serenitatis (Figs. 9 and 10) and Mare Humorum (Fig. 12).

Other regions, showing local rather than mare-wide structural patterns, are portrayed in Figs. 6–8. Figures 6 and 7 show, under opposite illumination, the western part of Mare Tranquillitatis in the region of the crater Arago, containing the impact point of *Ranger VI.* It is

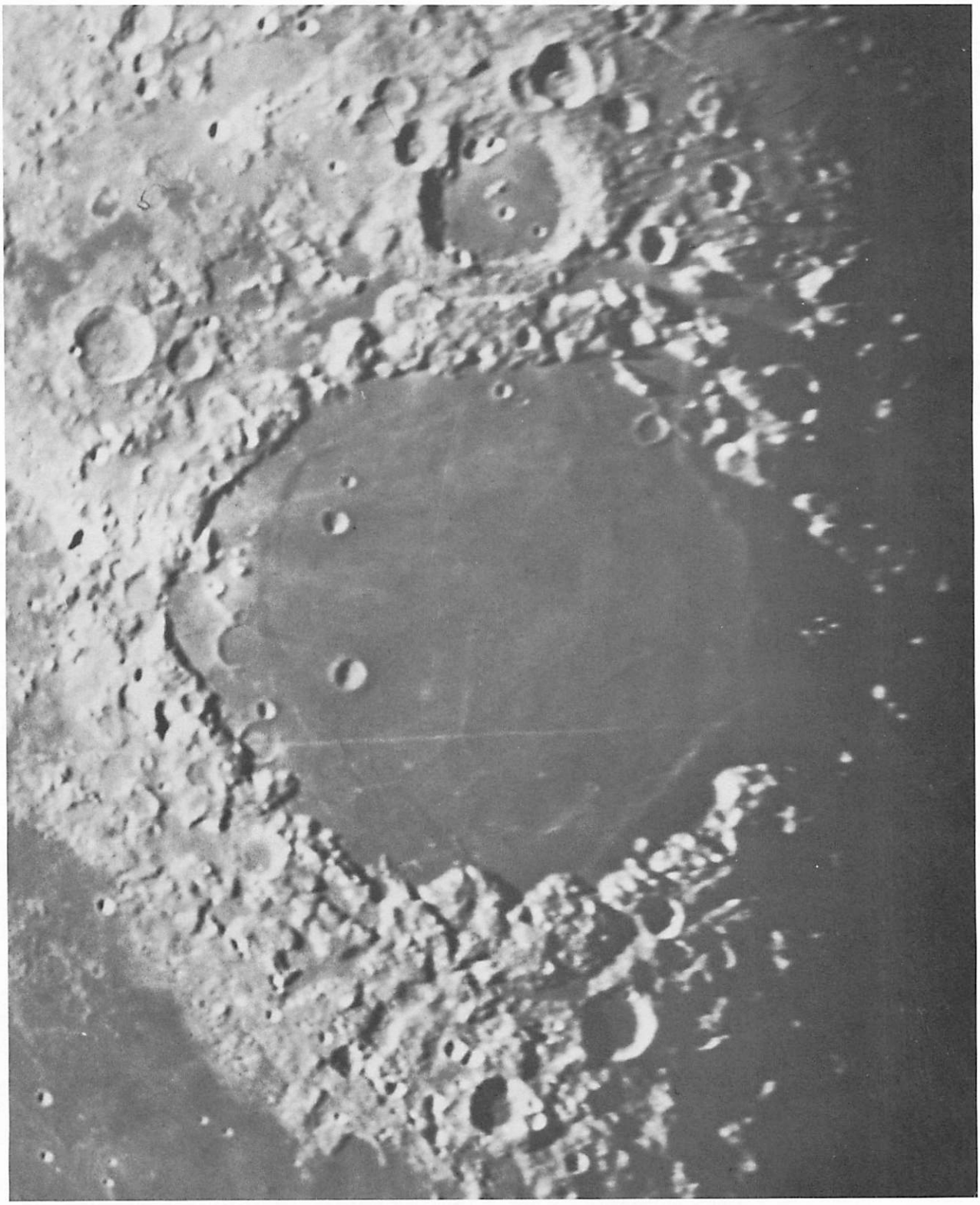

Fig. 1 Mare Crisium, rectified, showing surrounding walls (Plate Y369).

Fig. 2 Mare Crisium and neighboring small flooded craters, rectified (Plate Y738).

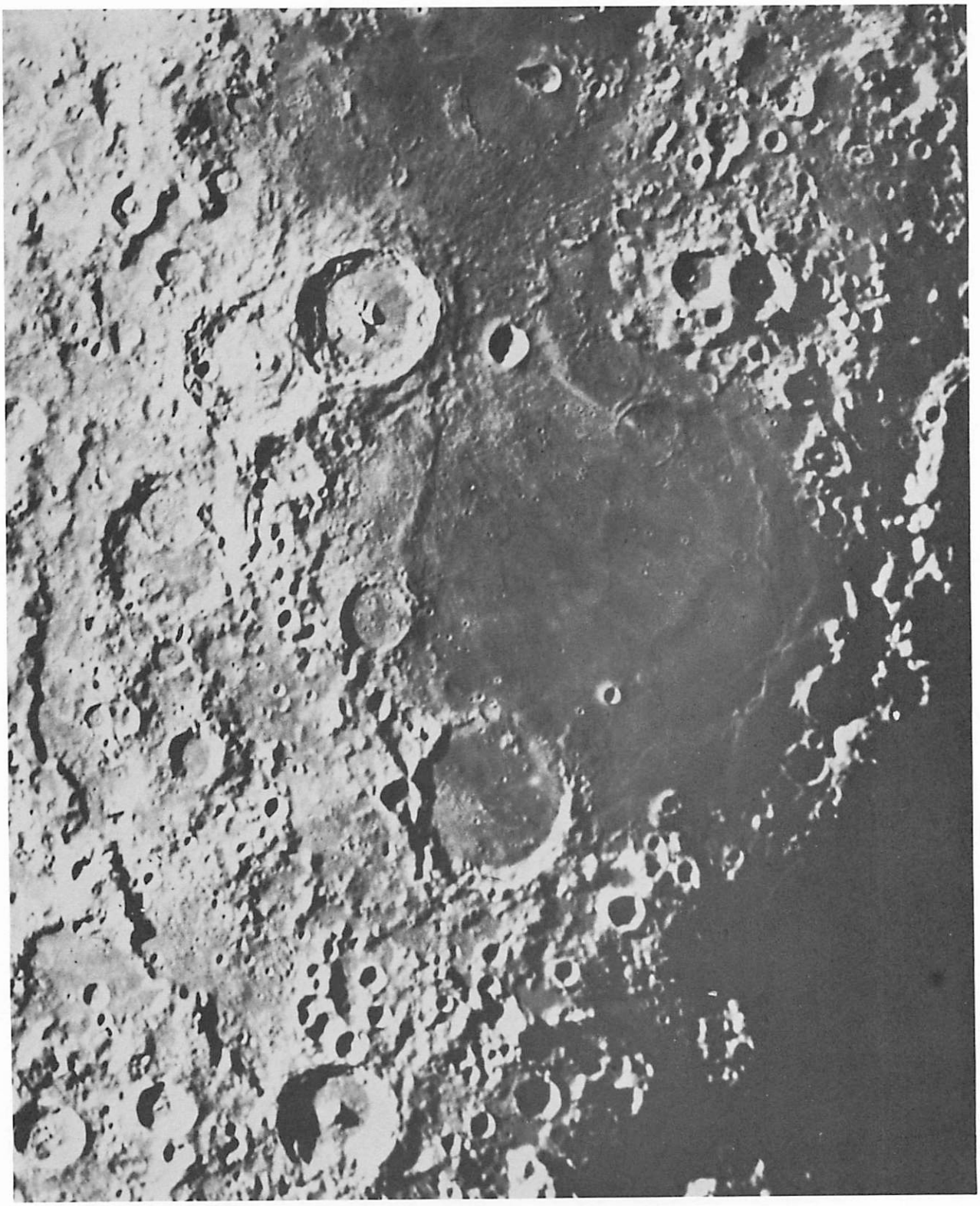

Fig. 3 Mare Nectaris, rectified, showing three surrounding walls (Plate Y1334).

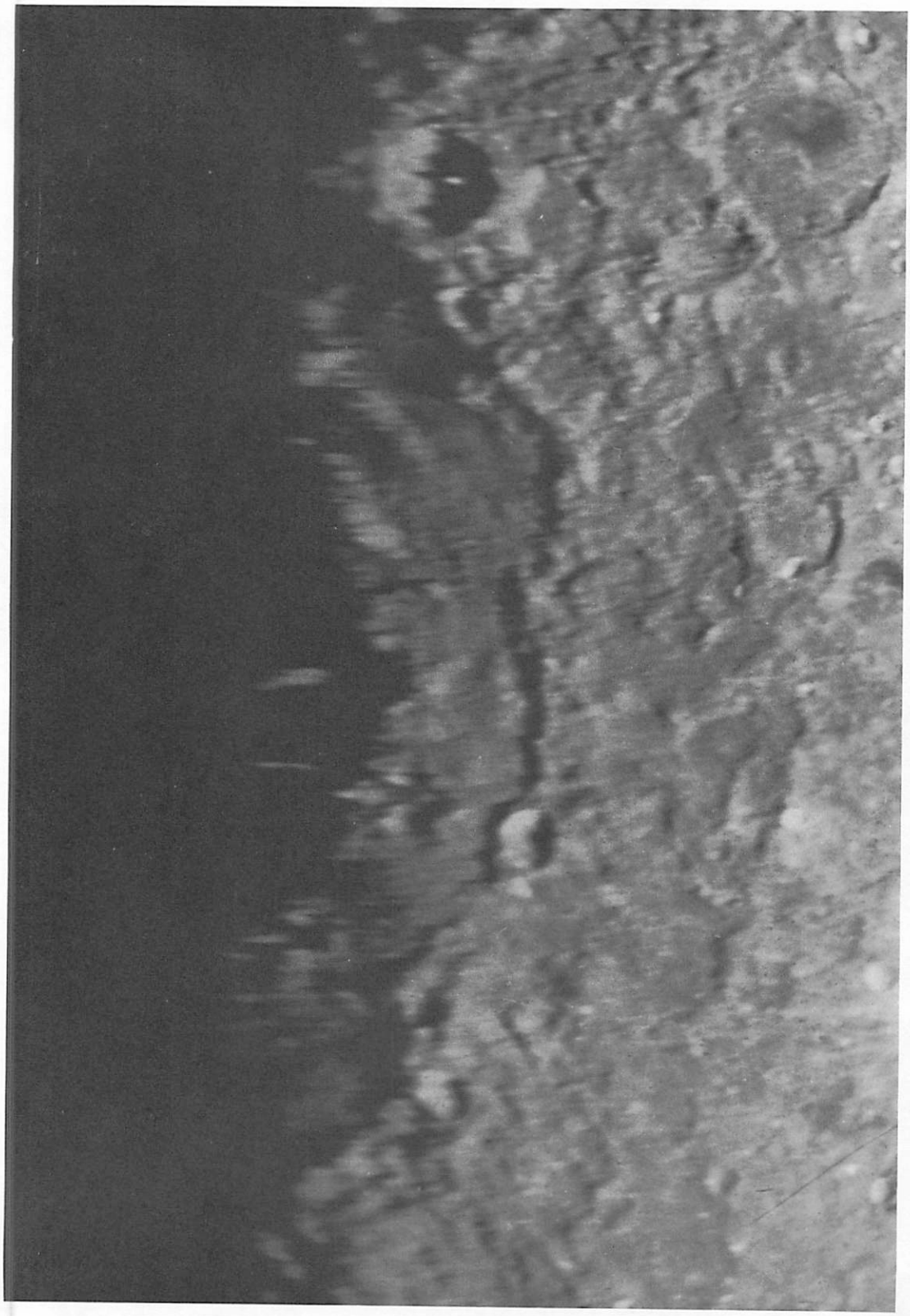

Fig. 4 Arcuate fault scarps surrounding Mare Orientale, rectified (Plate M372).

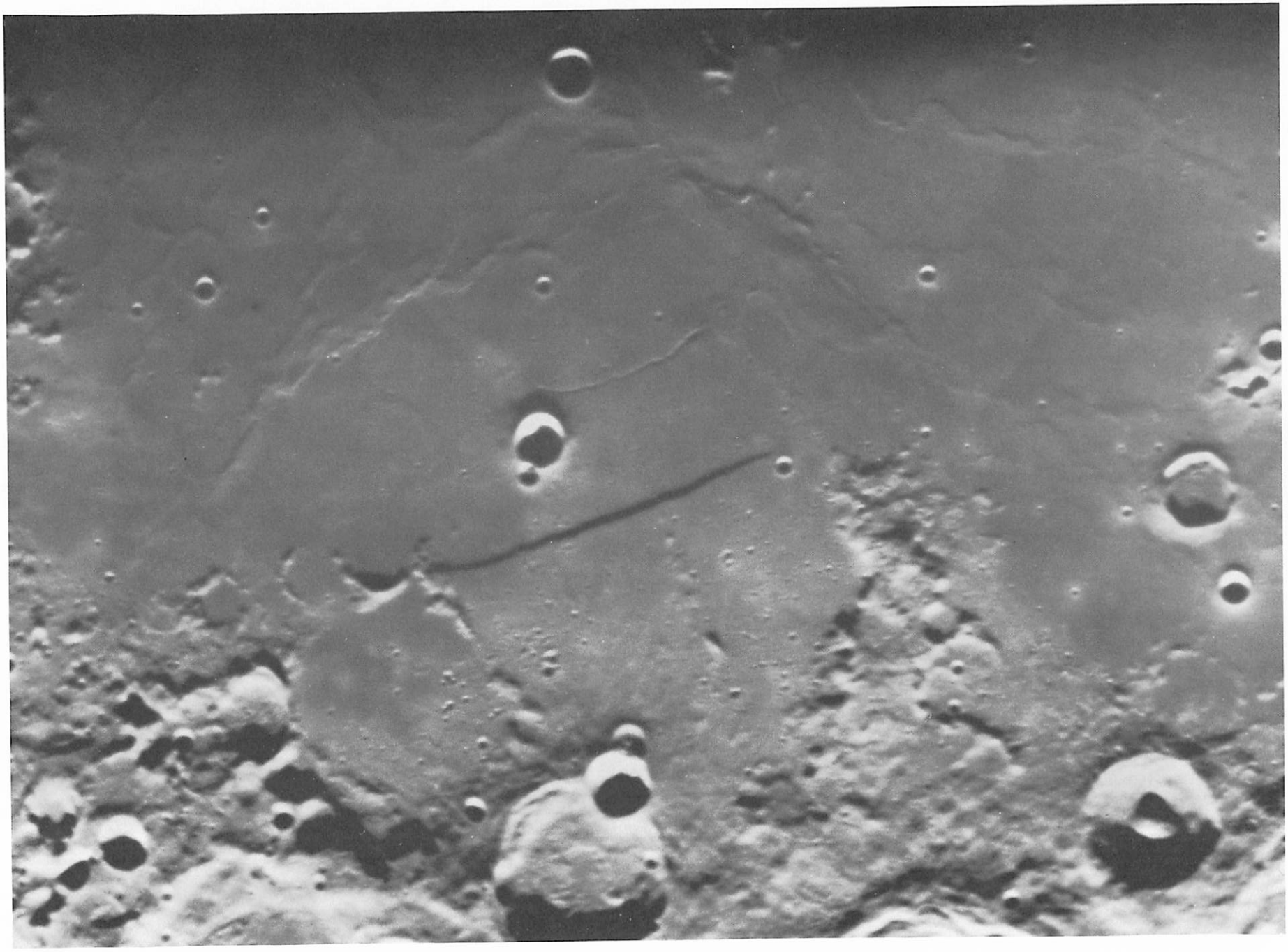

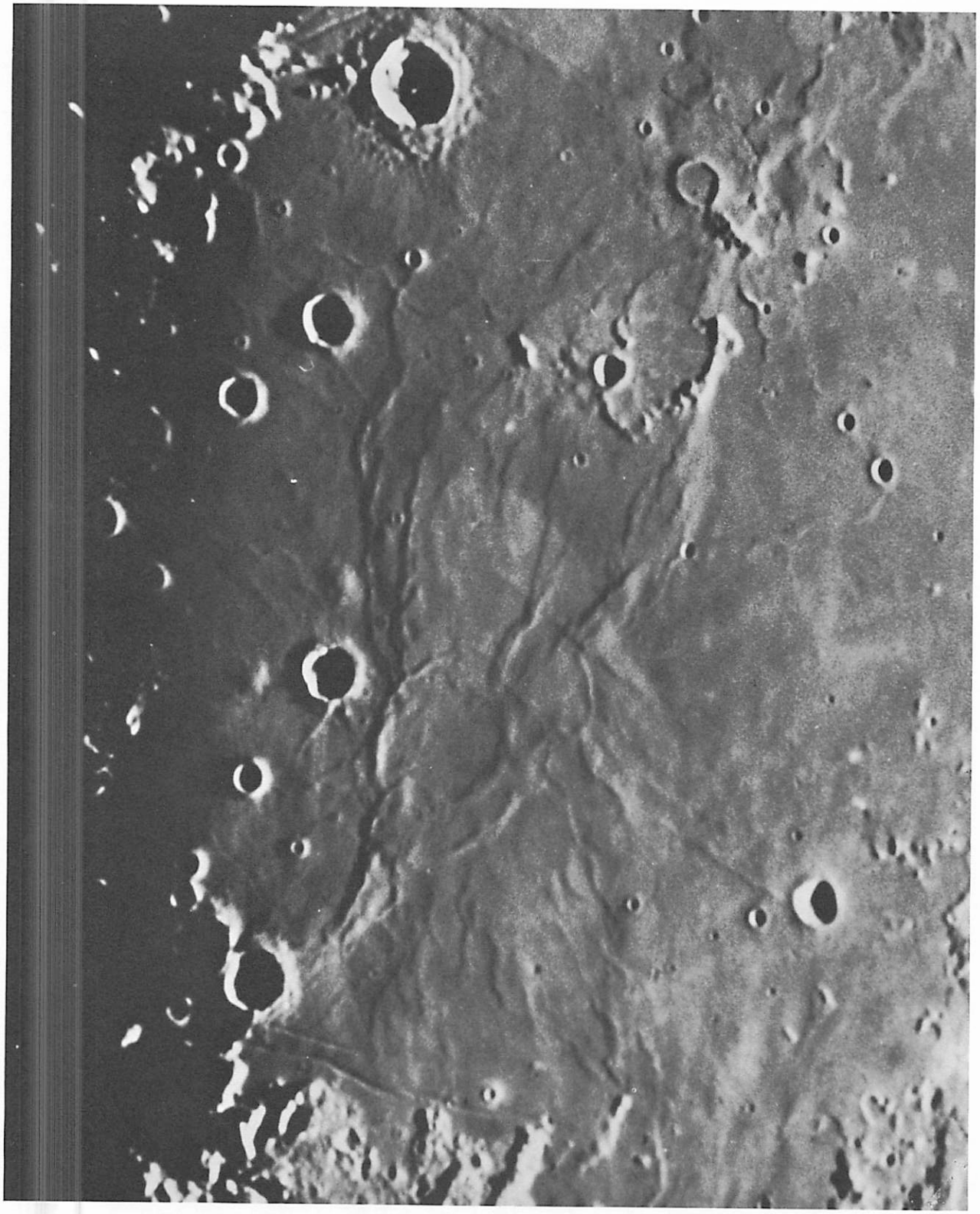

Fig. 6 Part of Mare Tranquillitatis near Arago, at sunrise (*Ranger VI* impact area; Plate Y936).

Fig. 5 Southeast corner of Mare Nubium, including Straight Wall (Plate C855).

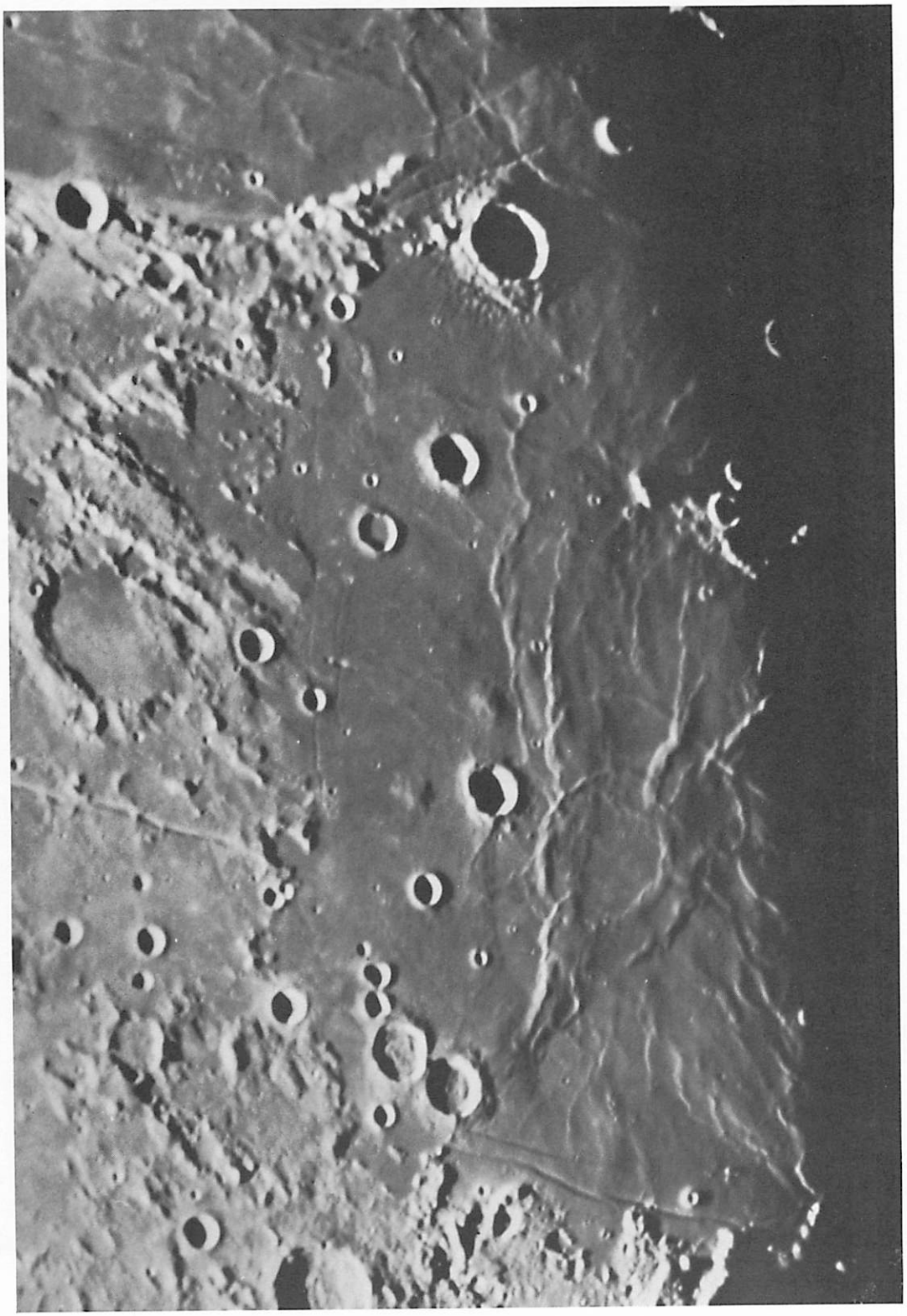

Fig. 7 Part of Mare Tranquillitatis near Arago at sunset (Plate M816).

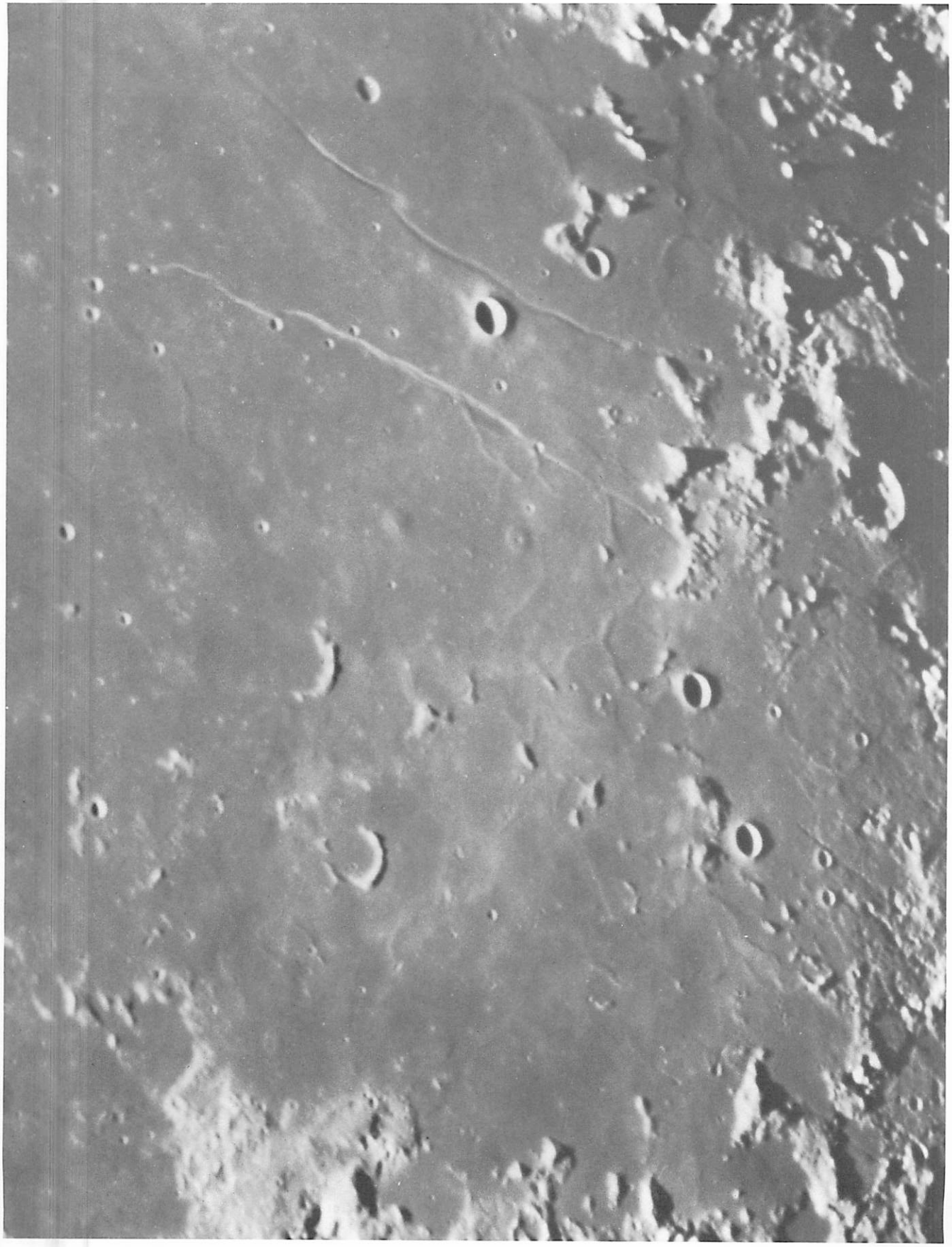

Fig. 8 Part of Mare Tranquillitatis, showing Cauchy Fault and numerous volcano-like structures (Plate C230).

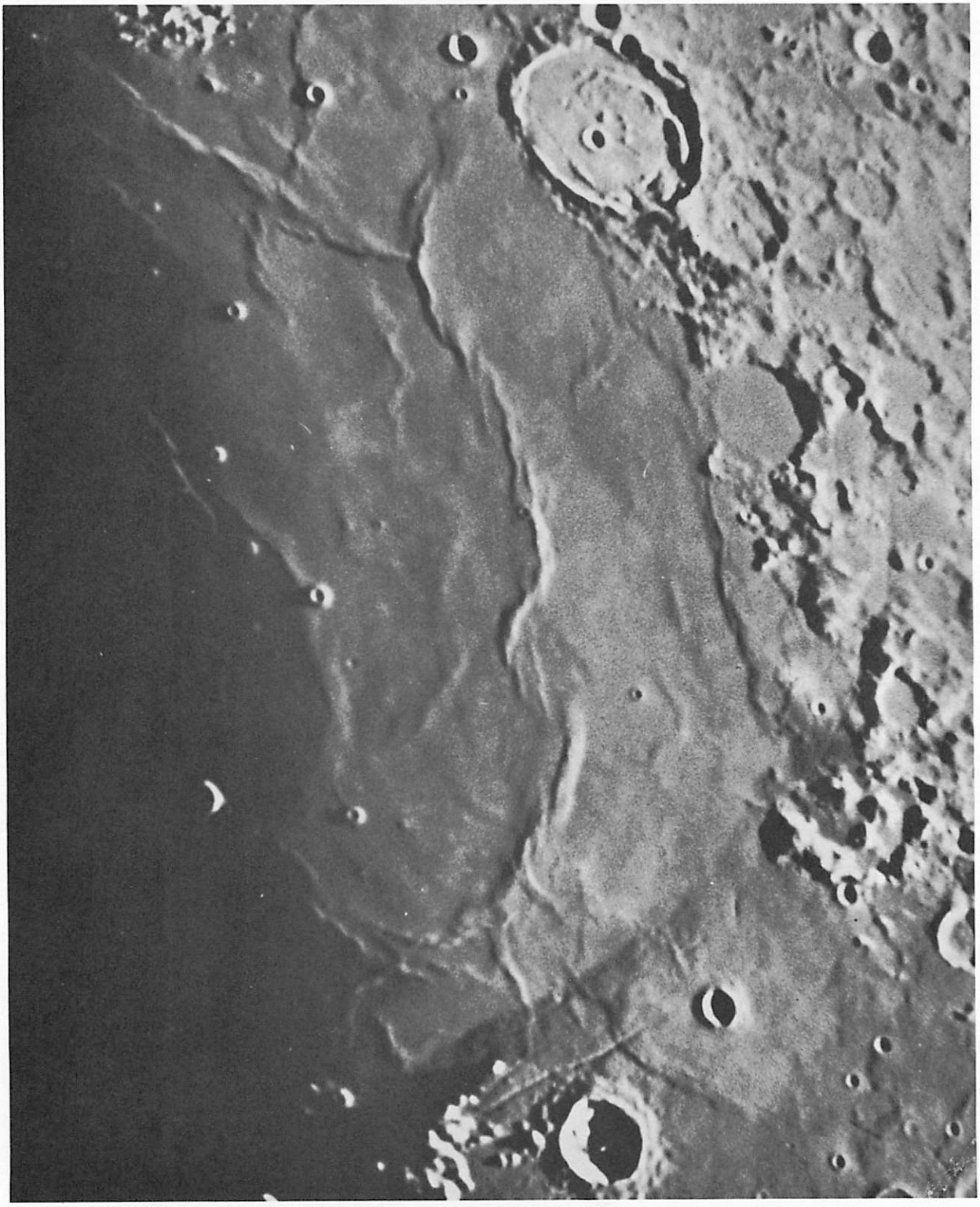

Fig. 9 Mare Serenitatis from Posidonius to Plinius. (Note *en échelon* structure in ridge system and Tranquillitatis flow entering Serenitatis north of Plinius, shown to be bluish on Fig. 14; Plate Y936.)

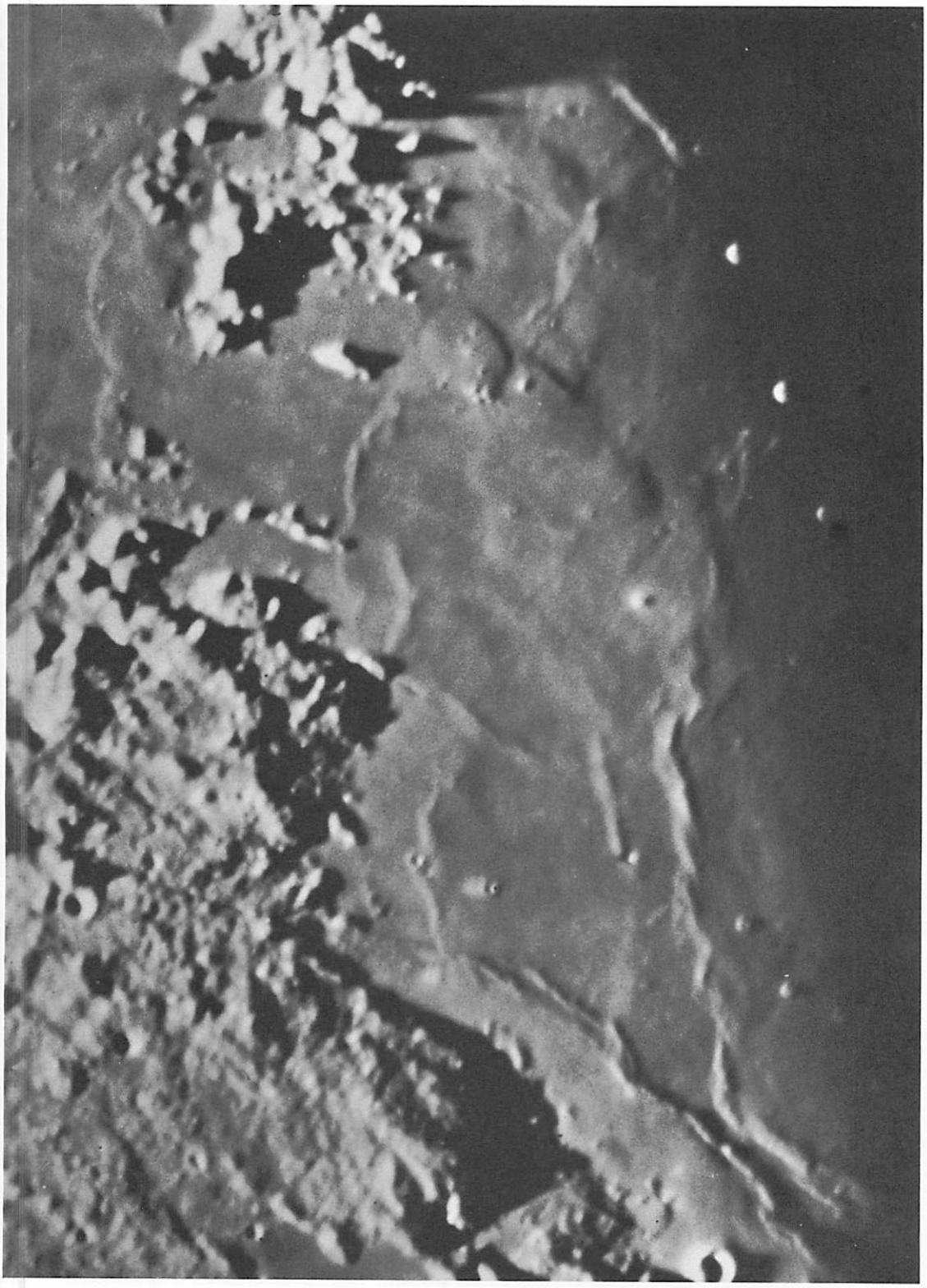

Fig. 10 Braided ridges, troughs, and flows in Mare Serenitatis (Plate M826).

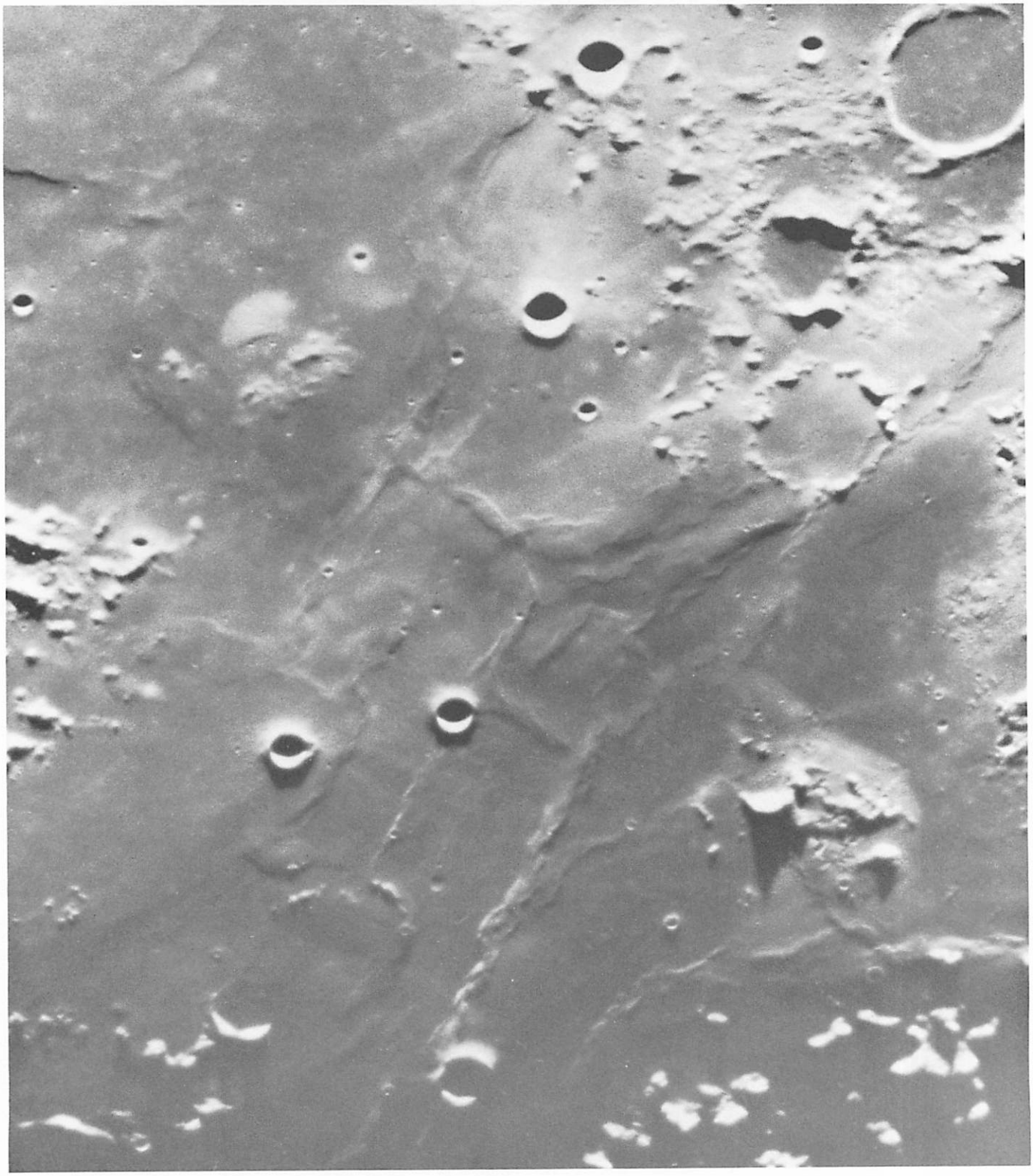

Fig. 11 Part of Oceanus Procellarum, south of Montes Riphaeus, showing ridges with braided structures, rimless craters, small crater strings, and domes. North is to the left (Plate C1201).

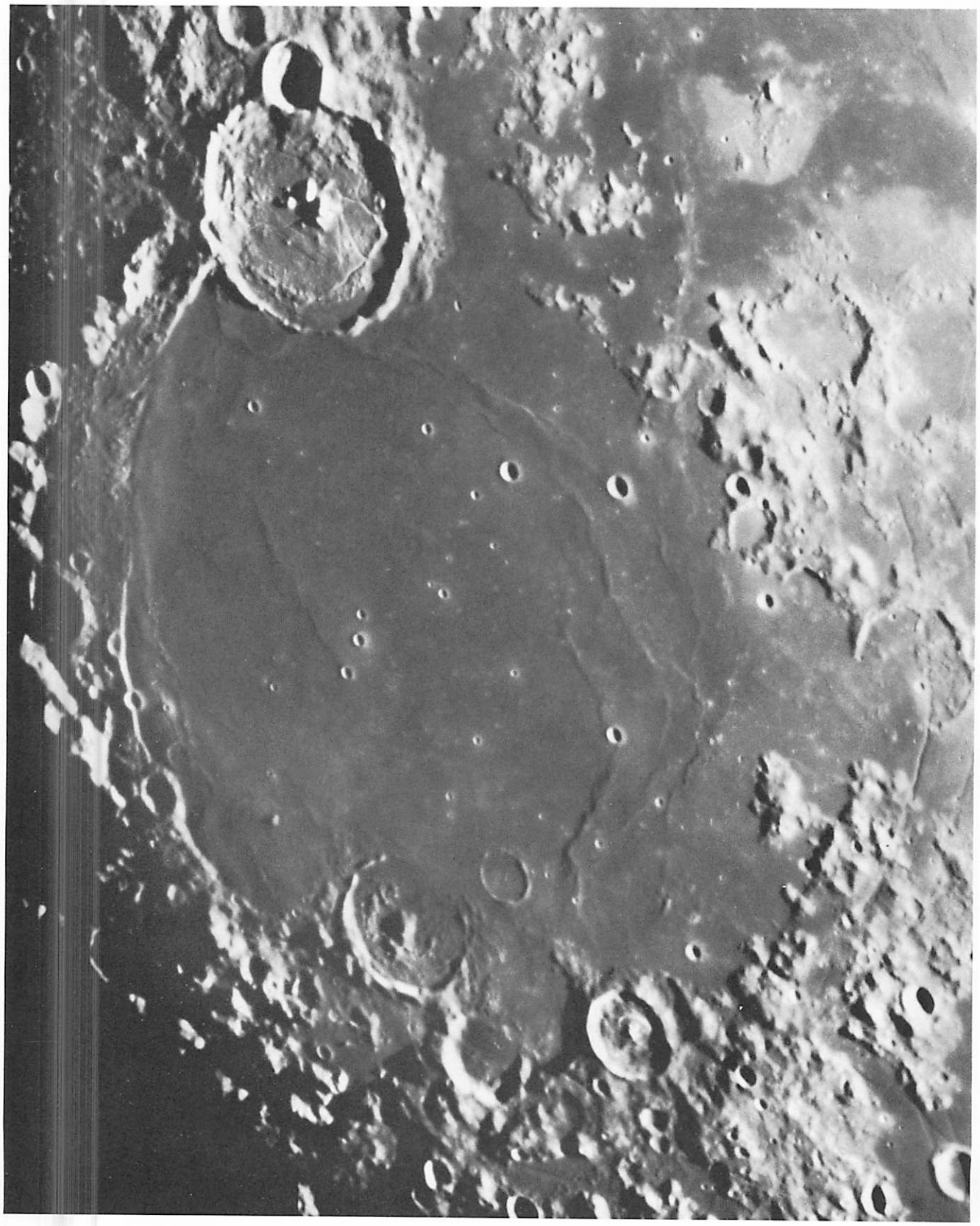

Fig. 12 Mare Humorum, showing concentric rilles and ridges and tilted craters on shoreline (Plate C1261).

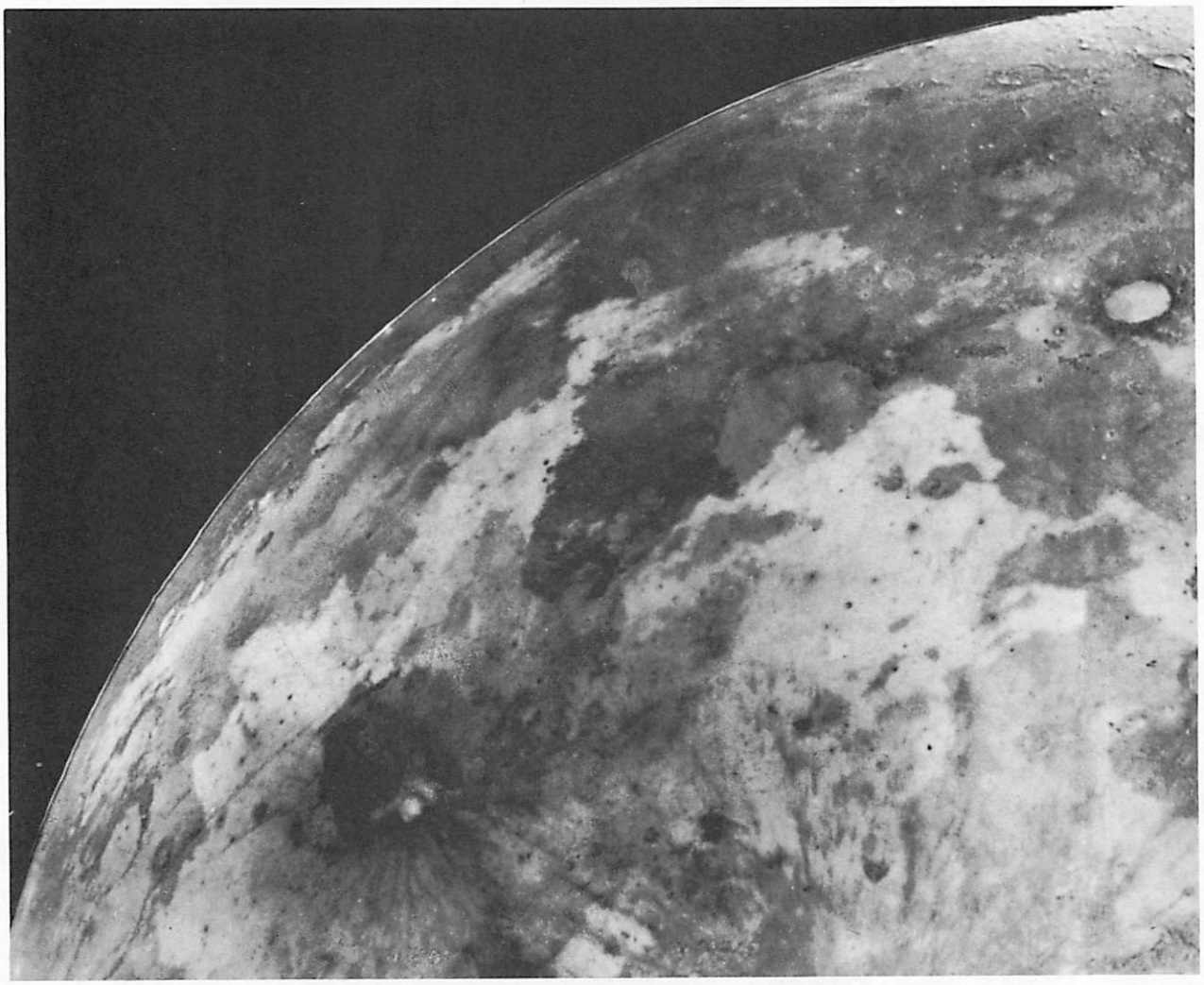

Fig. 13 Colors of the Mare Imbrium region. (The darker the tone, the redder the lunar surface. Printed from a sandwich consisting of an original negative ultraviolet plate and a positive copy of an original negative infrared plate, both taken at the 82-in. telescope of the McDonald Observatory of the University of Texas on May 29, 1964. The color differences were verified by photo-electric calibration by T. Gehrels of the LPL staff; E. Whitaker.)

Fig. 14 Colors of Maria Serenitatis, Tranquillitatis, and Crisium (E. Whitaker, Catalina Observatory plates).

Fig. 15 Colors in the third quadrant containing Maria Nubium, Humorum, and Cognitum (E. Whitaker, Catalina Observatory plates).

at once evident that the prominent ridge system reflects a complex deep-seated structure that is probably related to one or more major impacts and old craters, all preceding the filling of the mare basin. The complex structure is again in contrast with the rather simple concentric ridge patterns found in Mare Crisium, Mare Nectaris, and Mare Humorum; nevertheless, the pattern is not random and appears in principle interpretable in terms of one or two main events. Very close to the terminator, elevation differences of 3–10 m can easily be detected on ridges sufficiently long to be shown on the photographs. The straight diagonal ridges seen on Fig. 6 crossing the radial pattern emanating from Lamont agree in direction with lineaments found in the nearby terrae, indicating a basic crustal pattern continuing into the mare region. This fact and the detailed appearance of the ridge system, as well as the prominent mounds near Arago, are unmistakable signs of plutonic activity extending right up to the visible surface. The color differences within the mare (Fig. 14), to be discussed below, reinforce this conclusion.

Figure 8 shows the eastern half of Mare Tranquillitatis. No simple symmetry properties are apparent, but the Cauchy Fault, the numerous volcano-like structures (domes showing calderas), the prominent rille, and other structural features again point to tectonic and plutonic activity extending to the lunar surface.

Figures 9 and 10 show the eastern and western sectors of Mare Serenitatis. Because of its near-circular outline, its roughly symmetrical ridge pattern, and its surrounding mountain walls in the southern and eastern sectors, this mare is considered to have been formed by impact early in the lunar history (prior to the formation of Mare Imbrium). Attention is called to the *en échelon* structure of the Serpentine Ridge presented in Fig. 9, the dark threshold just north of Plinius, which is shown in Fig. 14 to have a bluer color than the remainder of the mare basin, and the very remarkable crossing and intertwining of ridges in the vicinity of Plinius. Figure 10 shows a complex system of ridges, plateaus, and the well known threshold of the "lava" flow directed toward Archimedes, just past the gate between the Apennines and the Caucasus Mountains. This entire complex of features again is unmistakably tectonic and plutonic in nature.

Figure 11 shows a region of Oceanus Procellarum just south of the Riphaean Mountains, at approximately the same latitude as Mare Cognitum but less than one mare diameter to the west. Certain structural directions clearly predominate. These are known to be part of the grid pattern that also pervades Mare Cognitum, as is shown in Section F. The "braided" structure of the ridges is noteworthy. The positions of the larger craters bear no relationship to the tectonic pattern, consistent with the hypothesis of their impact origin. That this conclusion does not extend to all of the small craters is evident from an analysis of the *Ranger VII* photographs. While the larger craters appear invariably to be of impact origin, some small craters are found by their linear arrangement or position on mountain tops to be related to plutonic effects.

Figure 12 illustrates the occurrence of several major craters near the shoreline of Mare Humorum, whose rims are not level but are inclined toward the mare. Similar structures are observed on the shorelines of Mare Crisium, Mare Nectaris, and elsewhere. Apparently these craters were caused by impact after the basin had formed (since they interrupt and locally destroy the mountain wall surrounding the mare) but prior to the flooding of the basin, as follows from the details of the mare level where the craters were invaded. The concentric ridge system of Mare Humorum is shown also, though not as well as on photographs taken at a low Sun angle.

B. Colors and the Meso-Structure of the Maria

An important source of information is the color of the lunar surface. Figures 13–15 show the color contrasts for the principal maria facing the Earth. It is seen that the color boundaries between bluish and reddish areas are usually very sharp; and by comparison with direct photographs, it is found that these boundaries often coincide with visible flows, as shown in Figs. 9, 10, 16, and 17. In Fig. 18, many flows have been mapped in a limited region of Mare Imbrium; the boundaries of five or six of these are recognizable also on Fig. 13 as edges of color provinces. These color contrasts indicate, first, that the lunar maria are not covered with even 1 mm of cosmic dust, which would have obliterated the color differences, and that the color contrasts seen on the lunar surface are, in many instances, related to observable structural units, such as the flows shown in Figs. 9, 10, 16, and 17. The uppermost flows, obviously the most recent ones, are often the bluest; the older deeper-lying flows, which are partly covered, are often (but not always) the reddest. The color differences may be due to differences in the state of oxidation, possibly related to variations in the water content of the magmas. On Mauna Loa, Hawaii, one often observes a reddish coloration of vents, which is attributed to escaping steam. Color differences might be due also to differences in age (cosmic weathering effects). The adjacent terrae, and particularly the islands

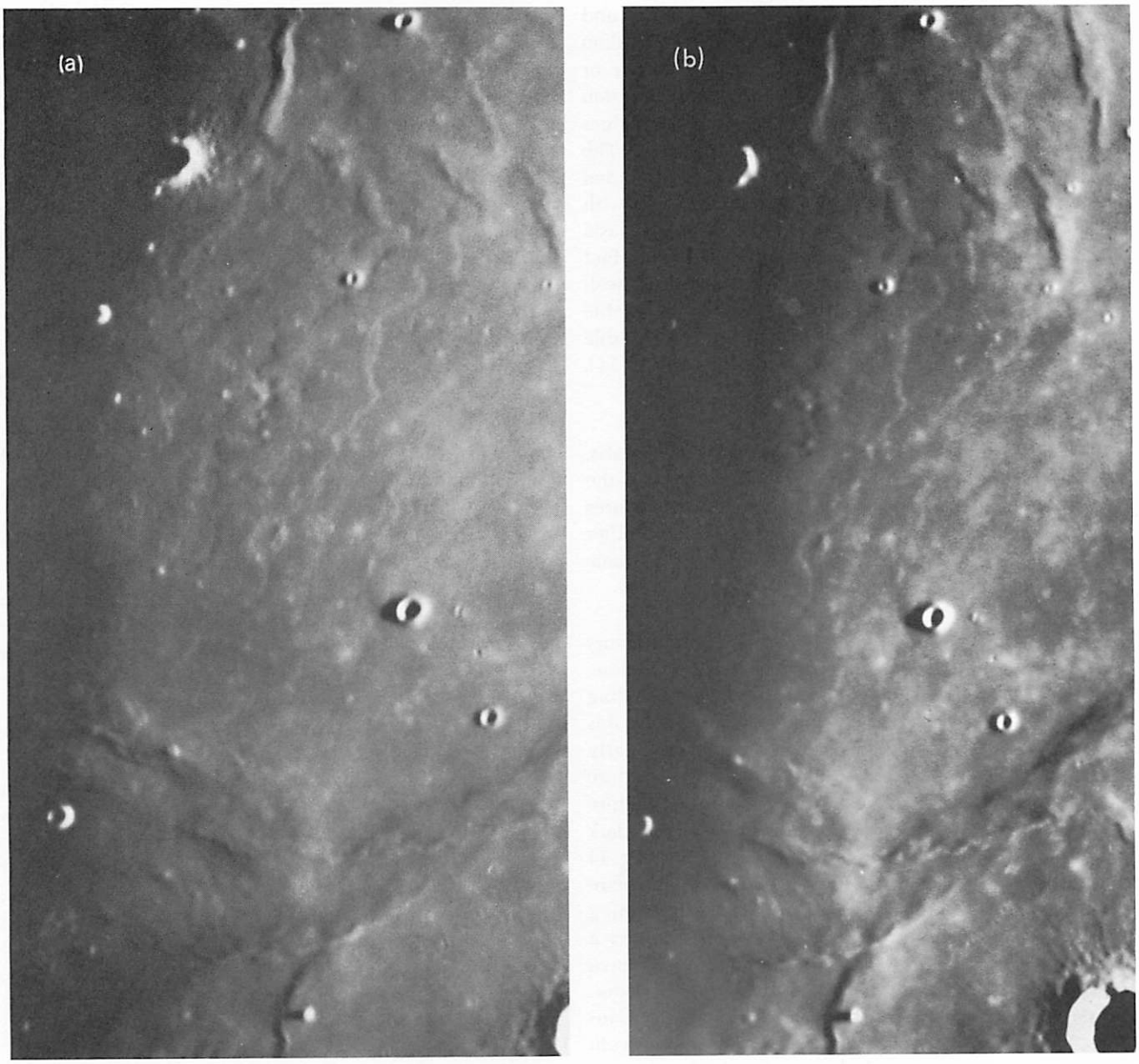

Fig. 16 Flows on Mare Imbrium in sunrise illumination (cf. Fig. 17a). Boundary of lower flow coincides with boundary of a color province shown in Fig. 13 (cf. Fig. 18); (a, Plate C1120; b, Plate M690).

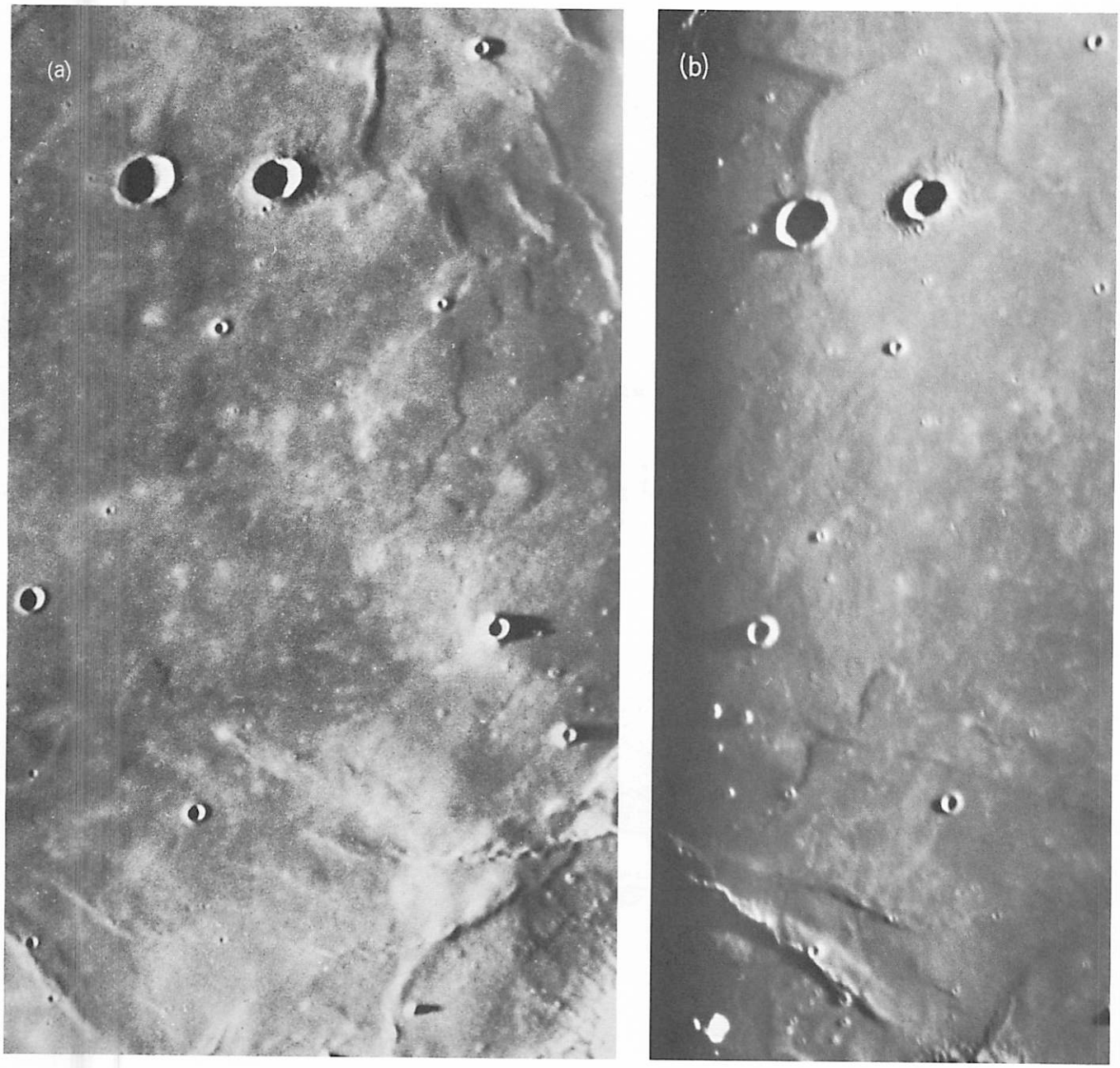

Fig. 17 Flows on Mare Imbrium. Fig. 17a (Plate W252) shows same area as Fig. 16 but with sunset illumination. Flow front in right upper margin coincides with color boundary of Fig. 13 (cf. Fig. 18). Fig. 17b (Plate C296) shows sunrise illumination of a prominent flow front near the main Imbrium ridge passing through Lambert (cf. Fig. 18 for connecting detail).

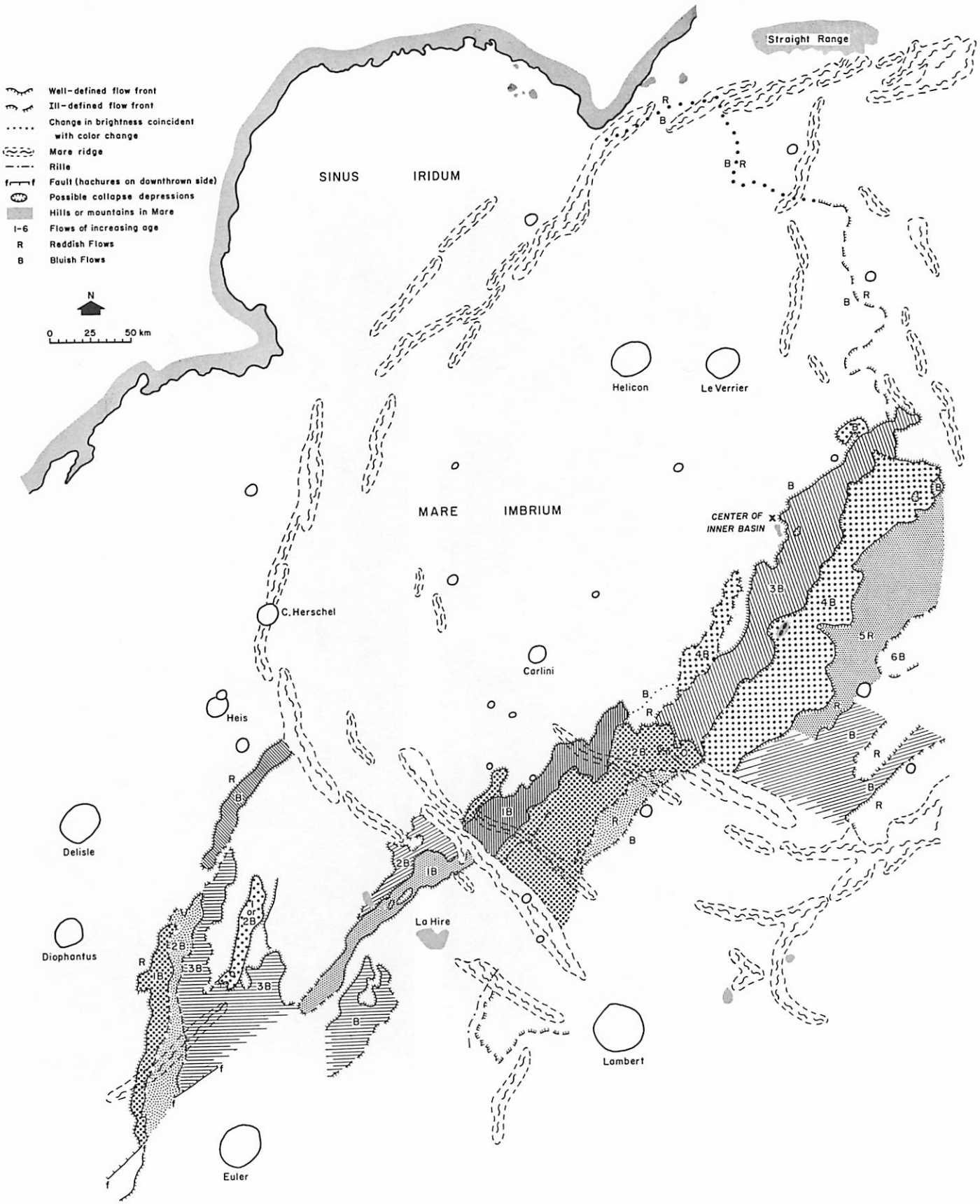

Fig. 18 Preliminary map of flows photographed in Mare Imbrium as interpreted by R. Strom (cf. Figs. 13, 16, and 17).

in the maria, are often redder than the maria themselves. This holds also for much of the crater-ray material deposited on the maria. Regardless of the causes of the observed colors, the existence of successive well marked flows as part of a general tectonic pattern unmistakably supports hypothesis 1 of Section A.

There is another important observation that bears on the choice between hypotheses 1 and 2. It is that the flooding of the circular maria did not occur immediately upon the formation of the basins but after a considerable interval, apparently different for the different basins, in some cases perhaps as long as a few million years. This follows from the study of the inclined and partly flooded craters near the borders of Mare Nectaris, Mare Humorum, Mare Crisium, and others. These craters are tipped, clearly having been formed on an inclined surface, apparently the floor of the basin before it was flooded. Since the number of such structures differs for different maria, it appears that the intervals between formation and flooding may not be constant. In any case, the intervals must have been many thousands or possibly a few million years. Hypothesis 2 does not explain this phenomenon, whereas it is compatible with hypothesis 1 provided the formation of the lavas was not the result of the impact itself but of a general heating process of the Moon, causing subsurface magmas to be available during a certain period of lunar history. The assumption of the Moon having passed through such a period of considerable internal heat and partial melting is consistent with the observation that the parent bodies of the meteorites, which by all indications were even smaller than the Moon, have gone through a similar process of melting, differentiation, and freezing. It is difficult, if not impossible, to explain various other lunar phenomena without the assumption of a period of maximum melting. Among these are the isostatic adjustment that has taken place in approximately twenty large pre-maria craters, such as Clavius and Hevelius, which show convex rather than concave floors, and the flooding and filling of many craters with elevated flat, dark floors, such as Wargentin (Fig. 19). The hypothesis that the flooding was indeed by available magmas, caused by previous lunar heating and not by the impacts themselves, is further supported by the fact that several very large pre-mare craters were never flooded, whereas even small craters dating from the period of maria formation are flooded (Fig. 2) and that distinctly post-mare craters, such as Tycho and Copernicus, show no sign of flooding.

There is a related observation bearing on the choice between hypotheses 1 and 2. Because of the severe damage to the walls of Mare Cognitum it would probably

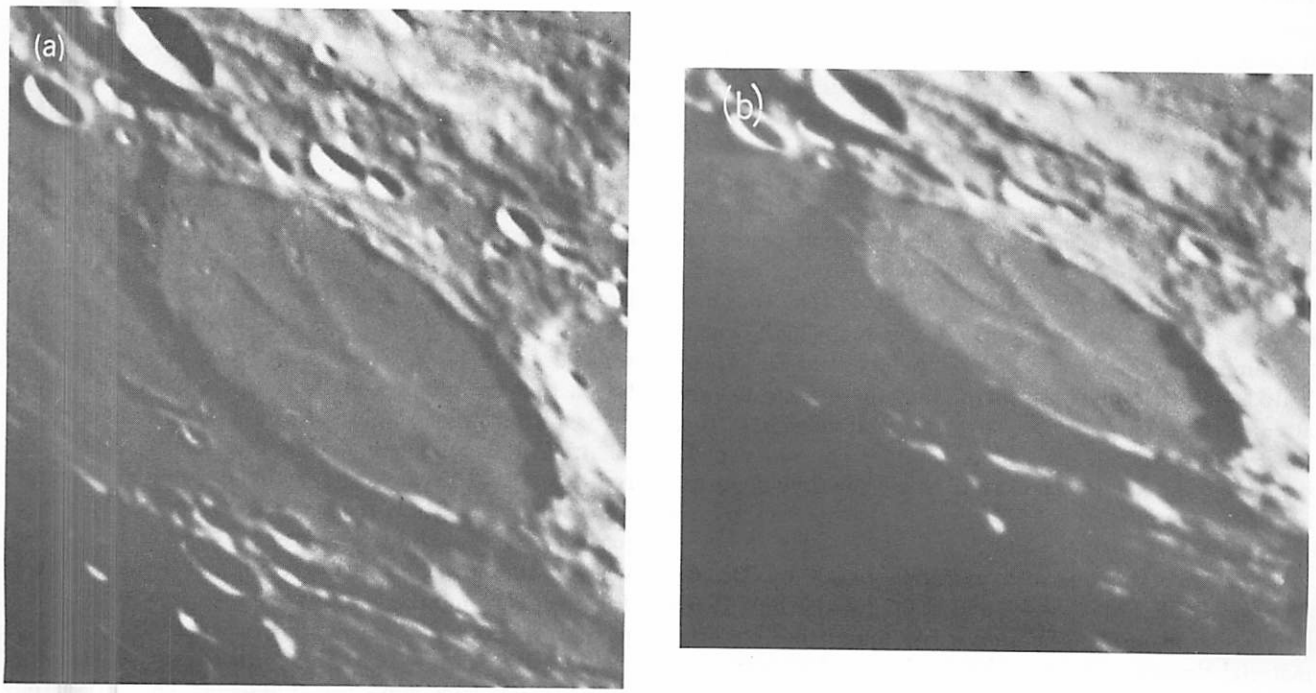

Fig. 19 Elevated floor of Crater Wargentin (a, Lick Observatory; b, Catalina Observatory 437).

be generally conceded that it is older than Mare Imbrium. If so, the striking color contrast between the islands in Mare Cognitum (such as Darney χ) and the mare itself proves that no dense dust cloud from the Mare Imbrium impact has struck there.

The conclusion that hypothesis 1 is consistent with the observed features does not mean that the structure and density of the lunar lava, as exposed in the maria, are the same as those of terrestrial lavas. The deposition in a vacuum, the much lower surface gravity of the Moon, and the subsequent erosion by particles and solar radiation will have caused departures which must be ascertained.

The lunar surface lavas will, upon deposition, probably be *extremely porous and vesicular,* like pumice or reticulite found, e.g., in Hawaiian lava flows, but probably more extreme. The pressures occurring in terrestrial lavas at a depth of 10 cm would be encountered on the Moon at a depth of some 120 m if the lunar surface rock has a bulk density of 0.5.

That the uppermost layers may have an even lower density is indicated by the experiments of Dobar *et al.* (Ref. 1), who found a value of about 0.12 for the bulk density of solid silica extruded as a liquid into a vacuum. These authors introduced the name "simolivac" for such material (silica molten in vacuum). Almost certainly, the surface of the original lunar laval flows will have had a rock-froth structure somewhat like simolivac. It will not be identical because the lunar rock will probably have no more than about 70% SiO_2 content, and dissolved gases will cause further complexities. In addition, a rapid boiling off of many substances will occur when the magmas reach the surface, since the sublimation points of SiO_2, MgO, BaO, ZnO, Al_2O_3, and other oxides, as well as the metals Ca, Cr, Cu, Fe, Mg, Ni, Si, Zn, etc., are much below the melting points even at such "high" lunar pressures as 10^{-5} mm Hg. We are indebted to Dr. Alvar Wilska of this University for calling these facts to our attention. Because of the low thermal velocities, the substances that boil off will precipitate on colder rock surfaces in the neighborhood and cause powdery deposits not unlike "fairy castles."

Recent experiments with extruded basalt by Dr. S. Hoenig at this Laboratory yielded 0.3 for the bulk density of this material. The author has found that basaltic material thrown up in liquid form by the Laimana volcano on Hawaii in 1960 and solidified in free fall (very low effective gravity) has a bulk density of 0.10–0.18. It is therefore very probable that at the time of deposition, the lunar maria were covered with a layer of material of bulk density 0.1–0.3.

Some estimate on the thickness of a rock-froth layer on each of the lava flows may be made on the basis of the Mare Imbrium (Figs. 16–18) and Mare Serenitatis (Figs. 9, 10) observations. The flows on Imbrium are about 50–100 m thick, and the most extensive are some 200 km long (Fig. 16). These Imbrium flows appear to have issued not from the mare shoreline but from fissures well inside the mare, within a rather confined area. The slopes of the flows have not been measured (this could probably be done photometrically) and may not be the original ones at the time of deposition. They seem to be of the order of 1 deg. In Mare Serenitatis, near the south shore (Fig. 9), a distinctly steeper slope of perhaps 3 deg occurs, though other flows are found nearby with very small slopes.

The composition of these flows cannot, of course, be inferred with any certainty by inspection from the Earth. O'Keefe and Cameron (Ref. 8) have drawn an analogy with terrestrial ash flows because of their great fluidity and suitable composition, if it be adopted that tektites are of lunar origin and their composition (about 70% SiO_2) is indicative of that of the lunar crust, and that lunar ash flows would lead to a material of similar composition as on Earth (ignimbrite). On the other hand, as R. Strom has pointed out, unlike the lunar flows (Fig. 16), terrestrial ash flows spread in all directions from the source and have no appreciable terminal walls, whereas the observed lunar flows rather resemble the Hawaiian flows illustrated in Figs. 20–22.

While most terrestrial lava flows have fronts inclined over 20 deg, Dr. H. Powers of the Hawaii Volcano Observatory informs us that some Hawaiian flows have fronts inclined less than 7 deg. Estimates based on Figs. 16 and 17 indicate average slopes of about 3–7 deg for the fronts there shown; the well known flow between the Apennines and the Caucasus, toward Archimedes, has a front slope of about 17 deg (R. G. Strom, E. A. Whitaker). These low figures are not necessarily representative, because the limited resolution used reduces the values. It is further noted that ash flows tend to sweep over low hills and other obstacles in their paths, whereas the slower lava flows avoid and bypass them. In Figs. 16–17, a number of hills are seen to have been bypassed, in curved arcs, by the principal flow. On the Earth, ash flows are associated with explosive volcanism, and basaltic lava flows are quiescent. The topography of the lunar maria appears to fit the second description

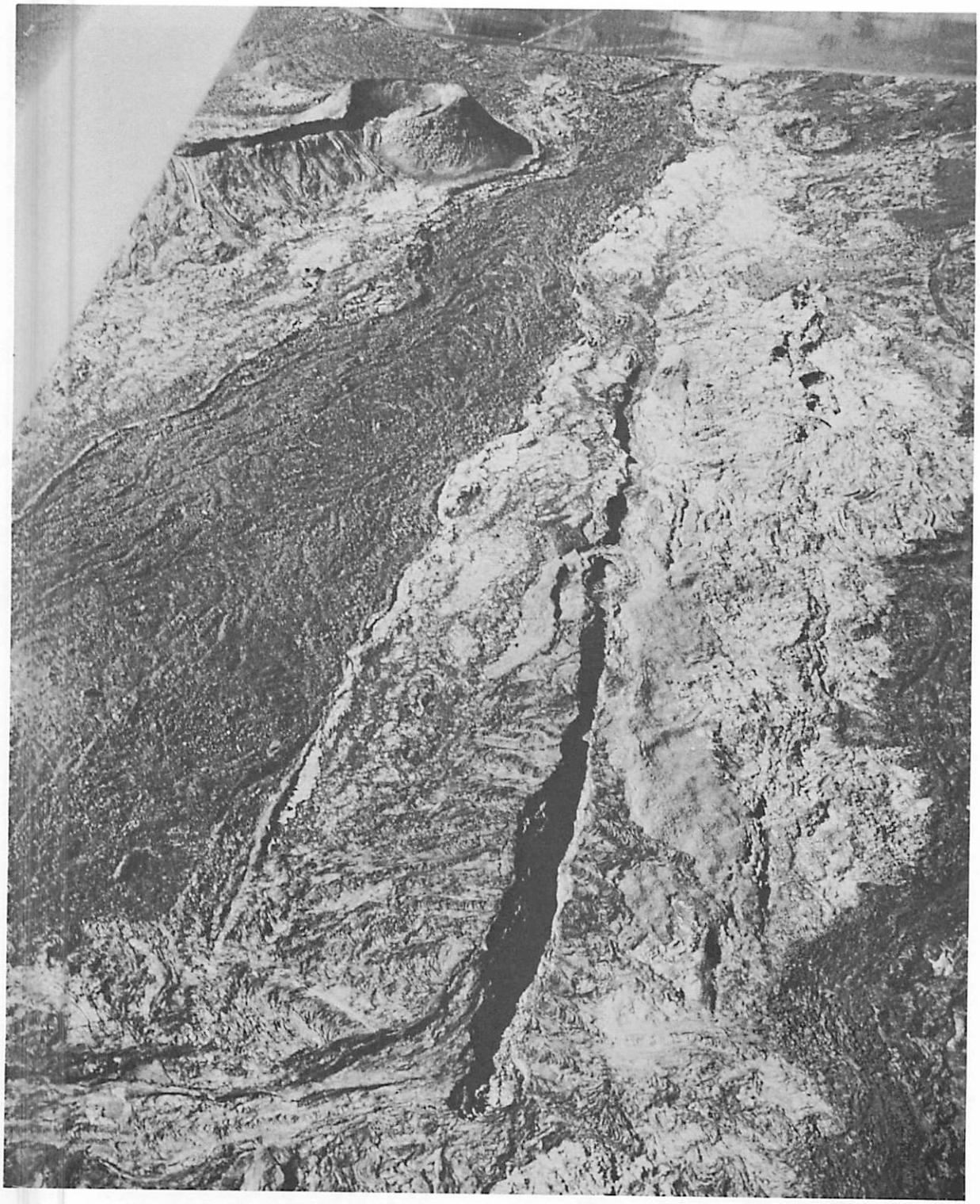

Fig. 20 Aerial view of lava fields and rifts on Mauna Loa, Hawaii. (Approximate elevation, 12,000 ft.; LPL photograph.)

Fig. 21 Crater, crater chain, rift, and edge of lava flow, Mauna Loa, Hawaii. (Window reflection superposed on upper right corner; LPL photograph.)

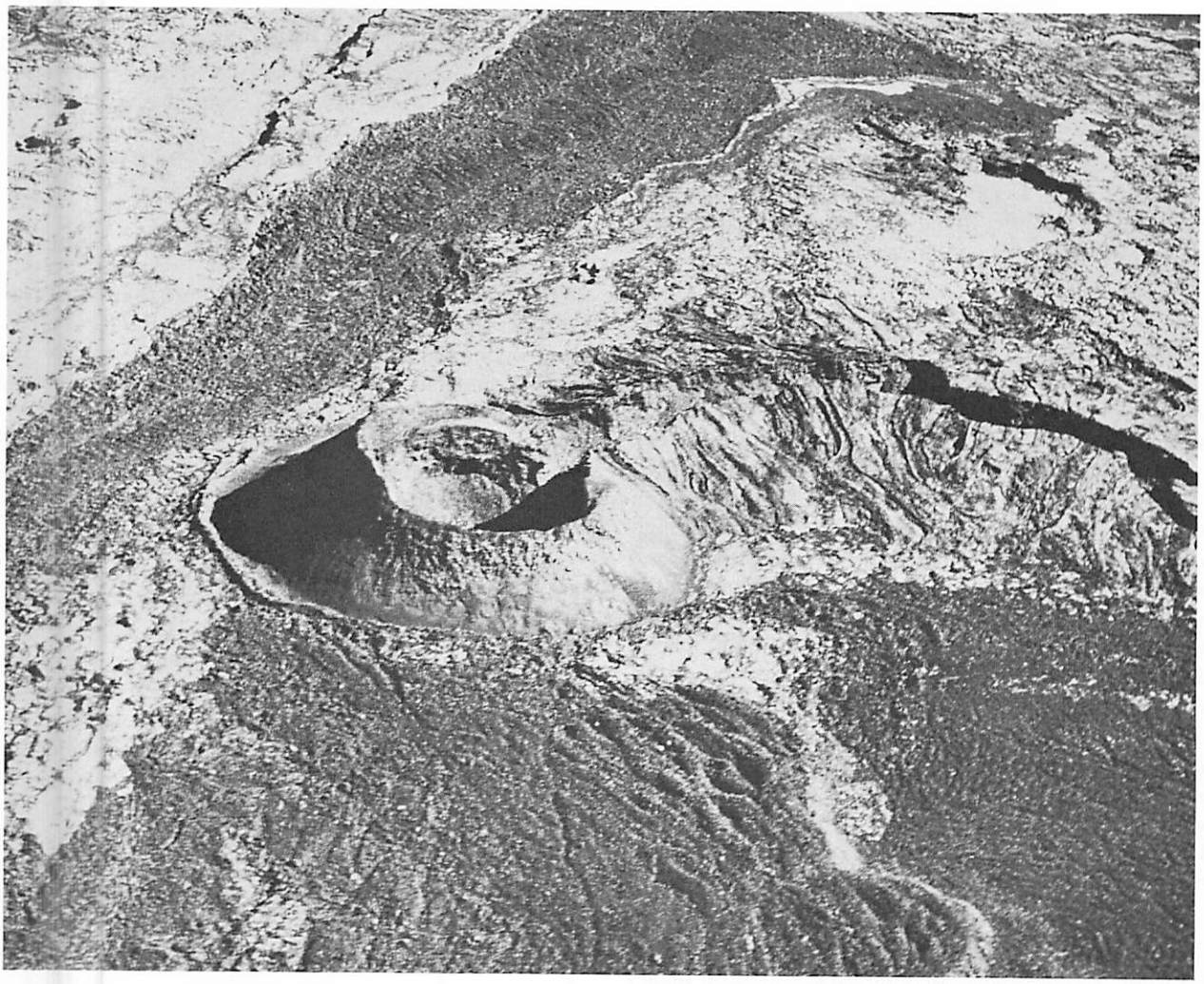

Fig. 22 View of lava vent and lava channel as well as surrounding lava streams showing "moraine" effect (LPL photograph).

better. It is true that some authors have assumed the craters on the maria to be of volcanic origin; however, there is nothing to indicate that the observed lava flows and the craters are related.

The retention of the carrier gas in an ash flow in the lunar vacuum would be difficult to understand unless it is assumed that the flow is promptly sealed off at the surface with a layer of sufficient strength to confine the gas. Also, ash flows are normally associated with lava flows. There thus appear to be reasons to assume that the observed flows are lavas, not ash, although allowance must be made for the different lunar conditions before one can be certain. If they are ash flows, the composition is likely to be rhyolitic; if they are lavas, they are likely to be basaltic.*

The *mare ridges* cut through the color provinces without visible interference. They are not the edges of lava flows. Instead, they appear to have a dynamical cause, some being related to the symmetrical pattern of the near-circular maria and others to the lunar grid system, of which some ridges are parts. This may be verified by inspection of Figs. 5–12, 16, and 17, and Fig. 25 in Section C. Also, the ridges are quite invisible at high Sun, showing that the lunar surface is essentially continuous across them. There are no close analogs of the lunar ridges on the Earth. Their non-interference with the color provinces and their invisibility at high Sun indicate that they were formed by uplift. In some cases, the uplift appears to have been so large that the surface has split open; and often it may be observed that out of such fissures, a new dike-like rock mass has been extruded, usually whiter in color than the original mare floor (and thus visible at high Sun). These whitish "lunar dikes" have been known to exist (Ref. 9), and some are clearly seen on several of the *Ranger* photographs.

The phenomenon of lunar dikes indicates that the ridges are surface manifestations of subcrustal structural planes along which upwelling of magmas has taken place. These structural planes presumably resulted from tension followed by compression. This model accounts for the presence of ridges as part of the grid system and also as roughly concentric and radial structural units of the impact maria, because, as the lava basins cooled to increasingly great depths, the deeper spherical layers of the Moon shrank, narrowed the support base for the overlying maria, and caused radial compression. Figure 11 shows a region adjacent to Mare Humorum where the grid-system pattern was deflected by the local stress pattern of the mare.

The formation of ridges by a laccolithic-type uplift of the lunar crust above dynamically determined fracture planes is facilitated by the layered structure of the lunar maria noted above (individual layers typically 50–100 m thick), particularly if alternate layers are very vesicular and weak structurally. The low surface gravity would also facilitate the vertical displacements. Thus, it is not surprising that the equivalent of lunar ridges has not been found on the Earth.

The ridges are therefore assumed to date from an early post-mare period and to have resulted from effects accompanying the cooling of the mare basins. Later in lunar history, magmas will not have been available except possibly in isolated "volcanic" regions. The apparent absence of ridges from the terrae is consistent with their presumed nature as consolidated dust to great depth and the absence of near-surface magmas.

On the basis of the findings discussed in Sections A and B, the following conclusions about the lunar maria have been drawn that may be used as a basis for the discussion of the *Ranger VII* data. The maria are low-level areas flooded by lunar lavas. Some of these depressions were caused by large impacts that resulted also in extensive surrounding tectonic structures, both peripheral and radial. The lavas were not caused by the impacts themselves but resulted from extrusion of available magmas. Some mare surfaces show clear evidence of several successive lava flows. Each flow is found to have a homogeneous color throughout, but different flows may have different colors. The most recent (upper) flows tend to be the bluest, but the age sequence is not everywhere the same as the color sequence. Composition differences, rather than mere age differences, are therefore held responsible. These composition differences may reflect the state of oxidation, possibly related to the water content of the magmas. There is again a remarkable analogy with recent terrestrial basaltic lava flows; on Mauna Loa, Hawaii, each flow has a characteristic uniform color, but the colors of adjacent flows may differ markedly.

The lunar flows are bounded by terminal walls, and some large flows (up to 200 km in length) are comparatively narrow. By terrestrial analogy, this would indicate

*R. Strom points out that gradations exist such as described by R. L. Smith in the *Bulletin of the Geological Society of America*, Vol. 71 (1960), p. 809, that might closely resemble the lunar flows.

that the flows are basaltic lavas rather than ash. According to the small slopes of the flows and their great lengths, the lavas must have been very fluid. Yet their terminal walls show the presence of a substantial solid crust during the flow. On this basis, and in view of the presumed rock-froth nature of the upper layers, it is assumed that the lunar flows consist of two layers each, an upper viscous and later highly vesicular layer, some 10–20 m thick, and a layer of more compacted rock that resulted from the low-viscosity lava.

Subsequent meteorite or cometary impacts as well as cosmic abrasion will have occurred in this multilayered structure. Very small craters will have formed in the rock froth only, and larger craters will extend into the denser rock; but the succession of flows on the maria may have caused irregular local alterations between very vesicular and denser rock material. Regional unevenness in crater shape is therefore to be expected.

Dobar *et al.* (Ref. 1) found the bearing strength of simolivac to be 1–4 tons/ft^2 or 1–4 kg/cm^2 for static loads. For the low-*g* Hawaiian basalt, the author found essentially the same value (2–3 kg/cm^2), which increases to about 6–8 kg/cm^2 after surficial crushing of a few millimeters. It is probable that the bearing strength of the lunar maria will be of the same order of magnitude, with impacts that have pulverized and compressed the rock froth having caused some local fluctuations in value. The expected occurrence of cavities and lava tunnels makes it unsafe to use this number indiscriminately.

The *Ranger* photographs, with their high resolution, potentially add much information on the texture of the upper 10–20 m of the mare surface. The upper layer is not likely to react like solid rock or even like sand or alluvium because of its very high compressibility, over 90% of the volume being open. This is particularly true for material stemming from the unconsolidated upper layers of a terra region impacting on a rock-froth mare.

C. On the Structure of Mare Cognitum

Figures 23–25 are Earth-based photographs of the Mare Cognitum region showing the aiming and impact points as well as two low obliques. The mare is less regular than Mare Crisium, presumably because of the greater age of the basin, and is only two thirds of its size (diameter roughly 280 km versus 450 km for the inner wall of Crisium). In size, the mare resembles the inner basin of Mare Orientale (inner ring 320 km), the inner ring of Mare Humboldtianum (300 km), or the giant craters Bailly and Pingré near the South Pole (ring diameters 320 and 300 km) (Ref. 6). As is true for Mare Crisium, the east wall is destroyed, although the destruction is much more severe in Mare Cognitum. The ridge system shown in Fig. 25 and the area of the Riphaean Mountains are the most regular remaining parts of the mare. Most of the ridges are visible with more resolution on the *Ranger* photographs despite the higher Sun angle (23 deg).

A group of islands occurs in the mare at 12°S, 26°W, the largest of which is called Darney χ. These islands are remarkable for their deep yellow color (in stark contrast with the dark gray, slightly yellow, mare floor; cf. Fig. 15) and for the large number of crater pits piercing their surface (several dozen can be seen telescopically). The islands appear to be remnants of the pre-mare lunar crust.

Figure 26 shows the full-Moon appearance of Mare Cognitum. The mare is seen to be traversed by a number of narrow crater rays, most of which are traceable to Tycho or Copernicus, although a single thin ray issuing from Lalande passes almost squarely through the impact area. The craters responsible for these rays are denoted by symbols in Fig. 26.

All rays in Fig. 26, particularly those in the eastern half of the mare, are readily identified on the *Ranger* photographs. The Copernicus ray in the far eastern part of the mare (11°S, 18°W) is found to contain a band of craters up to about 500 m in diameter, seen in B frames 165, where the band of craters occurs in the upper central section of the frame, through 180, after which the area moves out of the field. Apart from a few minor features, grooves are found to be nearly absent on these photographs. The resolution on B180 is 100–150 m. The photographs strongly indicate that *the brightness of the ray is not due primarily to secondary craters but instead to uniformly spread fine ray material.* The area is well mapped on the AF-ACIC chart RLC 2, scale 1:500,000. The distance from Copernicus is 20 deg or 600 km.

The second Copernicus ray, crossing the mare just east of the prominent mountain ridge near the mare center at 10°S, 21.3°W, is shown clearly on the A frames as a brighter fan-shaped area, but right up to the last frame (A183, resolution 250 m) showing an appreciable area of the ray, few if any secondary craters appear. Again, the uniformity of the ray indicates that its brightness is not primarily due to unresolved secondary craters. The distance from Copernicus is 20 deg or 600 km.

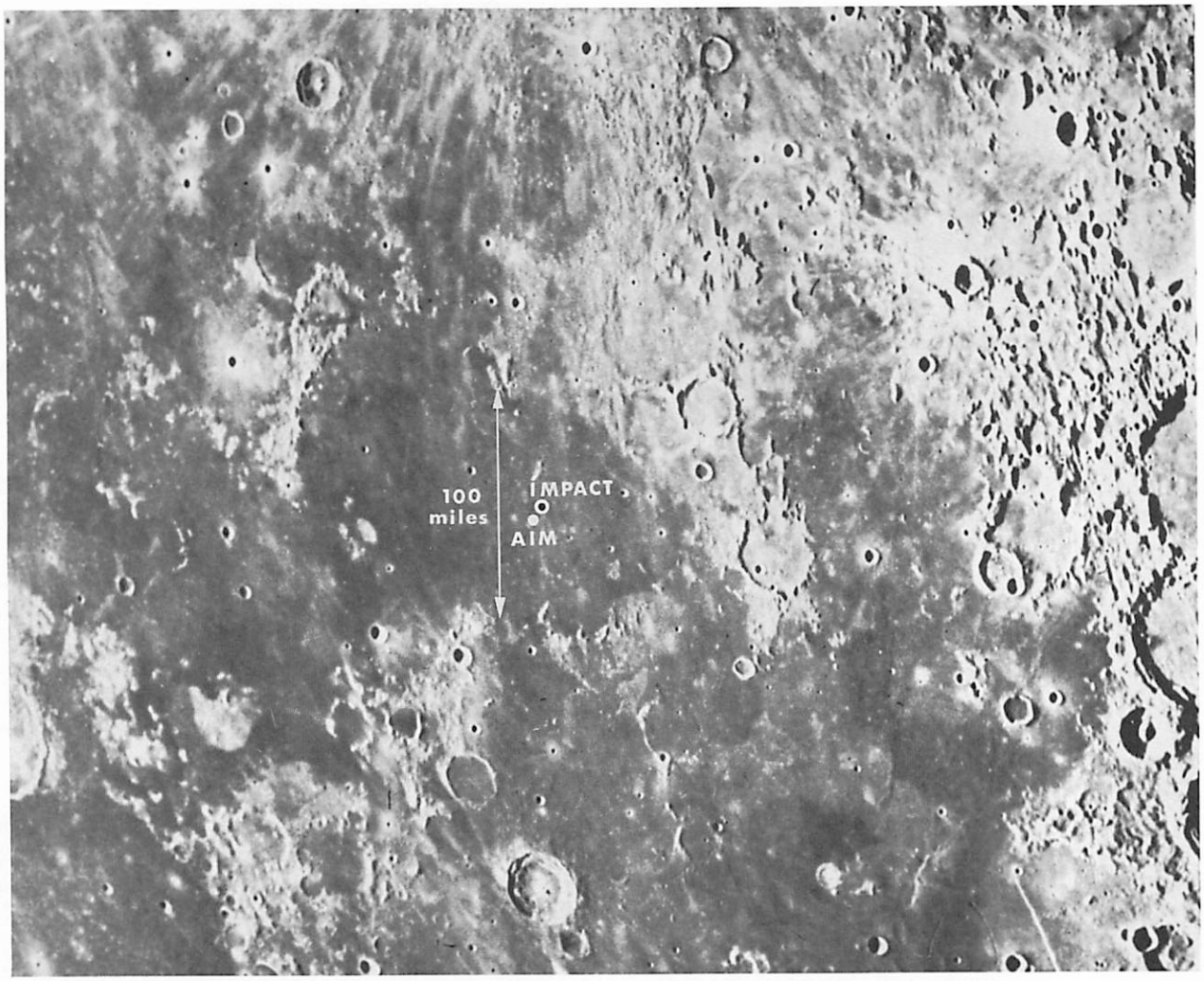

Fig. 23 Earth-based photographs of Mare Cognitum showing aiming and impact points of *Ranger VII*. (Illumination similar to that in *Ranger* photographs.)

Fig. 24 Eastern half of Mare Cognitum and surroundings under low Sun, showing ridge system in mare and several examples of white linear mountains (Plate C1129).

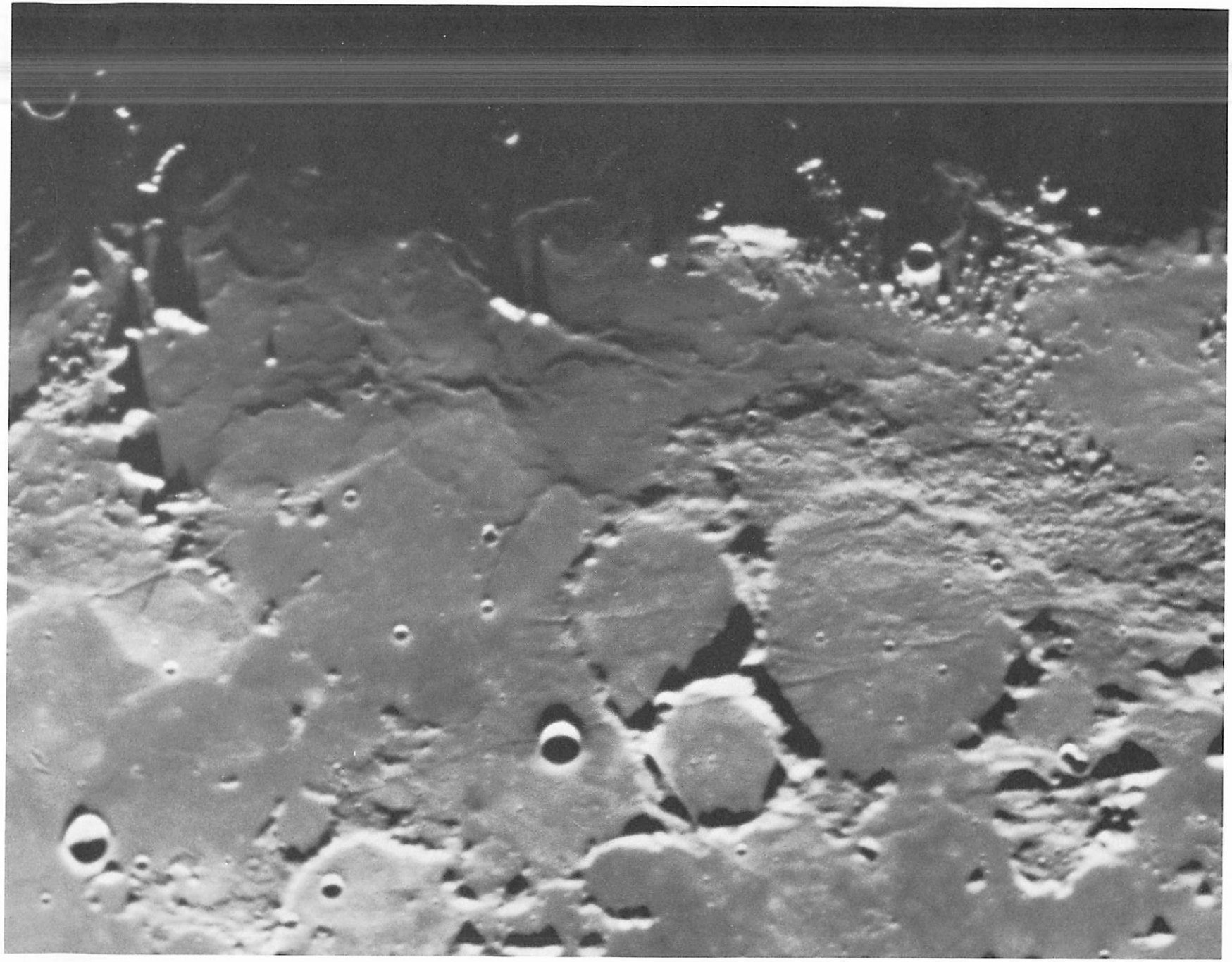

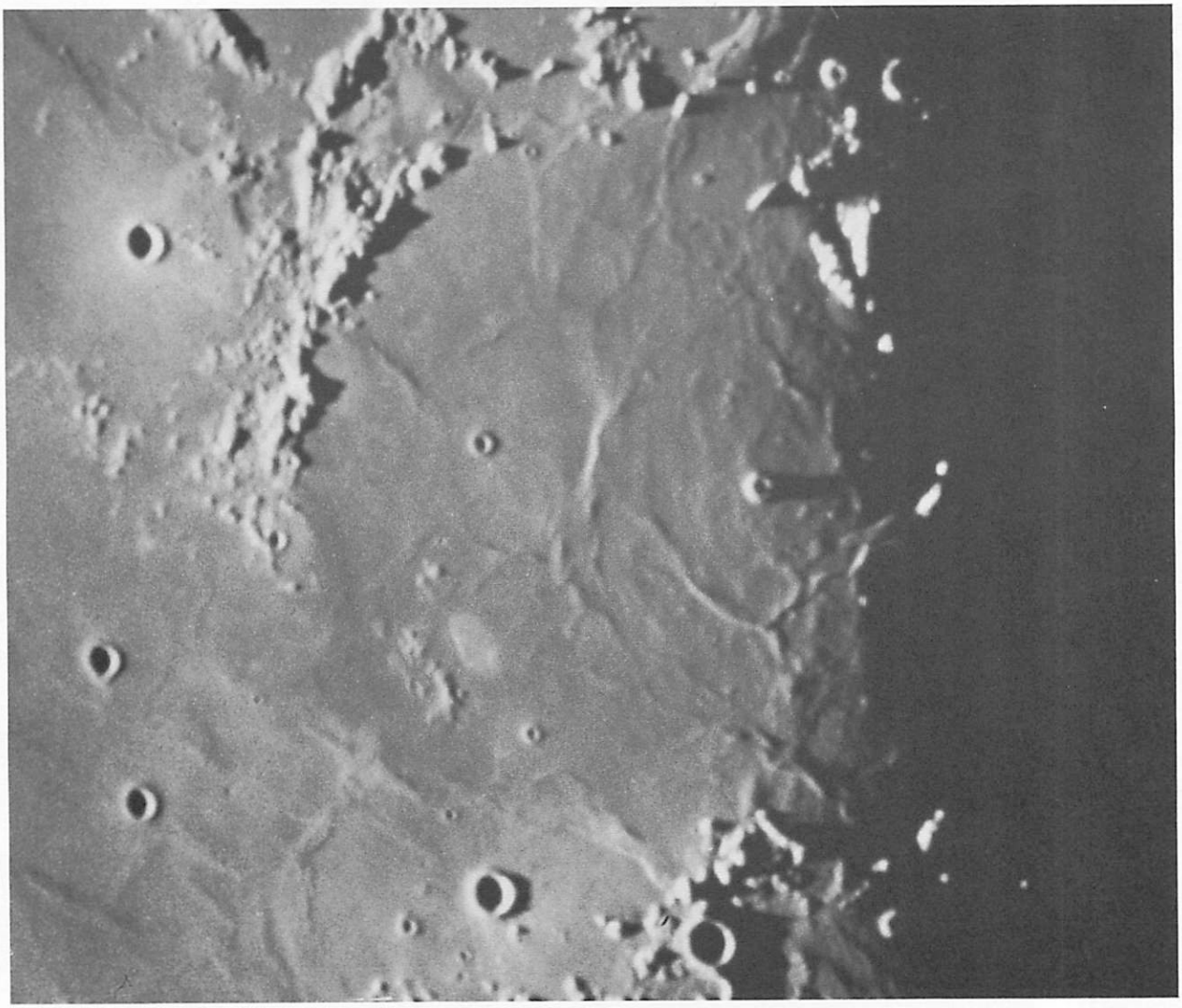

Fig. 25 Western half of Mare Cognitum under low Sun, including Riphaean Mountains (Plate M195).

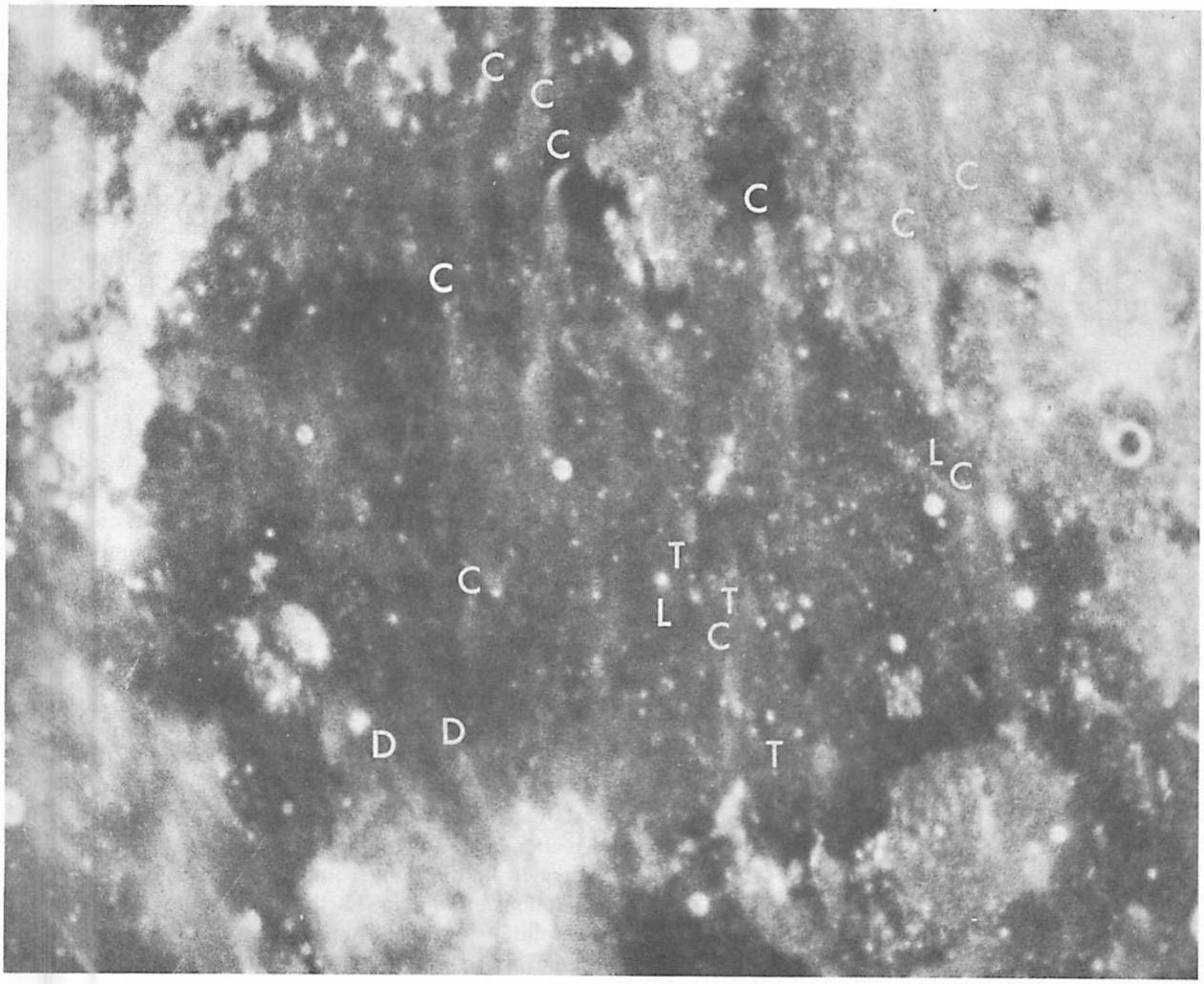

Fig. 26 Full-Moon view of Mare Cognitum, showing numerous crater rays and some dark areas essentially free from ray material. (Four sets of rays are identified as follows: *C*, Copernicus; *D*, Darney; *L*, Lalande; *T*, Tycho. The Lalande ray stretches between the two *L's* crossing the impact area. The Darney rays issue from Darney, within the Figure. The Copernicus rays extend downward from the symbols, the Tycho rays upward.)

Several small Tycho rays and some Copernican rays occur close to the impact area of *Ranger VII* and are thus shown with higher resolution. The *Ranger* records have provided the first information on the detailed structure of such rays.

D. The Structure of Crater Rays

Figure 27 shows a reprojected photograph of the Tycho ray system, with Tycho itself placed centrally on the lunar disk. The strongest Tycho rays are seen to miss Mare Cognitum, but numerous smaller rays spread toward the mare. Comparison of Figs. 26 and 27 will clarify the Tycho ray pattern in this region.

On A180, the prominent mountain at 10°S and 21°W, referred to before, is seen near the upper margin, with its crest pierced by a small crater. About 3.5 cm southwest of this crater, a cluster of five whitish craters occurs (at 10°30′S, 21°04′W; see ACIC map RCL-3, scale 1:100,000) from which a whitish band approximately 2 cm long extends upward. This feature is readily identified in Fig. 26, where it is marked with a **T**, and may be observed with increasing resolution (from approximately 300 to 75 m) in the successive A frames, 180–195. It is also shown on the upper central margin of Fig. 28, reproduced from A187. On these A frames, it is seen that the ray starts at a cluster of four or five prominent craters and numerous smaller ones in a confined area, from which a whitish band extends like a comet tail from the comet head. This whitish band crosses a complex ridge, shown in Fig. 28, and contains some shallow craters and grooves oriented North and South, in the direction of the ray itself, which is away from Tycho.

A similar observation may be made with respect to the Tycho ray that passes through the impact point of *Ranger VII*. The "head" of this ray is seen as early as frame A170, with two craters shown located at 10°52′S, 20°37′W, each about 1 km in diameter. On A180, many smaller craters are seen, and a fan-shaped ray issues from the cluster northward for about 1 cm. In Fig. 28 (A187), some structure is visible in the ray and evolves in the later A frames (cf. Fig. 29, frame A194). The analysis is complicated by the proximity and partial overlap of four Copernican clusters also identified on Figs. 28 and 29. In fact, there may be a continuous arc of minor Copernican secondaries extending through the entire central and upper central section of Fig. 29, crossing the Tycho cluster.

A spectacular event has occurred in the crater (1.4 km in diameter) just below and left of the central reticle on Fig. 28. The splashing Tycho material has cut through its rim and caused a bright ray about 0.5 km wide to extend northward from the crater for about 4.5 km. This is best seen on frames A194 (Fig. 29) and A195.

The concept of secondary impact craters occurring at the head of short crater rays is not new. It was observed many years ago, both visually and photographically, on the three or four short but prominent Tycho rays on the floor of Pitatus (Ref. 10). This floor is notable for its absence of confusing surface detail. At the head of each of the rays, a shallow crater can be seen.

In considering (e.g., in Fig. 29) the shapes of the secondary craters in the crater rays, it must be borne in mind that a given impact area can be struck by ejecta arriving at different angles and with different velocities. For example, the distance from Tycho is 32 deg or 980 km, so that the impact velocity for Tycho secondaries must have exceeded 1.1 km/sec (Ref. 11). Velocities of up to 2.0 km/sec could have occurred, provided that the impacts were nearly vertical. For velocities less than 1.67 km/sec, both low-angle and high-angle impacts could have reached the target (Ref. 11), but clusters are unlikely to contain both types in comparable numbers. Near-vertical impacts probably lead to roundish clusters, low-angle impacts to elongated clusters. Since the observed clusters are roundish, it is assumed that they are due to high-angle impacts. This is consistent with the fact that most craters are also round. Two exceptions occur in the first cluster, being groove-like craters, visible in Fig. 29 but best seen on A197. Figure 29 also shows some shallow grooves in the tail part of the ray. A larger groove of similar orientation, marked **b**, is seen in Fig. 28. The direction points to Bullialdus, which is 10 deg or 300 km away from the *Ranger* impact point. Figure 30 shows the relationship on an Earth-based photograph. With the resolution of Fig. 30, however, the Bullialdus scars or grooves are seen to only about half the distance from the *Ranger* impact point, marked **I**.

While there is little doubt that a causal relationship exists between clusters of secondary craters and their ray elements pointing away from the central ray crater (Tycho or Copernicus), the nature of the lesser features within the rays is not obvious. We shall return to this subject after a more general review of lunar craters and depressions seen on the *Ranger* photographs.

The presence of clusters of secondary craters at the head of ray elements appears to represent a rather general phenomenon, as was noted upon re-examination of high-resolution Earth-based photographs. It became

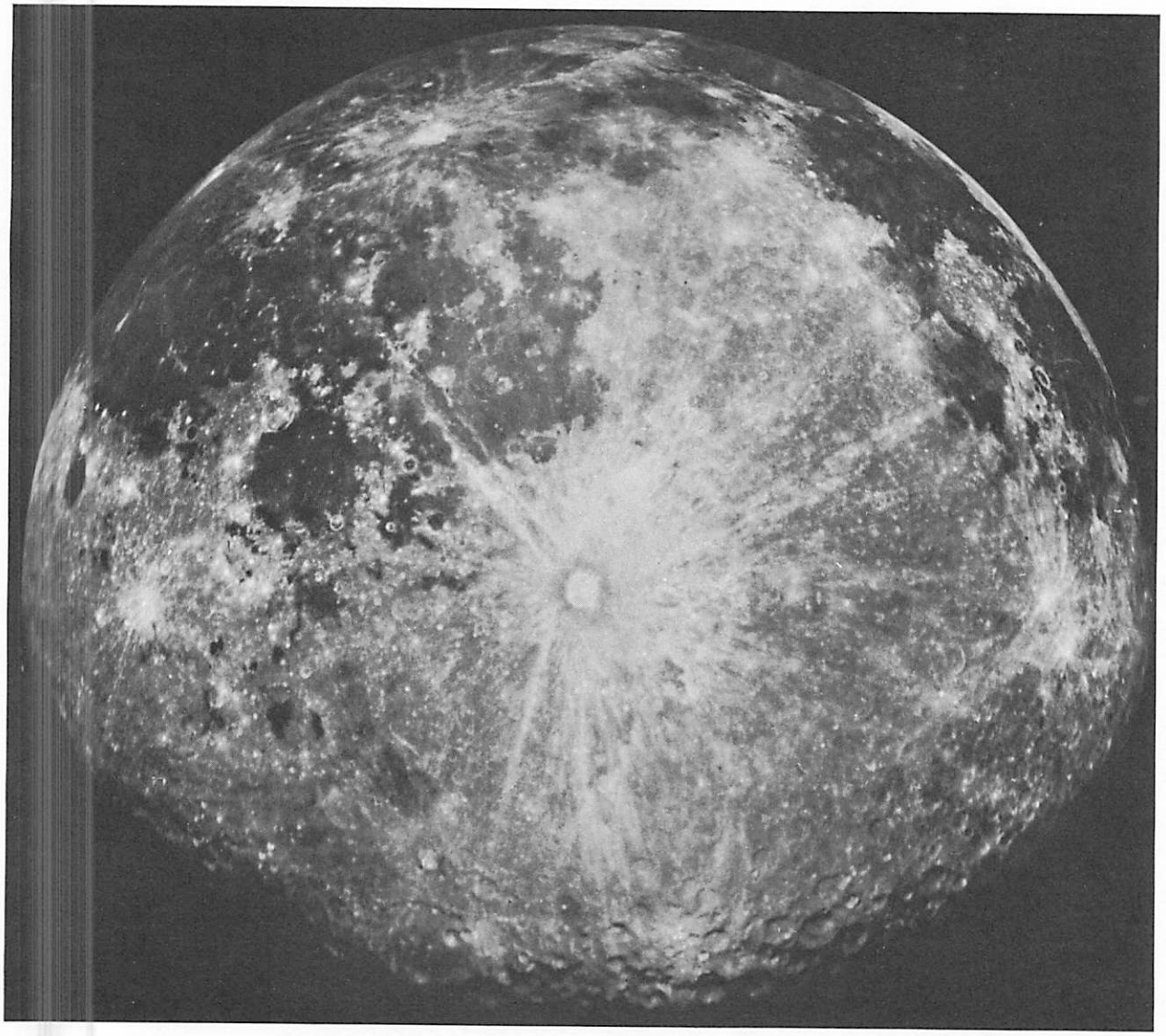

Fig. 27 Tycho ray system seen from above, reprojected.

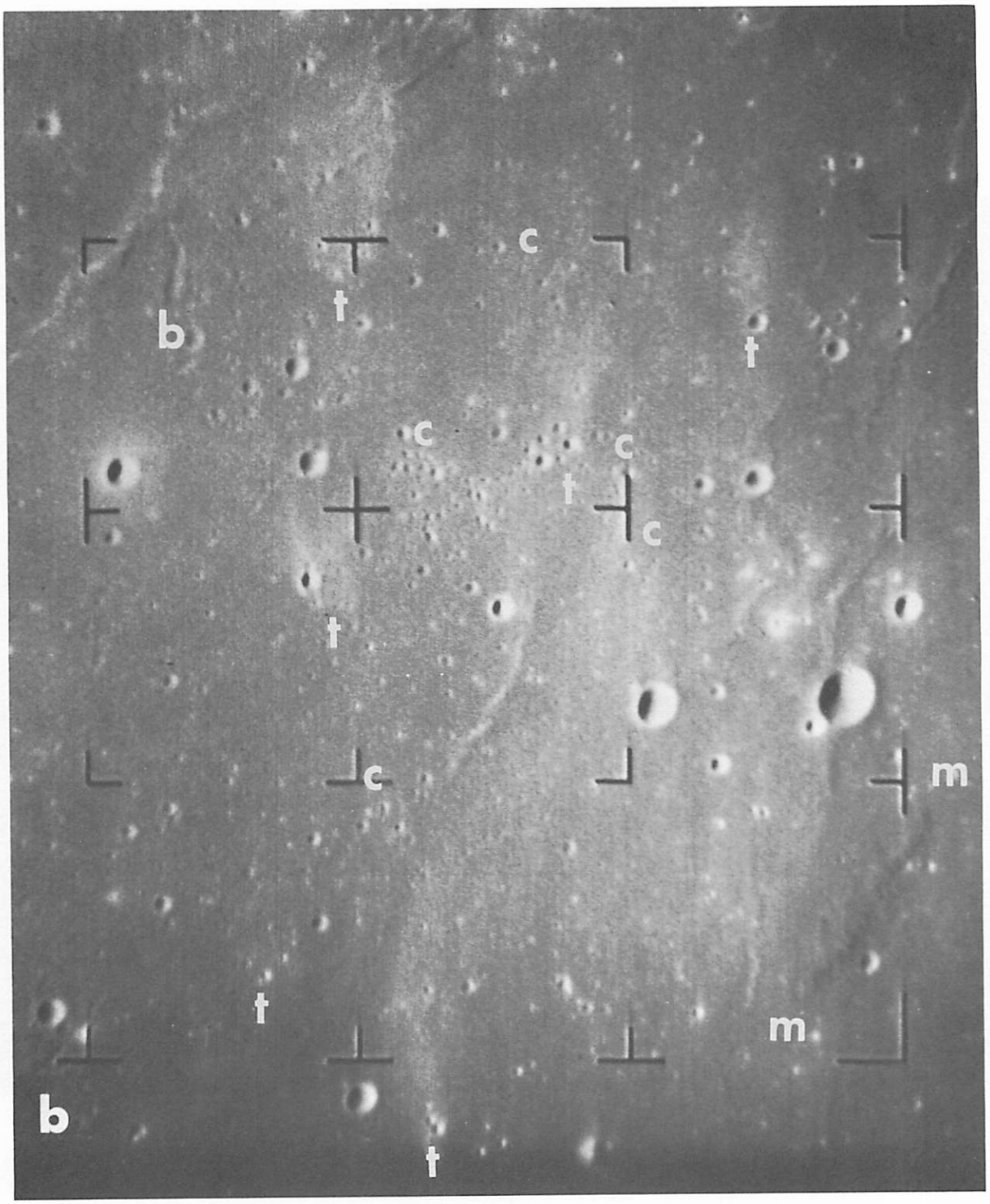

Fig. 28 Part of *Ranger* photograph A187 showing Tycho *(t)* and Copernicus *(c)* clusters of secondaries and associated rays, identified. North is up; the Tycho rays point North, the Copernicus rays South; b = Bullialdus groove; $m - m$ is a nearly black mountain range which appears distinctly post-mare.

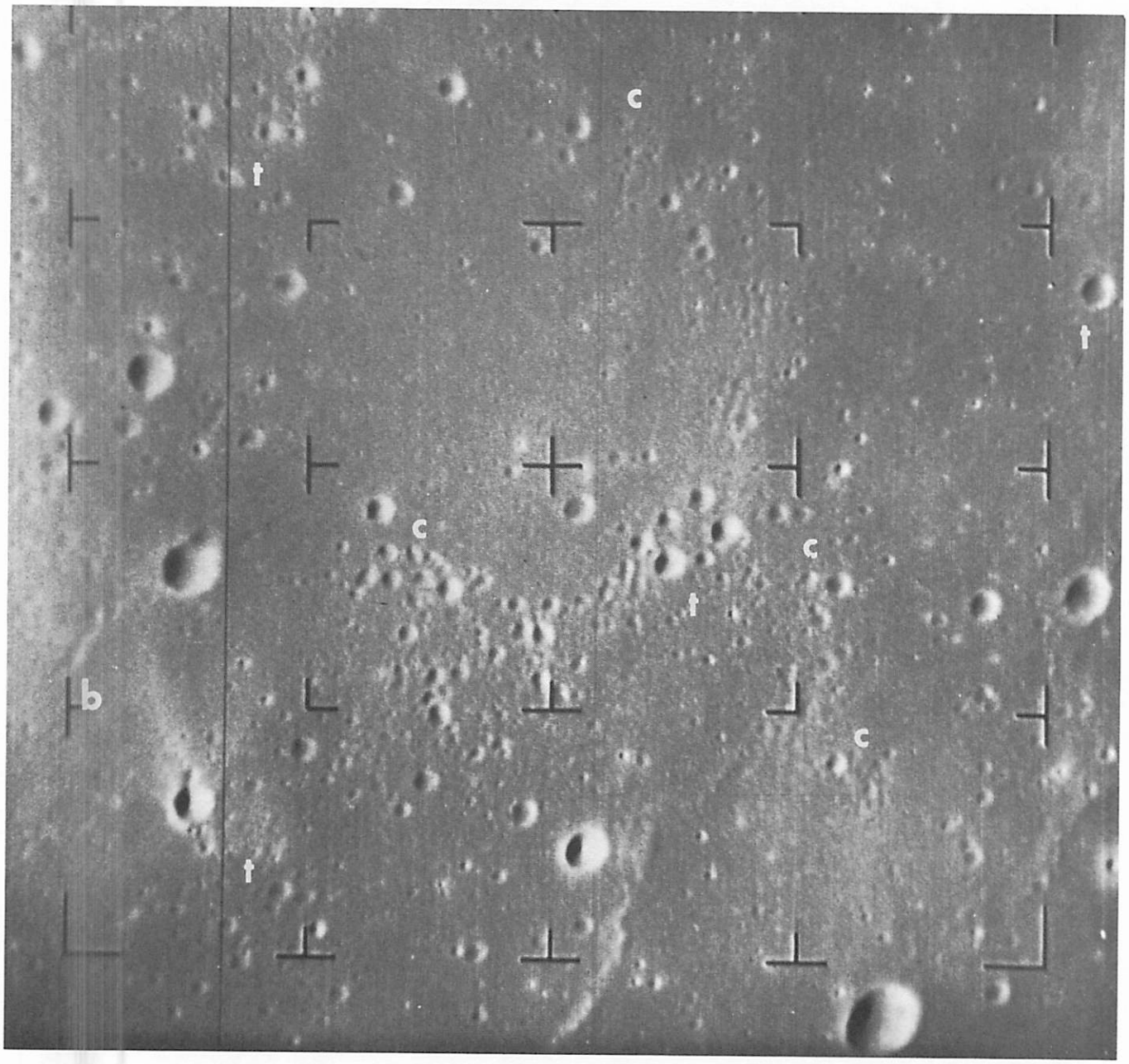

Fig. 29 Reproduction of A194 showing with higher resolution several features marked on Fig. 28.

Fig. 30 Earth-based photograph of Bullialdus and *Ranger* impact region *(I)* showing grooves caused by crater in its immediate vicinity. (Distance from crater to impact point is 10 deg or 300 km. Plate Y160.)

apparent that the ray craters have *two classes of secondaries*, those with normal dark walls and scattered at random around the crater, very frequent within about 4 crater diameters from the main crater walls and rapidly thinning out beyond; and those with bright walls, usually having ray elements associated with them, not distributed at random near the crater but falling along great circles passing through it. These bright secondaries, together with their oriented ray elements, form the observed ray pattern.

E. A. Whitaker shows in No. 59 that the relationship between the secondaries and the ray elements can be understood by assuming that a blast from the central crater (Tycho or Copernicus) was responsible for the deposition of the ray material originating from the secondary impact. This interesting suggestion would require the central crater to have been formed by an explosion whose ejected gases did not condense upon cooling during the flight time (15–30 min). A comet might serve this requirement. The mass of a Halley-type comet has been estimated to be 10^{17}–10^{19} g (Ref. 12). If its velocity of impact was 52 km/sec (corresponding to the comet radially approaching the Sun with parabolic velocity), the kinetic energy was 10^{30}–10^{32} ergs. Baldwin (Ref. 13) estimates that the energy required to produce Tycho (and Copernicus, having nearly equal dimensions) was 10^{30} ergs. The kinetic energy of Halley-type comets is thus adequate to produce these craters, even if the cometary nucleus is a composite body.

A rough calculation suffices to show that the expanding gas cloud would have cooled rapidly as a result of radiation losses to space. With a total energy of 10^{30} ergs, the thermal energy of the cloud is estimated to be of the order of 10^{29} ergs. If it expands as a hemisphere, initially optically thick to its own radiation, with a velocity $v \sim 10^5$ cm/sec, then its radius will be 10^7 cm after 100 sec and its total luminosity $L = 2\pi R^2 \sigma T^4 = 3.6 \times 10^{15}\ T^4$ ergs/sec. This quantity must be less than 10^{29} ergs/100 sec, the initial radiation presumably having been the most intense. Hence, T (100 sec) $< 730°$K. Adiabatic effects will reduce the temperature further. One finds similarly that T (1000 sec) $< 130°$K, a value probably too low because it neglects solar irradition, reduced optical opacity, and possible sublimation.

In order for the Tycho gases not to sublimate before reaching Mare Cognitum ($\Delta t \simeq 1000$ sec) and thereby lose their aerodynamic effect on the particle spray ejected by the clusters of secondary craters, the gases must have been highly volatile, consistent with their proposed cometary origin and contrary to a meteoritic origin. The comet hypothesis thus appears to be self-consistent. It appears very plausible that some material from the comet nucleus, being additionally separated from the main mass by the Moon's tidal effects, should be propelled to greater distances from the central crater than the lunar surface materials that produced the non-ray secondaries near the rim.

It remains to be shown that the frequency of comets passing the Earth is adequate to account for the occurrence of cometary impacts on the Moon. I am indebted to Dr. G. Van Biesbroeck for deriving the number of cometary encounters with the Earth since the year 1800 to within 0.1 AU, as based on the *Table of Cometary Orbits* published by J. C. Porter. Among the 648 parabolic comets that have been well observed since 1800, three have passed within 0.1 AU of the Earth, namely, Tebbut 1881 III, Morehouse 1908 III, and Jurlof 1938 III. It is certain that, in addition, uncounted smaller comets have passed the Earth; and it is significant also that all three of the comets listed fall within the past century, when the observers were more active. Among the 125 known periodic comets, five have *orbits* which come within 0.1 AU of the Earth; again, this list is incomplete for faint comets. All but one of the five (Tempel–Tuttle, $P = 33.2$ years) have periods of 5–7 years. It can be shown from probability considerations that statistically much less than one of the five came within 0.1 AU of the Earth since 1800. With three bright parabolic comets during the past 100 years having come within 0.1 AU, we derive that impacts on the Moon by such objects will occur at the rate of 1 per 2.5×10^9 years. On the basis of Oort's theory on the evolution of comet orbits, it may be assumed that the rate was greater in the early history of the solar system. With the strong reasons presented in favor of the major ray craters on the Moon having been caused by comet impacts, the argument may be reversed and the comet size distribution for the interior part of the solar system derived from the observed ray-crater distribution on the Moon. This subject will be dealt with elsewhere.

E. Classes of Craters and Depressions

In Section D, we referred to two classes of secondary craters associated with major ray craters such as Tycho and Copernicus. The rayless secondaries are crowded around the main crater, with elongated grooves or scars found sporadically at greater distances; these craters and scars do not have bright walls and are essentially invisible at full Moon. The second class are the bright secondaries,

often occurring in small clusters and associated with ray elements. These are located in the crater rays, which may extend to great distances from the main central crater.

In addition to these two rather easily identifiable classes, a third category is found, scattered rather uniformly over the Moon, consisting of primary craters. These primaries, where they occur in the maria, are usually very regular in shape, showing a rather deep floor and elevated crater walls often surrounded by a small white halo, a few crater diameters in size.

The *Ranger VII* pictures have shown the existence of a fourth class of craters or depressions, without surrounding walls but having a form approximating an inverted Gaussian curve rotated around its vertical axis of symmetry. The majority of these *depressions* are quite shallow, and their bottoms, though roundish, are nearly flat at the center. Examples of such depressions are found on the last A and B frames, particularly A199 (Fig. 31). There appears to be a variant of these depressions shaped somewhat like dimples and aptly called *dimple craters* by H. C. Urey. Figure 31 shows some examples of such formations. These depressions and dimple craters occur in a variety of dimensions and depth-to-diameter ratios. In Fig. 31, the depressions vary from less than 150 to 300 m in diameter, the dimple craters from less than 60 to 150 m. It is probable that at a lower Sun angle than 23 deg, even shallower depressions would be seen and that most of the mare surface would be found covered by them. These shallow depressions show no sign of explosive violence, the slopes being extremely smooth. The deeper depressions have breaks in the walls or even rock ledges, as seen in Fig. 31.

One might at first suppose that these structures could be explained by a surface heavily cratered by post-mare impacts and subsequently buried by dust. But this is most unlikely on several grounds: (1) no single thickness can explain both the large and small dimple craters of similar proportion, and the shallow and deep depressions; (2) fine fractures (scale $\sim$ 1–2 m) are observed that are structurally related to the depressions in a manner suggesting a brittle rock surface; (3) lineaments are observed over the entire mare surface to the smallest resolved dimension, apparently part of a global lineament pattern (see Section H); (4) an observable primary cosmic dust layer and a lunar secondary dust layer of distant origin are essentially absent (see above), while the post-mare impact rate of particles below 10^4 g is only about 1 g/cm^2/4.10^9 years (Ref. 2); and (5) the fractures in the walls of these depressions are unlike those seen in impact craters.

Instead, one appears to observe here collapse formations, which have recently been recognized as a very general property of certain types of basaltic flows on Earth (Ref. 14). A morphological resemblance exists also with the milder forms of karst formation, but the latter are due primarily to surface solutions of limestone and not to collapse over subsurface cavities. The terrestrial collapse depressions are often surprisingly circular in outline (cf. Fig. 32) as are the lunar depressions; their shapes and dimensions are also similar.

There are three causes that could have led to collapse depressions on the lunar maria: (1) the relocation or even local drainage of magmas below the surface rock-froth layer into lower subsurface vesicular lava beds; (2) the volume decreases in the subsurface materials resulting from solidification and cooling; (3) the escape of gases. Cave-ins of the ceilings of cavities will lead to dimple craters. On the basis of the above identification, the sinkholes and dimple craters are early post-mare in age. The absence of an appreciable straight conical section on the slopes of the dimple craters, so typical of Hawaiian drainage craters (Fig. 33), indicates that the profile is not due to drainage but cave-in. The shallow depressions shown on the *Ranger* records are reminiscent of the much larger round and very shallow depressions observed on the floors of Ptolemaeus, Albategnius, and Hipparchus. The score of Ptolemaeus depressions are typically about 10 km in diameter, the others 2–5 km. They are seen only at very low Sun angles. The fact that the Ptolemaeus depressions are so large may be connected with the high elevation of the Ptolemaeus floor, well above Mare Nubium or the floor of Alphonsus. The shallow craters within the Tycho rays shown on A199 (Fig. 31) appear also to be of the collapse type, not due to flying fragments. This conclusion is supported by the orientation of the tree-bark structure reviewed in Section F and the lineaments shown over the entire region, well portrayed on the ACIC maps. The relationship between the crater rays and the collapse features has not been fully elucidated; it may be in part photometric, the ray deposit enhancing the visibility of pre-existing structures; or due to stimulated collapses by ray material.

One of the craters in Fig. 31 is found to have several rock masses on its floor and step-wise rock ledges on one of its inner walls. Because of their dark color and dimensions, the rock masses are assumed to be unrelated to the impacting material and to be extrusive igneous masses instead.

At least half a dozen craters on the B frames have rock-like masses on their floors, sometimes more than one per crater. Presumably, these are either remnants of the impacting masses, such as shown on the Hawaiian craters of Fig. 34, or the result of slumping of the crater walls.

A test of the impact hypothesis is readily made. B200 shows one crater with a central rock mass about 15 × 20 m in size. The crater is 90 m in diameter. According

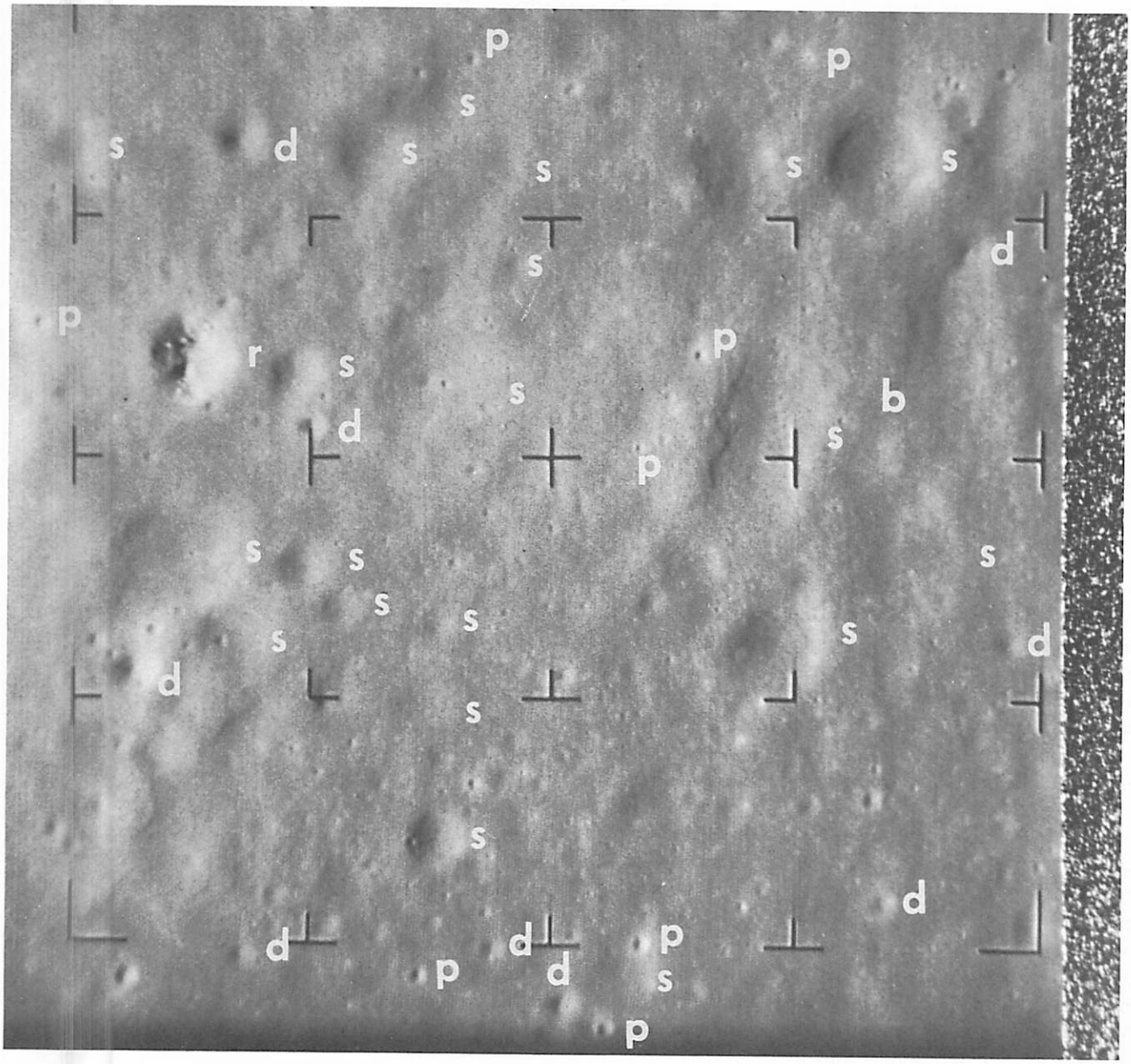

Fig. 31 Reproduction of A199 showing examples of small primary impact craters *(p);* depressions (sink holes) *(s),* dimple craters *(d),* and a crater with internal rock masses *(r).* (*b* designates the location of the "boat" [Figs. 36–38]. The distance between the central reticle and the mark to the left is 0.65 km on the Moon. Smallest craters visible are about 10 m diameter. Approximate scale 1:15,000; 1 mm = 15.5 m.)

Fig. 32 Aerial view of part of basalt flow 40 mi south of Socorro, New Mexico, showing collapse depressions partially filled with desert sand (LPL photograph).

to a table by Baldwin (Ref. 13), the energy required to make the crater was $10^{19.7}$ ergs. If the rock mass struck with $v = 1.0$ km/sec and all the kinetic energy was used in making the crater, the rock mass was $10^{10.0}$ g or 22 m in diameter if spherical and of mean density 1.9. With half the impacting velocity, the mass required would be 4 times, the diameter 34 m. The secondary nature of the crater and the impacting mass are therefore confirmed.

Frame B199 yields additional tests. A crater of 220 m diameter contains a rock about 30 × 50 m in size; a crater 320 m diameter contains three masses, measuring approximately 30 × 40, 15 × 20, and 30 × 30 m. These two craters required approximately $10^{21.0}$ and $10^{21.5}$ ergs to produce, that is, spherical rock masses with $v = 1.0$ km/sec and diameters 58 and 87 m, respectively. Again, these figures are consistent with the hypothesis of secondary origins of the craters and rocks.

It remains to be shown that these rock masses can indeed be propelled to the velocities assumed without break-up. If the velocity of 1.0 km/sec was acquired during a uniform acceleration over an interval equal to the radius of the primary crater ($R = 45$ km for Copernicus), one finds $g = 1100$ cgs. If, for simplicity, the rock mass is now assumed cubical, with one surface normal to the pressure gradient, the pressures required to accelerate a $(30\text{ m})^3$ and $(100\text{ m})^3$ rock mass to $v = 1.0$ km/sec are, respectively, 5.3 and 21 × 10^6 dynes/cm^2 (5 and 21 atm). The peak pressures will be higher than these averages, but the figures suffice to show that rock masses of the sizes considered can indeed be hurled over the lunar surface to several hundred kilometers. They also suggest, however, that this is not true for much larger masses without rupture. In fact, impacts at the largest distances from their primaries appear invariably as complex scars or depressions, indicating that they were formed not by single bodies but clusters of fragments. This correlation of crater shape with distance from the primary was called to my attention by R. Le Poole of this Laboratory.

Many larger craters observed on the B frames have a banded, almost flame-like pattern on their inside walls. The pattern resembles that shown, e.g., on the outer wall of Puu Poliahu (13,630 ft, 4160 m), one of the summit mountains of Mauna Kea, Hawaii (Fig. 35). This pattern is due to a combination of weathering and slumping which has exposed fresh deposits.

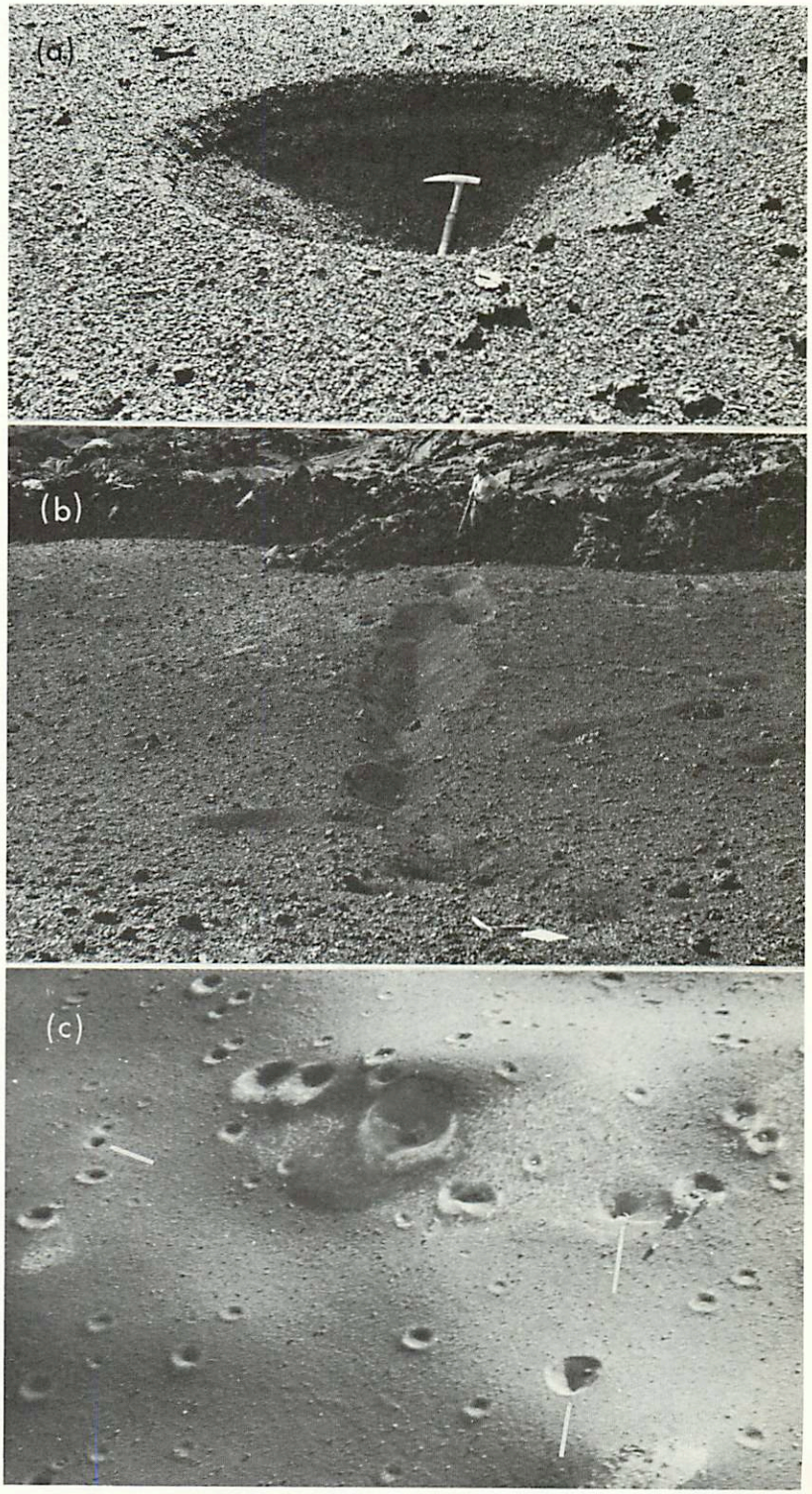

Fig. 33 Examples of craters and a crater chain on a slope of Laimana Crater, Hawaii, due to drainage of surface materials: *(a)* a 6-ft crater, *(b)* a crater "chain" due to drainage into a crack, *(c)* a field on a moderate slope covered with scoria showing conical drainage craters (marked with white lines) and "secondary" impact craters. (Note that impact craters in this material show crater walls accentuated on the down side; LPL photograph.)

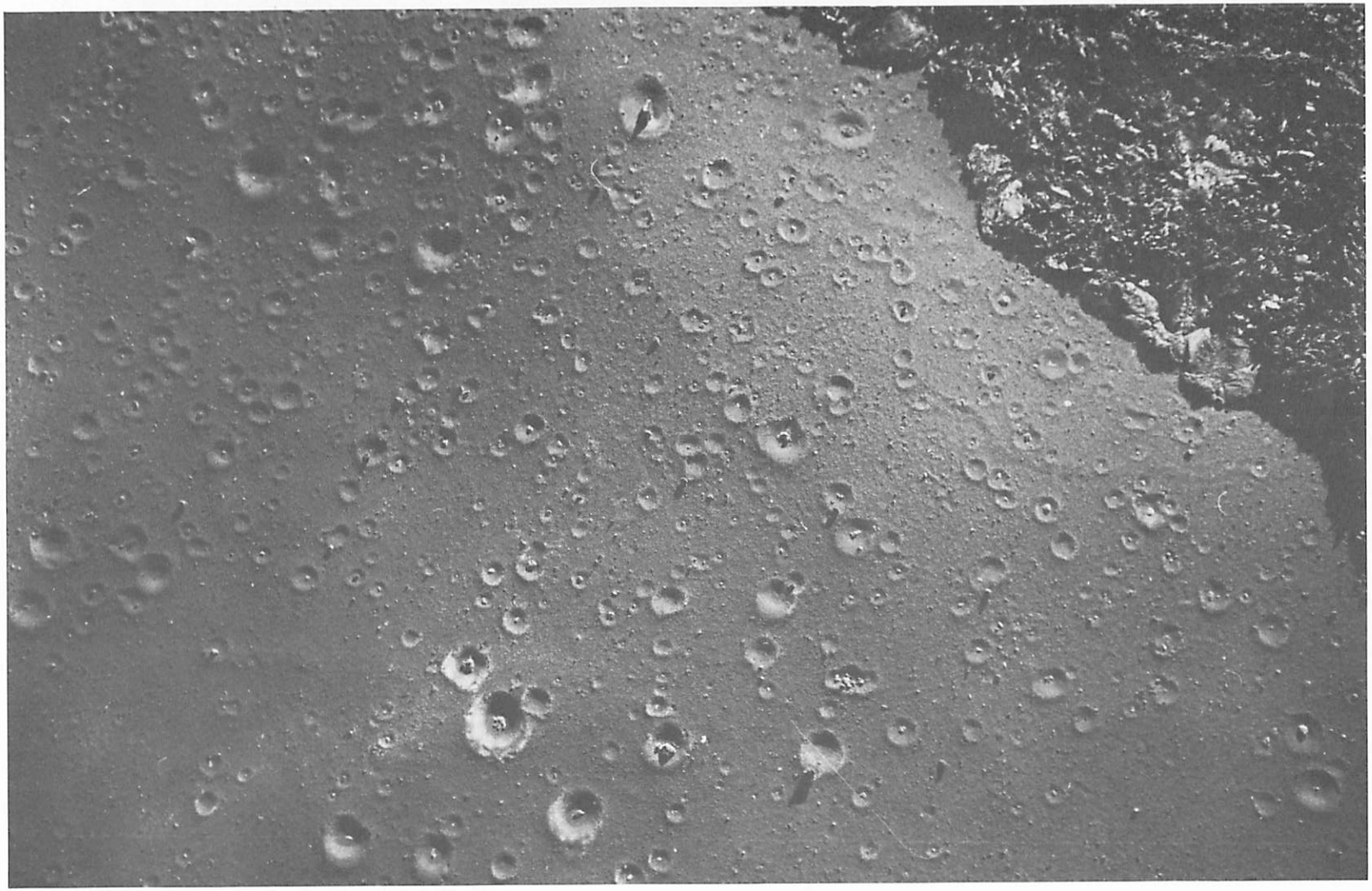

Fig. 34 Aerial photograph of impact craters produced February 1960 on a gentle slope covered with scoria of Laimana Crater, Hawaii. (Lava stream in upper right. Craters up to 3 m diameter formed by solid basalt blocks ejected nearly vertically from volcano. Sun angle corresponds to *Ranger VII* photographs; courtesy L. Nichols.)

Fig. 35 Patterns of slumping on weathered surface of Puu Poliahu, Hawaii, resembling patterns on interior walls of lunar craters.

A fuller discussion of the different types of craters encountered on the *Ranger VII* records will be published elsewhere (Ref. 14).

F. The Structure of the Mare Floor

The mare floor was observed with the highest resolution on the last several P frames. Two photomosaics of these were made by placing appropriately enlarged P frames on enlargements of A199 (no rectification was applied to A199 for the 25-deg deviation from normal viewing). The best one is shown in Fig. 36. It is seen that the darker areas running between the various shallow craters as continuing bands are resolved into much structural detail, similar in appearance to tree bark (e.g., Ponderosa pine) or glacial moraines. The continuing flow pattern on the P frames somewhat resembles patterns observed in terrestrial lava flows, as seen in Figs. 20–22. These are aerial views of recent (uneroded) lava flows on Mauna Loa, Hawaii, at approximately 12,000 ft elevation, near the northeast fissure emanating from the main caldera. Particularly, the pattern shown in the foreground of Fig. 22 is similar to the pattern seen in Fig. 36. The Hawaii pattern is that of a basaltic flow of aa, a clinkery mass pushed in place by an underlying lava flow. Its resemblance to a glacial moraine stems from the similarity of the mechanism of motion and deposition, a two-layered process.

Reference has been made to extensive flows in Mare Imbrium (up to 200 km long) which indicate highly fluid lavas as the carriers. The terminal walls of some of these flows (Figs. 16, 17) are very similar to those shown in Fig. 22 (right edge) and indicate a damming action by the solid crustal cover. Since pumiceous lavas are viscous and do not produce the nearly level flows shown in Figs. 16 and 17, one surmises that only the upper 10 m or so of the mare surface are structured as pumice, reticulite, or rock froth, the deeper layers being much less vesicular.

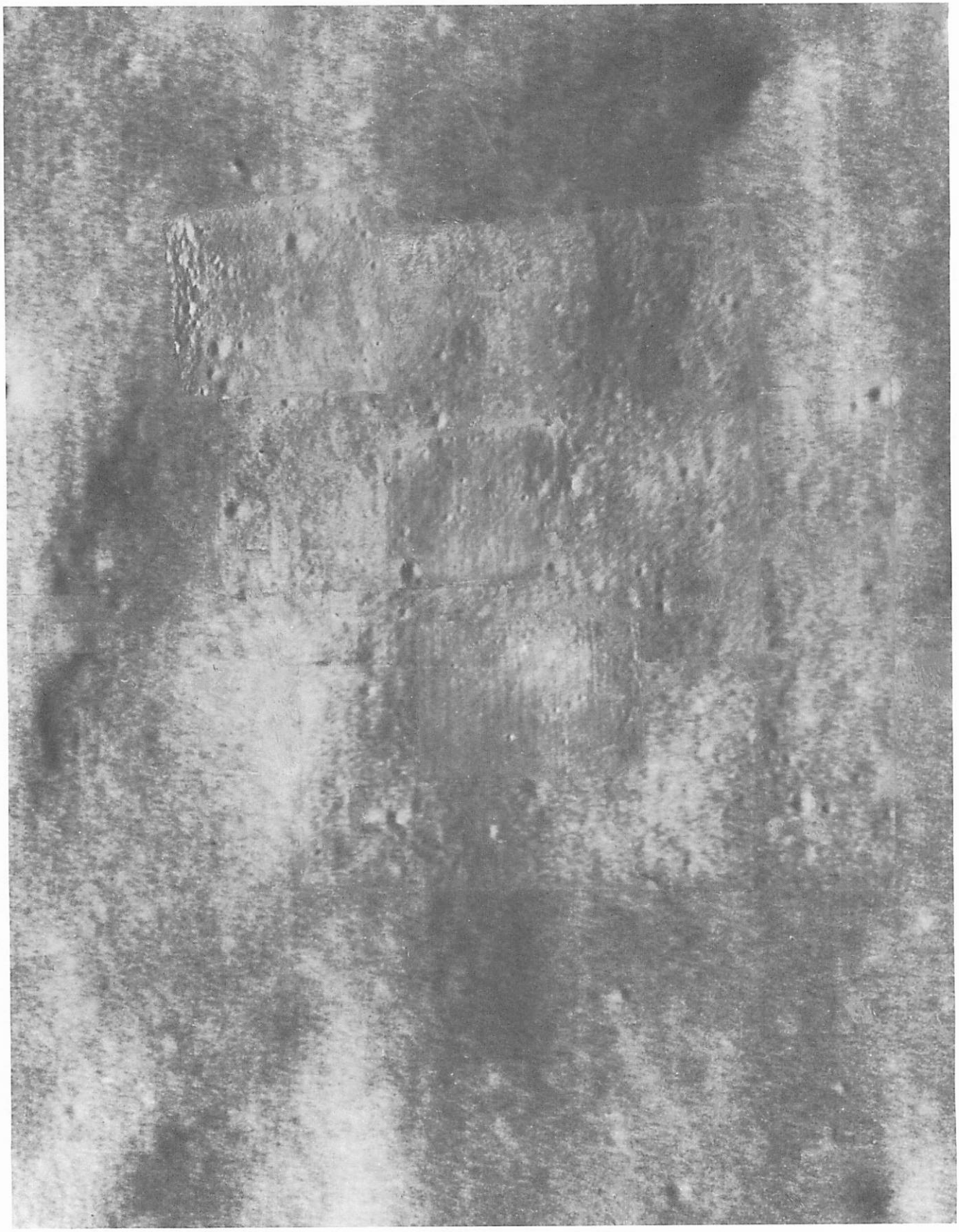

Fig. 36 Photomosaic on A199 with several P frames superposed (E. Whitaker).

The darker areas on Fig. 36, resolved into the tree-bark structure, could, in principle, either be slopes inclined away from the Sun and thus be both darker and show more detail; or they could be nearly level terrain and actually be darker (true mare surface, without the overlay of Tycho ray material), as well as possessing more true relief. The first factor appears to dominate. Some tree-bark-type relief is weakly shown even on frame P189(2), which is in a brighter area. The pattern is seen over a somewhat wider area on the mosaic composed by E. A. Whitaker, presented in *Comm. LPL* No. 59.

One striking impression gained is that the fine ridges and troughs shown on the last P frames have a rounded appearance, with a rounding-off scale of roughly 1 m, as if a buffeting action on the lunar surface had reduced all sharp relief. If further study sustains this conclusion, the effects of micrometeorite bombardment and spray of secondary material may be held responsible.

Essential in further studies will be a maximum effort of picture clean-up and enhancement. Preliminary results by analog methods on the "boat" structure are found in Figs. 37a, b, and c. A scale model at 1:500 of the region best covered has been composed with great care by the sculptor R. Turner at this Laboratory, with the author's collaboration, using A199 and the last P frames. Marginal detail was entered only when confirmed on at least one other frame. The smooth areas in the model are not necessarily devoid of structural detail on the Moon but are areas where the Sun angle was too high to bring out the low relief. A photographic reproduction of this model, exposed to the Sun at 23 deg elevation, is shown in Fig. 38; its scale is about 1:2600.

The gain of about 5 in average resolution over the last A frame (Fig. 31) has clearly been of decisive importance for revealing the mare surface. The field of Fig. 38 partly overlaps with ACIC map, RLC 5 (scale 1:1,000), but our model was constructed directly from the *Ranger* records and somewhat exceeds the ACIC representation in detail extracted. Many of the lineaments shown in Fig. 38 appear to belong to the lineament families reviewed in Section H.

The last eleven B frames, 190–200, show that the shallow dips noted in Fig. 31 are typical of the mare surface, also outside the Tycho ray. They appear to cover an appreciable fraction of the lunar surface and, on the B frames, are mostly between 150–300 m in diameter, in agreement with the prominent dips seen in Fig. 31.

This distribution indicates that the dips antedate the (recent) Tycho event and that instead, as suspected earlier, their visibility on the lower-resolution photographs was enhanced by the ray, much as snow may enhance the aerial visibility of terrestrial topography.

In addition to several extremely shallow dips and a few deeper ones, again mostly in the diameter range of 150–300 m, frame B200 shows a prominent dimple crater near the center of the frame nearly 100 m wide and some 10 m deep. A very similar object is seen in the extreme upper margin. The fields of B197, 198, and 199 are covered by the shallow dips for at least half the surface area. Frames B193–197 indicate that *the dips avoid mare ridges*, not inconsistent with the structure of these ridges as sills, as discussed in Section I, and with the explanation of the dips as due to collapse.

The depressions appear to have some preferential depth, near 10 m, although both much shallower and somewhat deeper dips also occur. This depth may conceivably be related to the depth of the rock-froth layer.

There is some evidence for a second preferred depth, at about 100 m; at least, some craters are found that single out this depth by showing a layer of a different color. Bonpland G has a dark band at about 100 m on B185–186; Bonpland HB shows a light band on B196; Bonpland JJ seems to have a flat layer on A197, and a crater just northwest of Bonpland JF shows a band on A198 at this depth.

Several members of the Experimenter Team have commented on the low frequency of ray craters with diameters less than about 30 m (although exceptions are found; cf. Fig. 31). This also could be attributed to the thickness of the rock-froth layer. A 30-m primary crater will have a depth of 6–8 m. A small crater found in the rock froth would probably not show crater rays; but a larger crater, penetrating into the denser rock below, could have such rays. The thickness of 6–8 m might possibly be a measure of the average depth of the layer of rock froth.

The absence of rocks strewn all over the lunar surface is a striking aspect of the *Ranger* photographs. As reviewed above, this absence is likely to be attributable to the rock-froth structure of the upper layers of the mare.

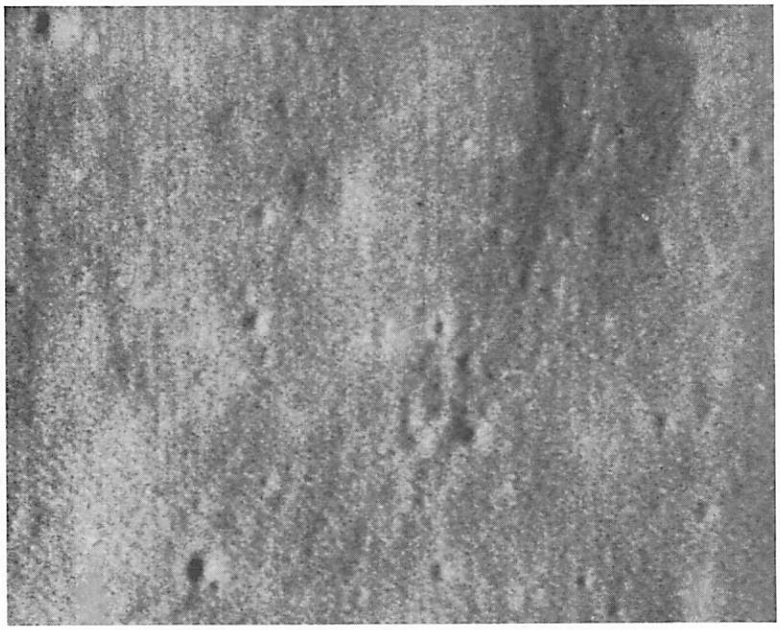

Fig. 37a Reproduction of *Ranger VII* frame 188 P_4; one of several frames used in the construction of the model shown in Fig. 38. Fiducial marks have been removed.

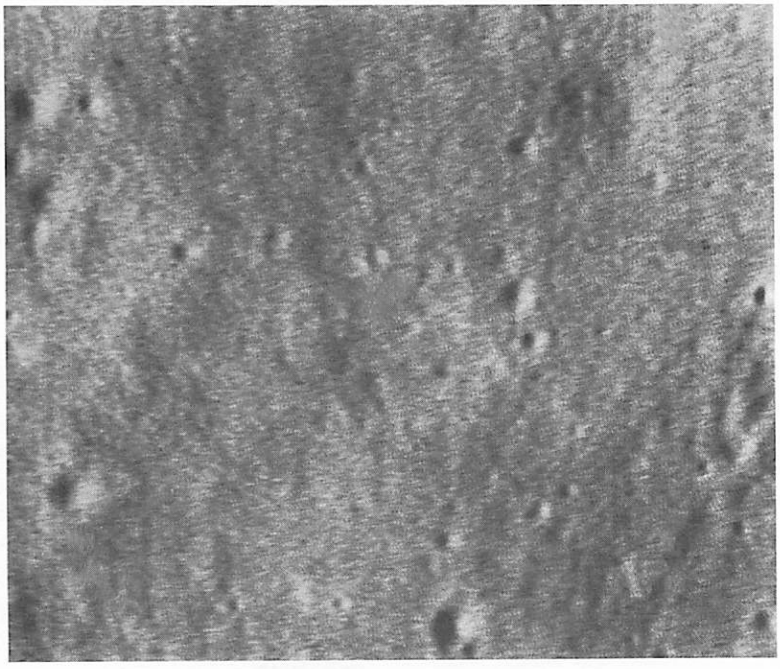

Fig. 37b *Ranger VII* frame 189 P_3. Electronic interference lines have been suppressed by superposition technique. Used in production of the model shown in Fig. 38.

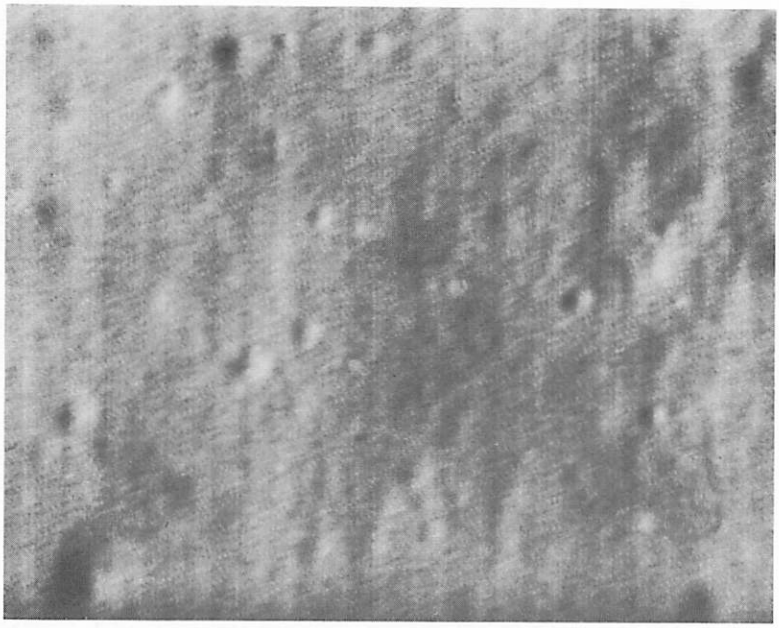

Fig. 37c *Ranger VII* frame 188 P_2. Electronic interference lines have been suppressed by superposition technique. Used in the construction of the model shown in Fig. 38.

G. The Frequency of Lunar Craters

The frequency distribution of crater diameters can be used both to estimate the age of lunar formations and to investigate the nature of the craters themselves. The following account is based on W. K. Hartmann's work.

The age of a lunar province can, in principle, be determined from the number of its craters and a knowledge of the mean rate of crater formation since the formation of the maria. A preliminary estimate of the latter has been made on the basis of studies of the current influx of meteorites and of fossil meteorite craters on the Earth. It is found that the lunar rate for craters of diameters larger than 1 km is approximately $5 \times 10^{-4}/\text{km}^2/10^9$ years.

Earth-based photographs have been used to determine the number of craters per square kilometer in the mare regions of the Moon. Resolution limitations prohibit complete counts below 5 km diameter. The *Ranger VII* photographs have been used to extend the counts to craters much smaller than 1 km. These counts, which apply to Mare Nubium and Mare Cognitum, fall precisely on the curve for all the maria in the northern hemisphere, as determined from the Earth-based photographs. The number of craters larger than 1 km was found to be about $18 \times 10^{-4}/\text{km}^2/10^9$ years and, based on the mean cratering rate given above, implies an age of about 3.6×10^9 years. This agrees well with estimates of the age of the Moon based on isotopic age determinations of meteorites, i.e., 4.5 to 4.7×10^9 years.

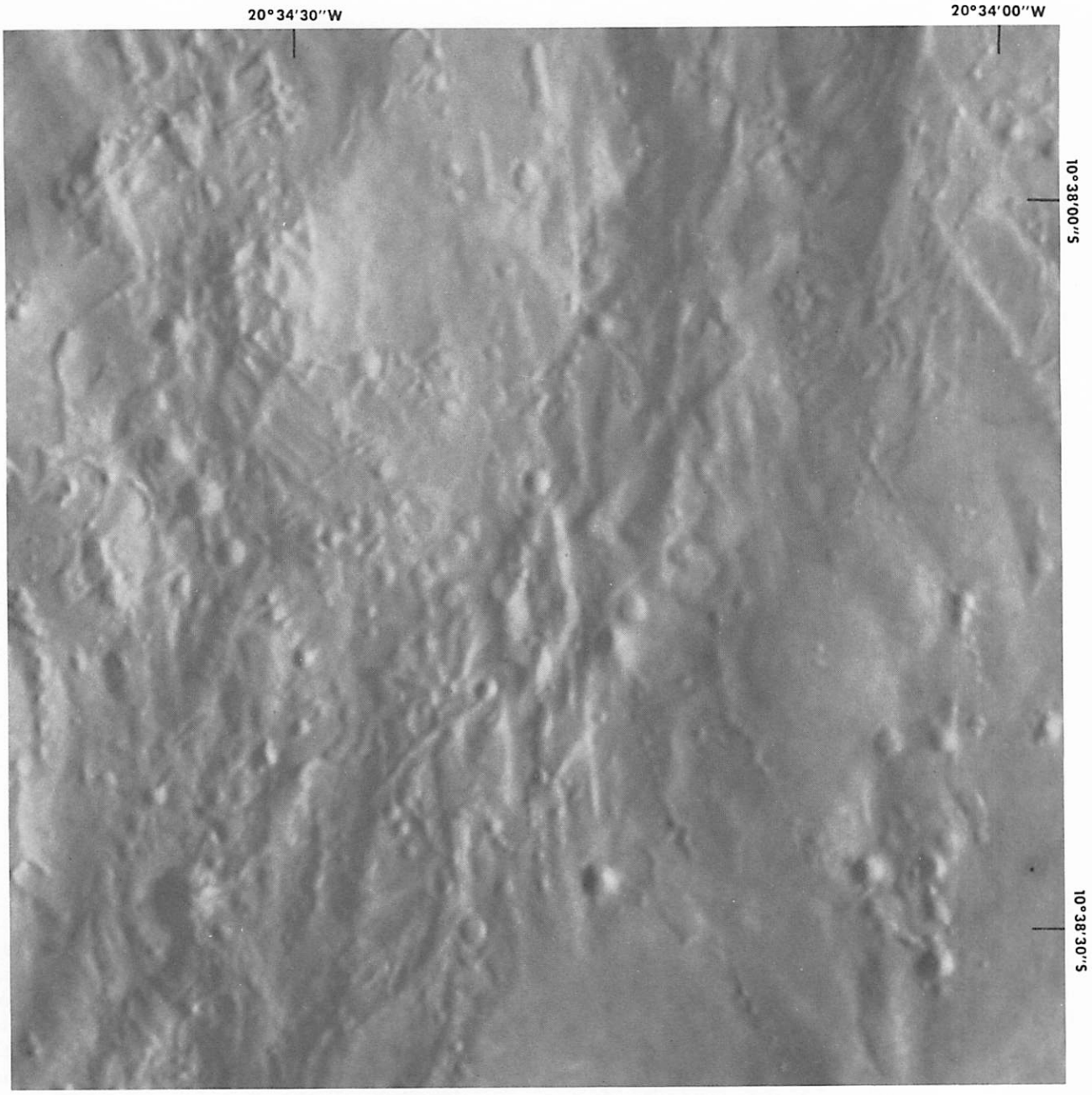

Fig. 38 Photograph of a scale model of the part of the lunar surface covered by high-resolution P frames. (Produced by the sculptor Ralph Turner with the collaboration and supervision of the author, using shadow lengths and stereo viewing to estimate vertical relief. The model is the result of a painstaking intercomparison of all *Ranger* data available. Approximate scale, 1:2600.)

Hartmann's studies are based on the new catalogs of crater diameters published by Arthur, Agnieray, Horvath, Wood, and Chapman (Ref. 15). With the numbers of post-mare craters plotted on a log-log diagram in equal increments of log diameter, Hartmann has found that for them, the relationship is linear over the entire range of 5 to 100 km. Older groups of craters show a linear relationship only at larger diameters, and it appears that among the oldest groups, some erosion or destruction mechanism has erased the smaller craters.

The *Ranger VII* photographs allow these studies to be extended by nearly four orders of magnitude. The areas selected for the crater counts were, for each range of crater diameter (i.e., image resolution), those that were as free as possible of clusters of secondary craters. The last frames were in a region in which crater rays were nearby or partly overlapping, so that secondary craters were not completely absent. Since *Ranger VII* impacted in a mare, we are concerned with the post-mare distribution, which is illustrated in Fig. 39. The linear relationship found from Earth-based photographs extends down to at least 5 km. The fitting of the *Ranger* data to the Earth-based data is very good, which means that the crater density in Mare Nubium and Mare Cognitum is close to that for the maria in the northern hemisphere. At diameters of 32–1000 m, however, there are more craters than expected on the basis of a linear extrapolation from larger diameters. The craters from 250–1000 m give rise to a new slope in the distribution curve, whereas at diameters less than 32 m, the numbers again approach the extrapolation.

The interpretation of this curve is not complete. The excess of craters from 32 to 1000 m probably represents the inclusion of secondary craters in spite of efforts to avoid them and of the depressions and dimple craters noted in Section G. It is possible that the diameter distribution observed of primary craters is linear over the entire diameter interval from 2 m to 1000 km and that the depressions and dimple craters cause the excess from 32 to 1000 m, peaking at 250 m.

Since (1) there is no clear evidence for a shortage of primary craters less than 1 km in diameter, (2) the shapes of the secondary craters and the depressions cannot simply be used as a criterion for age because they are formed in all shapes and depth-to-diameter ratios down to 1/20 or less, and (3) the Tycho impact is probably a comparatively recent event in lunar history in any case, it is concluded that the varied shapes observed are not a reliable basis for an estimate of the rate of lunar erosion.

A direct estimate of the erosion rate may be made from the influx of particles onto the Moon. The term erosion with reference to the Earth includes all processes by which matter or rock is loosened and moved. On the Moon, erosion is caused by incoming particles ranging in mass from asteroidal to atomic.

The influx rates are such that for particles of mass greater than 1 g, impacts are infrequent and widely dispersed; they result in distinct craters, so that we can refer to the effect of large masses as "cratering." Cratering does not erode the surface in-between except insofar as secondary throwout strikes such areas, and this must be estimated for a given spot, such as the *Ranger VII* impact point.

In the mass range from 1 g to atomic masses, a given square centimeter of mare will have been hit repeatedly; this effect is referred to as "sandblasting." Most of the sandblasting mass influx is concentrated in particles of the order of 10^{-4} to 1 g in mass. A total mass of about 1 g/cm^2 has fallen on the maria in the form of sandblasting particles. Secondary particles of lunar material thrown out onto the lunar surface in the sandblasting process form a layer of perhaps 20 g/cm^2. It should be noted that when impacting particles of less than 1-g mass strike an open, porous surface such as hypothesized for the Moon, ejection of secondary particles is severely impeded. Therefore, although the impacting particle may dislodge up to 100 or 1000 times its own mass, the secondary throwout will be much less. Each sandblasting particle may knock nearly its own mass off the Moon, and the net effect of sandblasting erosion may be a slight mass loss by the Moon.

Atomic-sized particles and radiation cause "sputtering" of material. It has been estimated that a layer on the order of 10 cm deep has been lost in this way.

The net effect of sandblasting and sputtering will be a softening of relief on a scale of 10 to 100 cm. The secondary throwout by cratering in the region of the *Ranger VII* impact blankets the surface by a layer probably less than 1 m in depth. This follows from the fact that not even the brightest rays are as much as 10 m deep, as their relief cannot be detected from the Earth, and the *Ranger VII* impact site is only very weakly rayed.

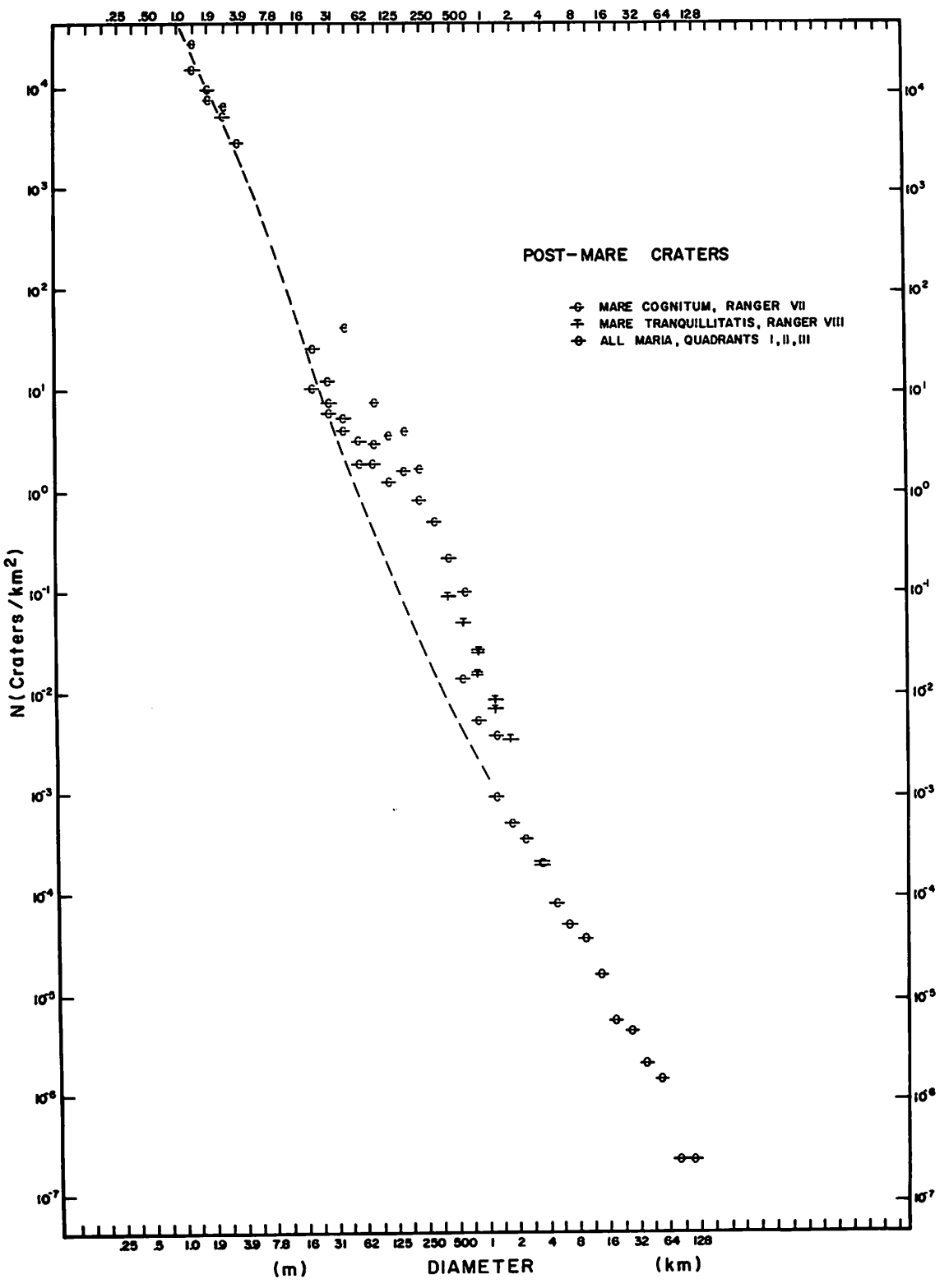

Fig. 39 Incremental diameter distribution of post-mare craters from Earth-based and *Ranger* photographs. All craters were counted by Hartmann. Dashed line indicates the distribution of "sharp" craters alone and is thought representative of the primary impacts.

It is concluded that the total effect of the direct influx of cosmic material and secondary throwout material in the region of the *Ranger VII* impact has been a softening of vertical relief and a mixing of surface layers on the order of 10 to 100 cm in depth.

The impact origin of lunar craters as a class is given strong support by both the frequency distribution and the form of the primary craters as revealed by the *Ranger VII* photographs. Since the frequency distribution of meteoritic and asteroidal masses is known, one may use the theory of cratering to predict the diameter distribution of primary lunar craters. This has been done, and it is found that (1) the straight line in the log-frequency–log-diameter plot in Fig. 39 is predicted, (2) the slope of the predicted line is very close to that observed, and (3) the number of lunar craters is compatible with the observed flux of meteoritic material. If the lunar craters were volcanic, the correctness of these conclusions would be fortuitous, and one would have to explain why no meteoritic craters were present.

In addition, the *Ranger VII* photographs give detailed views of craters of about 1 km diameter, which we may compare with terrestrial examples. The lunar craters are shown to be bowl-shaped, as are the nuclear explosion craters on the Earth. They do not have vertical walls, as do volcanic collapse craters such as Halemaumau in Hawaii. Furthermore, there is no evidence of cinder-cone structures, which are common in regions of collapse craters on the Earth. Yet, in the continental regions, which are not covered by the mare material, one can commonly see small craters (up to a few kilometers in diameter) arranged in chains, graben, and other structures that attest to volcanic activity. In addition, the maria themselves give every evidence of being lava flows, eroded by the same rain of material discussed above. Therefore, the Moon's surface, considered *in toto*, has been shaped both by internal volcanic agencies, responsible for the flooding of maria, small volcanic structures, and probably the collapse craters mentioned; and by external meteoritic and cometary impacts, responsible for primary and secondary craters and the mild surface erosion.

*H. Small-Scale Lineaments on the Ranger VII Photographs**

The *Ranger VII* photographs reveal faint linear structures consisting of crater chains, elongate craters, shallow linear depressions, and several ridges. These features have been mapped on three rectified ACIC photomosaics of the *Ranger VII* photographs and are visible on the last P_1 and P_3 frames. Several of the lineaments are clearly shown in Fig. 40. The three photomosaics cover areas of 2,856, 13.5, and 0.139 km² (R1, R2, and R3 in Fig. 40), while the last P_1 and P_3 photographs encompass areas of approximately 1,200 and 1,600 m², respectively. Azimuth–frequency diagrams of the lineaments have been constructed and compared with similar diagrams of lineaments in the terra regions adjacent to the *Ranger VII* impact site. The latter lineaments were mapped from Earth-based photography in a previous study, and their length and true selenographic azimuths were computed on the IBM 7072 computer of the University of Arizona Numerical Analysis Laboratory. The terra regions consist of two areas (T1 and T2 in Fig. 41) to the south and northeast of the *Ranger VII* impact site. Each area encompasses 64,380 km². Figure 42 shows the area mapped for lineaments from *Ranger VII* photography and several neighboring major lineaments which are intermediate in size between those resolved on Earth-based photographs and those on the *Ranger VII* photographs.

Figures 43 and 44 are lineament azimuth–frequency diagrams of the terra areas adjacent to the *Ranger VII* impact site. They show that the lineaments are oriented in three principal directions (NE–SW, NW–SE, and N–S) and form parts of three global systems of lineaments (Ref. 16). The strong north–south peak in Fig. 44 is part of the Imbrium radial system, while the peak in Fig. 43 may be part of the global north–south system or the Imbrium radial system.

Small-scale lineaments in the *Ranger* photographs were separated into negative features (linear depressions, crater chains, and elongate craters) and positive structures (linear segments of ridges). Azimuth–frequency diagrams of the negative structures are presented in Figs. 45–49. Figure 50 is a similar diagram of linear portions of mare ridges in Mare Cognitum. These features occur within the area encompassed by the ACIC *Ranger VII* chart RLC 2, and were mapped from low-phase-angle Earth-based photography and the *Ranger* photographs. Figure 51 is an azimuth–frequency diagram of the small-scale segmented ridge structure in area R1. The directions of Tycho, Copernicus, and Bullialdus are shown on the diagrams of the negative structures in the *Ranger* areas. In addition, the azimuths of four major linear features, shown in Fig. 42, are illustrated in Figs. 43–47. These features are in the immediate vicinity of the mapped *Ranger* areas and consist of (1) a 10-km linear mountain

*This Section was prepared by R. G. Strom.

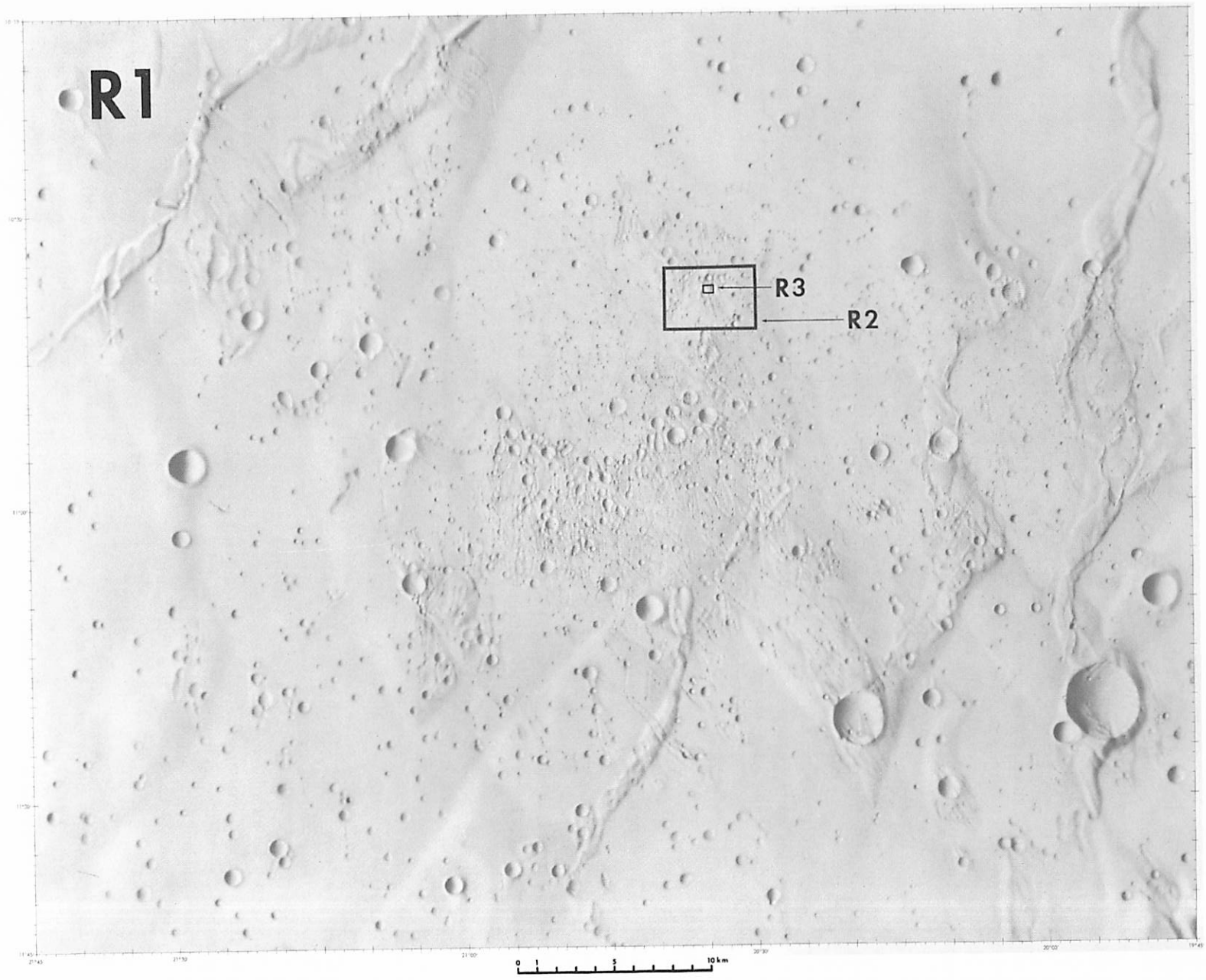

Fig. 40 ACIC *Ranger VII* Lunar Chart 3 showing location and relative size of mapped areas. Note distinct linear structures.

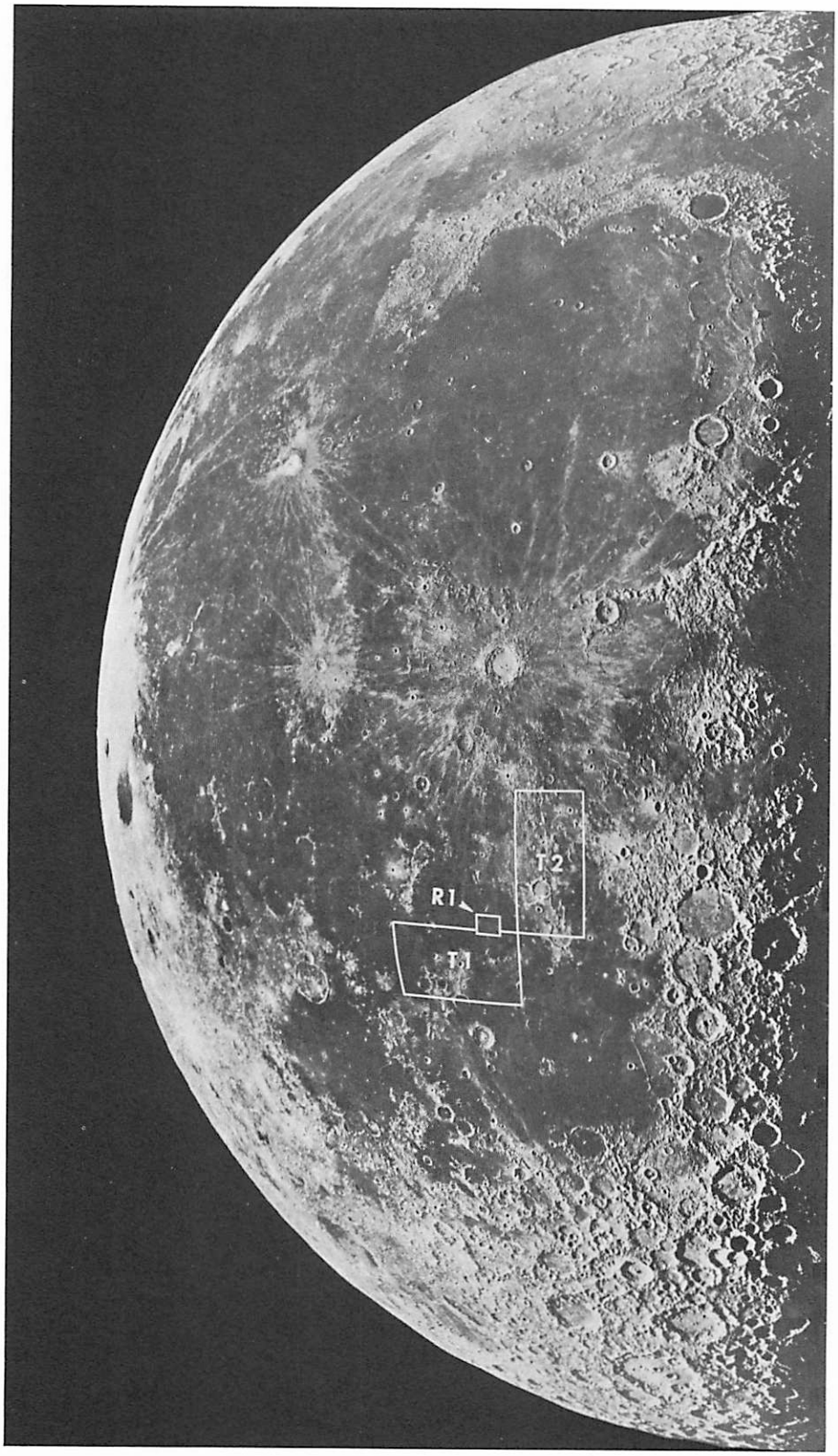

Fig. 41 Location of areas mapped for lineaments from Earth-based (T1 and T2) and *Ranger VII* (R1) photographs.

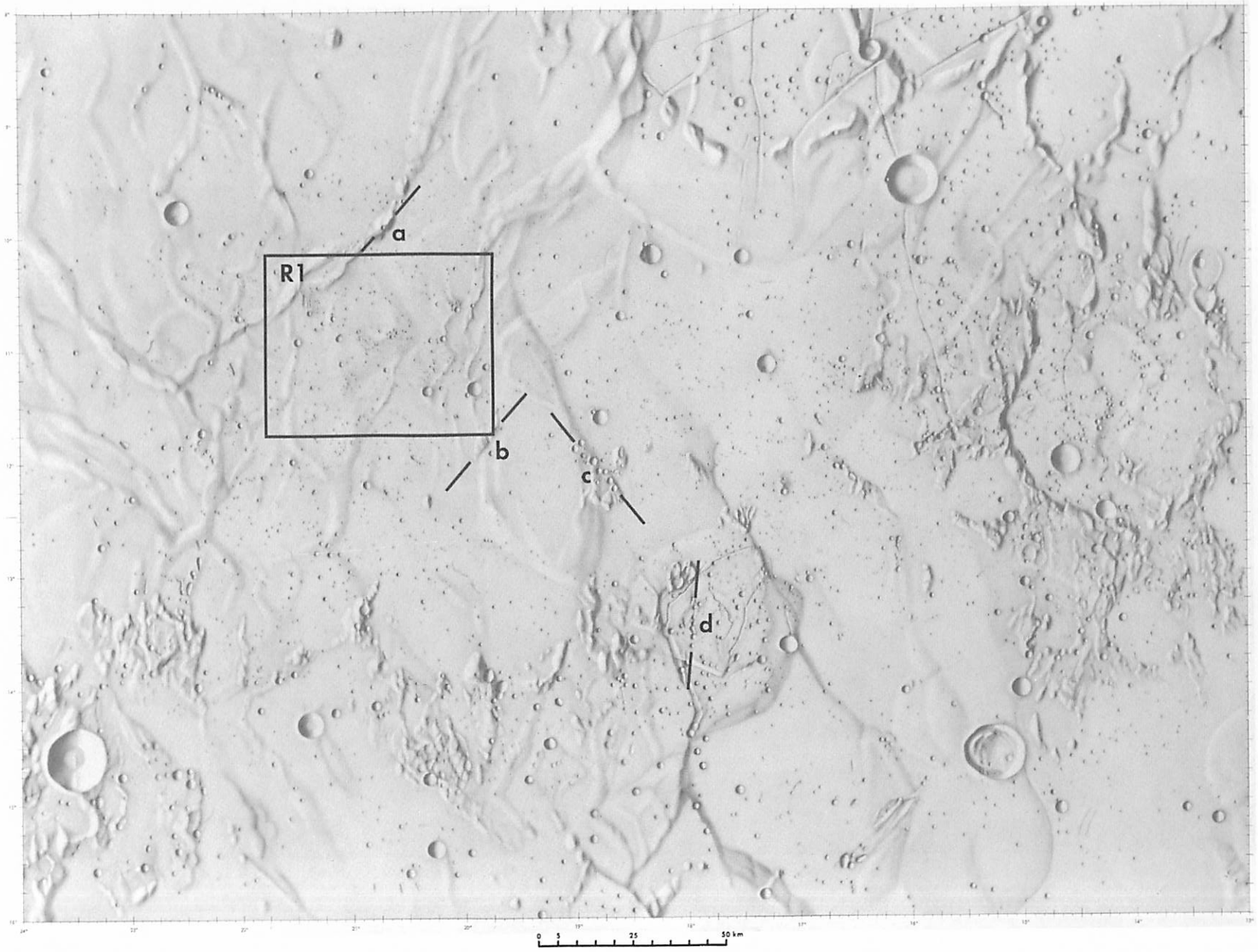

Fig. 42 ACIC *Ranger VII* Lunar Chart 2 showing major linear structures which coincide with directions of lineaments in areas R1, R2, R3, T1, and T2. (Linear structures are between black lines at *a*, *b*, *c*, and *d*.)

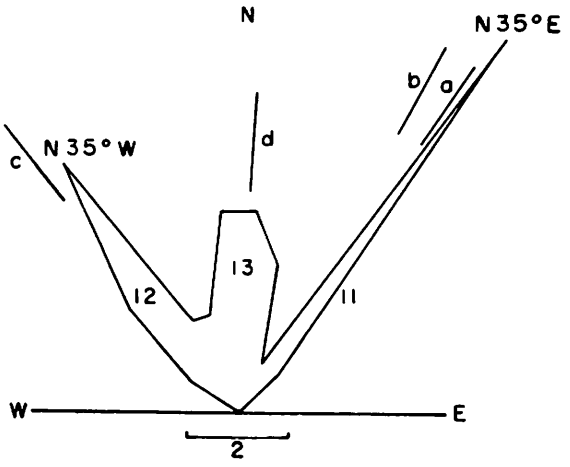

Fig. 43 Azimuth-frequency diagram of lineaments in area T1. (Number of lineaments represented by each peak and directions of lineaments *a*, *b*, *c*, and *d*, shown in Fig. 42, are indicated. Lineament length = 8–39 km; average length = 18.7 km.)

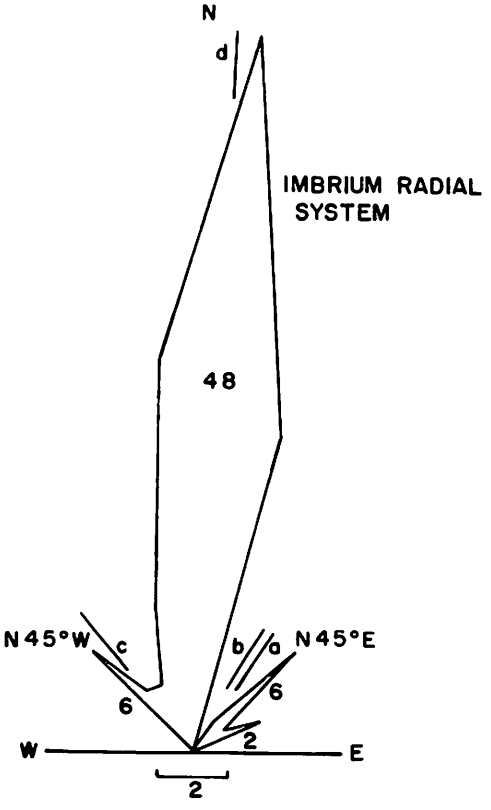

Fig. 44 Azimuth-frequency diagram of lineaments in area T2. (Indications are the same as in Fig. 43. Lineament length = 5–63 km; average length = 19.8 km.)

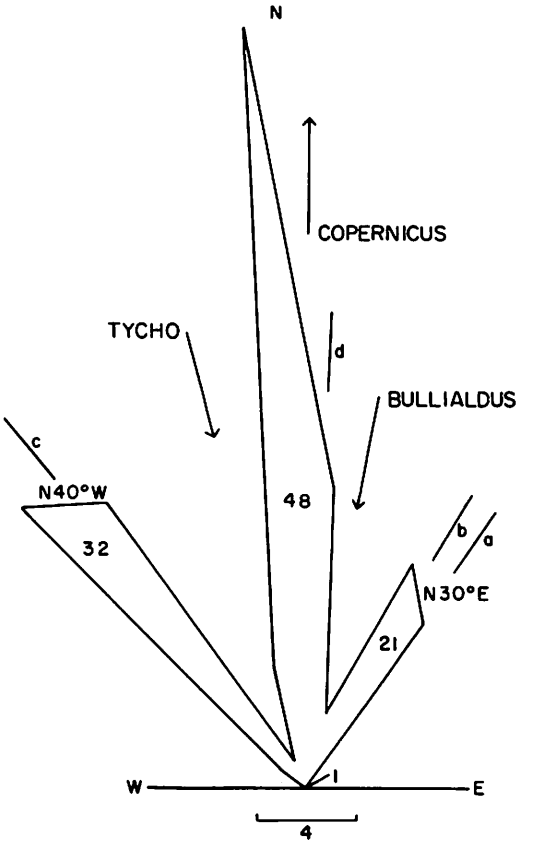

Fig. 45 Azimuth-frequency diagram of lineaments in area R1. (Number of lineaments represented by each peak, directions to Tycho, Copernicus, and Bullialdus and azimuths of lineaments *a*, *b*, *c*, and *d*, shown in Fig. 43, are indicated. Lineament length = 0.4–6 km; average length = 1.1 km; lineament density = 0.04 lineament/km^2.)

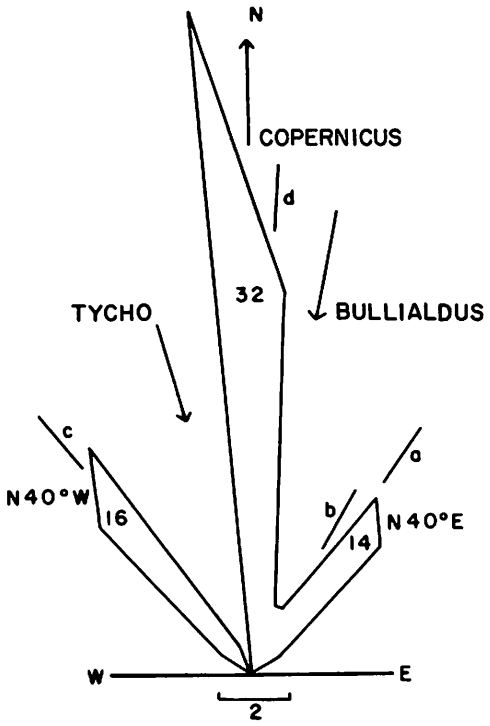

Fig. 46 Azimuth-frequency diagram of lineaments in area R2. (Indications are the same as in Fig. 45. Lineament length = 50–380 m; average length = 114 m; lineament density = 4.7 lineaments/km^2.)

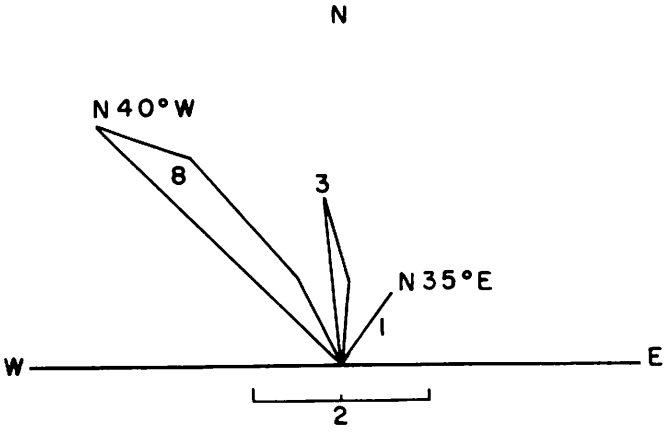

Fig. 48 Azimuth-frequency diagram of lineaments on last P_3 photograph. (Number of lineaments represented by each peak is indicated. Lineament length = 2.8–9.3 m; average length = 5.4 m; lineament density = 7094 lineaments/km^2.)

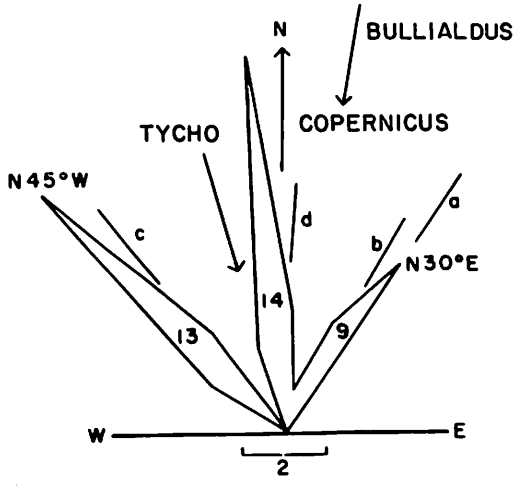

Fig. 47 Azimuth-frequency diagram of lineaments in area R3. (Indications are same as in Fig. 45. Lineament length = 12–53 m; average length = 21.4 m; lineament density = 252 lineaments/km^2.)

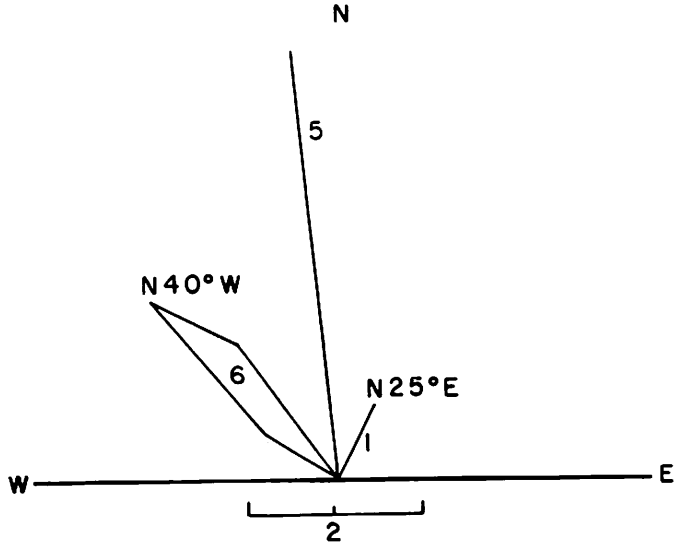

Fig. 49 Azimuth-frequency diagram of lineaments on last P_1 photograph. (Number of lineaments represented by each peak is indicated. Lineament length = 3–17.5 m; average length = 4.5 m; lineament density = 9876 lineaments/km^2.)

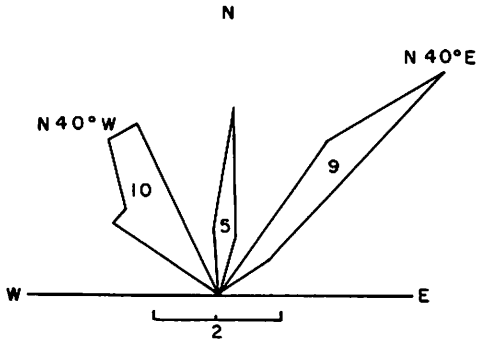

Fig. 50 Azimuth-frequency diagram of linear mare ridges occurring in western Mare Cognitum.

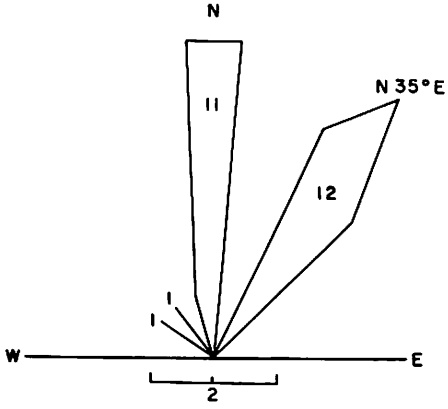

Fig. 51 Azimuth-frequency diagram of fine segmented ridge structure in *Ranger* area R1.

with a crater on its crest, (2) a 15-km dark ridge which is probably a lava extrusion along a fracture, (3) a 17-km linear cluster of craters, and (4) a 10-km-long crater chain.

A comparison of the azimuth–frequency diagrams demonstrates that the directions of small-scale negative and positive lineaments on the *Ranger VII* photographs coincide with the azimuths of large-scale lineaments in the adjacent terra areas (T1 and T2). The four linear structures shown in Fig. 42 also coincide with these azimuths. It has been suggested that the small-scale negative structures are secondary features which have resulted from clots of ejecta from Copernicus, Tycho, or Bullialdus. These ejecta could have rotated in flight and landed in three preferred orientations. To test this hypothesis, the azimuths of linear Copernican secondaries were measured in four areas radial to Copernicus. These areas are located in Mare Imbrium at distances of 6–16 deg north of the center of Copernicus. The *Ranger VII* impact site is 21 deg south of the center of Copernicus. Azimuth–frequency diagrams of the secondary features are illustrated in Fig. 52. The two lines near the top of each diagram are the radial boundaries of the areas. The diagrams show that the linear secondaries form fan-shaped patterns which coincide closely with the directions radial to Copernicus. There has apparently been some rotation of ejecta because not all lineations are exactly radial to Copernicus. Two notable exceptions occur in Fig. 52 (b) and (d). However, both these linear features coincide with the directions of lineament systems in the adjacent terrae and neither lies on ray material. Therefore, they may be structurally controlled and related to the major lineament systems. In any case, the Copernican diagrams do not resemble the typical three-peaked diagrams of the *Ranger* areas.

The fact that the directions of lineaments on the *Ranger VII* photographs coincide with the directions of the global fracture systems in the adjacent terrae indicates that at least the *Ranger* lineaments which trend in a NE–SW and NW–SE direction are structurally controlled and form part of the global lineament systems. Also, the similarity in direction of the linear segments of mare ridges—which are definitely tectonic in origin (see Section I)—and the small-scale negative lineaments supports the above contention. The north–south *Ranger* lineaments may be (1) fractures associated with the global north–south lineament system, (2) fractures related to the Imbrium radial system, or (3) secondary ejecta from Copernicus, Tycho, and Bullialdus. However, it is probable that some of the north–south lineaments are structurally controlled, because many of the segmented mare ridges and large-scale terra lineaments follow this direction.

The size of the small-scale lineaments has a bearing on the nature of the lunar surface. On the last P_1 and P_3 photographs, they average about 5 m in length and are as narrow as 1 m. The delicate nature of these lineaments —particularly those trending in a northeast direction— suggests that if a layer of fine debris is present, it is probably relatively thin (≤ 2 m); otherwise, these delicate features would be completely buried. If a debris layer were deposited prior to the formation of the fractures, then the layer would have to be relatively cohesive and strong in order to fracture.

I. The Mare Ridges

The *Ranger VII* photographs include many excellent records of ridges on Mare Cognitum. These ridges have been well portrayed in the ACIC *Ranger* series. Special

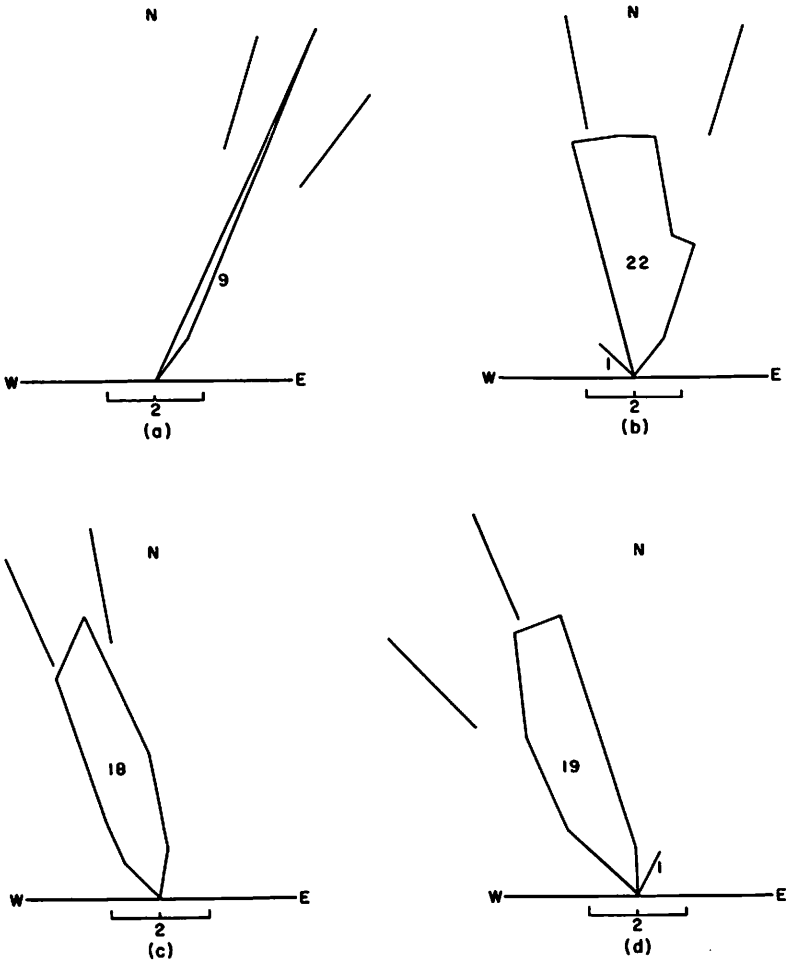

Fig. 52 Azimuth-frequency diagrams of linear features formed by Copernicus secondary ejecta.

reference is made to RLC 3 for the three ridges shown there, their structure and width, and the directions of the *en échelon* elements. It is noted that the ridges have these directions in common; they belong to the grid system discussed in Section H.

The narrowest dike-like ridge element shown on the *Ranger* photographs is found on B197. The element is about 50 m wide, 500 m long, and reaches about 10 m above the lunar surface. Except for the narrow dikes (and not in all of these), the ridges show no break through the lunar surface but are merely uplifted. The width of a ridge may be 250–500 m or exceed 1 km. That a dike has formed at depth, and that the general explanation developed in Section B applies, is seen from the test case on Bonpland HB, where a ridge crosses a crater. This crossing may be observed on B196 and on several P frames which were combined stereoscopically with B196. The dike crosses the crater floor centrally from southwest to northeast, casting a minor shadow below the northeastern half of the crossing. A bright band extends horizontally at a higher level (about 0.9 km down to the floor) along the west and north walls. This band appears to represent the cross section of the laccolithic intrusion by the dike responsible for the uplift of the western branch of the ridge, which continues narrow southwest of the crater. The broader branch of the ridge located just south of the center appears uplifted by a laccolith fed by three dikes that stem from a single main dike at depth and branch upward and outward along three planes. Together with the branch noted above, these would, in vertical cross section, resemble four branches in a river delta, spreading upward. This observation also explains how a ridge develops satellite branches roughly parallel with the main branch. Thus, the pattern of the dikes determines the number of branches; the width of each branch, if appreciable, may be due to a laccolith or sill. The concept of laccoliths is consistent with the result of the mare having bedding planes from successive lava flows, causing an alternation of weak and stronger

layers. If the structure planes possess *en échelon* fine structure, the ridges will likewise show this structure. This explains the "braided" appearance on lower-resolution telescopic photographs. A crossing of structure planes may lead to crossing ridges such as the remarkable system located northwest of Plinius (Fig. 9), the system in Mare Tranquillitatis near Lamont (Figs. 6, 7), and that shown in Oceanus Procellarum (Fig. 11).

It is also apparent from the *Ranger* photographs that some of the higher mountain ridges shown in Mare Cognitum are volcanic extrusions. The double-peaked mountain range Bonpland γ, shown central on Fig. 24, is located on the crest of a ridge and is seen on A180–186 to have several craters on its crest and two remarkably symmetrical low volcanoes on its southern toe. A number of similar mountains on the south shore also appear to be formed on structural lines and crowned with volcanoes on their crests. By implication, the many linear mountains of the Carpathians, oriented in the Imbrium direction, may similarly be regarded as being of extrusive origin.

It is very remarkable that these extrusives, be they segments of ridges broken out to the surface, linear mountain ranges such as Bonpland γ, or volcanoes such as occur near the toe of the Bonpland γ complex, are all *whitish*, much brighter than the mare floor. There seems to be again a parallel with Hawaii: the Mauna Loa lavas, which have been compared with the lunar maria (Sections B and F), do not show whitish coloration; but cinder cones, such as Laimana Crater, were initially covered with brilliant white material that was dissolved by rain. On the Moon, such deposits would remain, within the bounds of surface erosion and evaporation to the vacuum.

J. The Scientific Significance of the Ranger VII Mission

The comments in this Section are restricted to the impact of *Ranger VII* on lunar science. The tremendous technological achievements of the mission need no emphasis.

The scientific impact has several aspects:

1. *Gain in resolution.* The best resolution achieved in ground-based lunar photography is about 0".15 or 270 m in records together covering a small part of the Moon, obtained at the Mt. Wilson, Lick, and Catalina Observatories. Most high quality lunar photography has resolutions of 500–1000 m. Frame P190 has two records, one having a resolution of 25, the other of 40 cm. The gain in resolution achieved by *Ranger VII* is therefore 1000–2000 ×. This achievement may be compared with the invention of a powerful microscope in medical science.

2. *Quality of the records.* The quality of the records is uniformly good to excellent. This is attested by the photographic reproductions of the A, B, and P frames, now available. The B records in particular cannot fail to elicit the admiration of anyone familiar with astronomical photography. Steps are being taken to reduce the minor electronic interference that affects some of the P frames. Some additional information may be extracted from all records, particularly on small and shallow craters, by machine reduction methods.

3. *Ranger VII target selection.* In retrospect, no serious criticism can be made of the target selection. The mare region showed a variety of terrain, from the coastal area of Mare Nubium to a nearly bare mare floor to patches veiled by crater-ray material. Although nearly any site selected for a first *Ranger* mission would have yielded a wealth of new data, the choice of a mare has made it possible to solve, to a first order, several key problems and leads to a logical sequence of further steps in lunar exploration.

4. *Chief scientific results of the mission.* Outstanding among the results obtained are, first, the resolution of crater rays into clusters of secondary craters and their associated ray elements; the discovery that these ray secondaries are invariably bright at full Moon, contrary to the well known swarms of secondaries surrounding all post-mare impact craters, which are invisible at full Moon; the explanation, justified quantitatively, of ray craters as being due to impacts by comets. Next is the discovery of shallow depressions and dimple craters, covering much of the mare floor, and their interpretation as due to collapse. Third, the interpretation of the ridges as due to dikes extruded into fissures caused by both global and mare-wide tensional forces; with these dikes branching and also spreading locally as sills or laccoliths, thus causing *en échelon* or braided ridge structures and also giving the ridges locally considerable width. These broad expanses do not appear to contain depressions or dimple craters, consistent with the explanation of these features as due to collapse. Fourth, the discovery of the "fine structure" of the mare floor where it is exposed. This structure somewhat resembles lava flows, but there appears to be a "rounding off" effect on the surface blocks, presumably caused by

particle impact and solar wind; and after-effects due to subsidence of the depressions and dimple craters are evident. The numbers of primary craters appear to continue on a -2.5 power law in a log-frequency–log-diameter plot, with these craters covering around 10% of the mare surface down to the meter range. Non-ray secondary craters are observed, some with central rock masses still visible. It is shown that for these, the crater and rock sizes are compatible with being caused by ejecta from primary impacts less than 1000 km away, and that there will be a progression of secondary crater shapes with distance from the primary, with the most distant secondaries likely to be complex grooves caused by a cluster of fragments. Another important observation concerns the presence and the azimuthal distribution of lineaments. These findings lead to the conclusion that the structural pattern found on Earth-based photography in the lunar crust in regions adjacent to the mare persists in the mare itself, down to scales in the meter range. This shows that the fracture pattern in the lunar crust is very basic in nature and omnipresent, extending right up to the lunar surface. The diagonal patterns are not due to Tycho or Copernicus or even Mare Imbrium. They resemble the pattern to be expected from a general north–south compression, as first pointed out by R. Strom, who studied some 10,000 lineaments within 60 deg from the center of the face of the Moon (Ref. 16).

Important conclusions can be derived on the nature of mountain chains, both within Mare Cognitum and on the shore lines. These mountains show small craters on their crests, clearly by their distribution not of meteoritic origin, indicating the plutonic nature of these ranges. By implication, such mountain ranges as the Carpathians are not ejecta from Mare Imbrium either, but similarly due to magmatic upwellings along structural planes radiating from the Imbrium impact region. Fig. 28 shows a dark post-mare structure (m – m), noted by J. O'Keefe (Ref. 17), composed of some 20 nearly parallel blocks, steeply inclined to the main direction of the mountain, and exemplifying a composite pattern of the two diagonal lineament directions in Mare Cognitum. Its dark color is probably due to differential solar-wind denudation of crater ray material on a very rough, dark surface (Ref. 14, p. 243).

5. *The ACIC maps.* It is fortunate that the Aeronautical Chart and Information Center, with its experienced staff and excellent production facilities, has undertaken to construct a series of maps on the basis of the *Ranger VII* records. These maps are made in the best tradition of lunar mapping and are a most convenient summary of the new surface data obtained. They are especially useful for nomenclature, coordinates, dimensions, orientations, and the location of lineaments which are so important in the interpretation of the lunar surface.
6. *Required further research.* One of the principal questions left open is the detailed explanation of the variety of crater forms and depressions recorded on the *Ranger* photographs. This problem will require laboratory and field research (cf. Ref. 14).

   Another problem is the determination of contours by stereoscopy of the portions of the lunar disk suitably covered. A determined effort must be made to obtain improved Earth-based photography matching the *Ranger VII* records in solar phase angle. The construction of lunar section models would be incidental to this program.
7. *Economy of Ranger vs. Earth-based lunar photography.* In principle, very high image resolution can be obtained either by telescopes on the Earth with very large optics or by spacecraft near the Moon provided with modest equipment. As may be seen from the graphs included in the *Whitford Report on Astronomy* recently issued by the National Academy of Sciences, the cost of a 300–400-in. telescope would be in the vicinity of $100 million. Assuming that a site can be found for this supertelescope having sufficient atmospheric stability for its occasional use to the full limit of its potential, the resolving power obtainable would be 20–25 m. *Ranger VII* achieved a maximum resolving power 100 times larger. It is therefore obvious that detailed exploration of the lunar surface must be made by the general methods employed on *Ranger VII*. It is also apparent that the economy of the *Ranger* operation compares favorably with a maximum ground-based effort.
8. *Name of the mare.* It was fortunate that the impact area of *Ranger VII* was an unnamed small mare, situated between Mare Nubium and Oceanus Procellarum. With the mission successful and a wealth of entirely novel information on the mare obtained, it appeared appropriate to take advantage of this combination of circumstances in proposing a name for the mare that would henceforth commemorate and symbolize this scientific achievement. The name Mare Cognitum was proposed to and adopted by the International Astronomical Union on August 31, 1964, during its Twelfth General Assembly at Hamburg, Germany.

Acknowledgments. This paper was written with the collaboration of Messrs. R. G. Strom, E. A. Whitaker, and W. K. Hartmann of the Lunar and Planetary Laboratory, as indicated in the text.

REFERENCES

1. Dobar, W. L., Tiffany, O. L., Gnaedinger, J. P. 1964, "Simulated Extrusive Magma Solidification in Vacuum," *Icarus,* 3, 323.
2. McCracken, C. W., and Dubin, M. 1963, *Dust Bombardment on the Lunar Surface,* NASA TN D-2100; also in Salisbury, J. W., and Glaser, P. E., eds. 1964, *Lunar Surface Layer, Materials and Characteristics* (New York: Academic Press), pp. 179–214; Dubin, M. Personal communication on recent data evaluation.
3. van Diggelen, J. 1958, *Rech. Astr. Obs. Utrecht,* Vol. XIV, No. 2, reprinted as NASA TT F-188, 1965; Hapke, B. 1963, *J. Geophys. Res.,* 68, 4571.
4. Shorthill, R. W. 1962, *Measurements of Lunar Temperature Variations during an Eclipse and throughout a Lunation,* Report Dl. 82-0196, Boeing Scientific Research Laboratories.
5. Evans, J. V., and Hagfors, T. 1964, "On the Interpretation of Radar Reflections from the Moon," *Icarus,* 3, 151.
6. Hartmann, W. K., and Kuiper, G. P. 1962, "Concentric Structures Surrounding Lunar Basins," *Comm. LPL,* University of Arizona, 1, 51.
7. Hartmann, W. K. 1963, "Radial Structures Surrounding Lunar Basins, I: The Imbrium System," *ibid.,* 2, 1; 1964, "II: Orientale and Other Systems; Conclusions," *ibid.,* 2, 174.
8. O'Keefe, J. A., and Cameron, W. S. 1962, "Evidence from the Moon's Surface Features for the Production of Lunar Granites," *Icarus,* 1, 271.
9. Kuiper, G. P. 1958, *Vistas in Astronautics,* eds. M. Alperin and H. F. Gregory (New York: Pergamon Press), Vol. 2, pp. 299–302.
10. Kuiper, G. P., *et al.* 1960, *Photographic Lunar Atlas,* Sheet D5 (Chicago: University of Chicago Press).
11. Wright, F. E., Wright, F. H., and Wright, H. 1963, "The Lunar Surface: Introduction," *The Solar System,* eds. B. M. Middlehurst and G. P. Kuiper (Chicago: University of Chicago Press), Vol. 4, pp. 37ff.
12. Whipple, F. L. 1963, "Structure of the Cometary Nucleus," *ibid.,* Vol. 4, pp. 644–646.
13. Baldwin, R. B. 1963, *The Measure of the Moon* (Chicago: University of Chicago Press), Table 13, p. 157, and Table 18, p. 177.
14. *Ranger VIII and IX, Part II: Experimenters' Analyses and Interpretations,* Jet Propulsion Laboratory Technical Report No. 32-800, March 15, 1966, pp. 51–86; also, Kuiper, G. P. 1966, "The Moon and the Planet Mars," *Advances in Earth Science,* ed. P. M. Hurley (Cambridge, Mass.: M.I.T. Press), Chap. 2, pp. 49–57.
15. Arthur, D. W. G., *et al.* 1963, "The System of Lunar Craters, [redacted]," *Comm. LPL,* University of Arizona, 3,61.+Refs.
16. Strom, R. G. 1964, "Analysis of Lunar Lineaments I: Tectonic Maps of the Moon," *ibid.,* 2, 205.
17. O'Keefe, J. A. 1964, "Interpretation of Ranger Photographs," *Science,* 146, 514–515.

APPENDIX A*

Model of Area near Ranger VII Impact Site: Additional Views

Figure 38 in the text reproduces a photograph of the model under lighting conditions resembling those existing during the *Ranger VII* impact (Sun angle 23°). It was printed slightly out of focus to match the resolution on the best *Ranger VII* records. Supplementary views of the model are presented here with different lighting conditions and have been kept in sharp focus.

Figures A-1a and A-1b are a stereo pair of the impact region. Figure A-2 shows the area under eastern illumination, opposite that used in Figure 38. Figure A-3 illustrates the region viewed with a northern illumination. Comparison of these figures serves to warn us how surface detail changes its aspects under different lighting conditions and points to the difficulties of constructing a three-dimensional model based on a single lighting direction.

Approximate slope angles of the terrain can be deduced from the model. Measurements indicate that the lowest point is 38 m below the highest, over a distance of 445 m. This gives an average slope of less than 5°. The steepest general land rise is 21 m over a distance of 125 m — an average of nearly 10°. Some craters contain

*Prepared by the sculptor of the model, Mr. Ralph Turner.

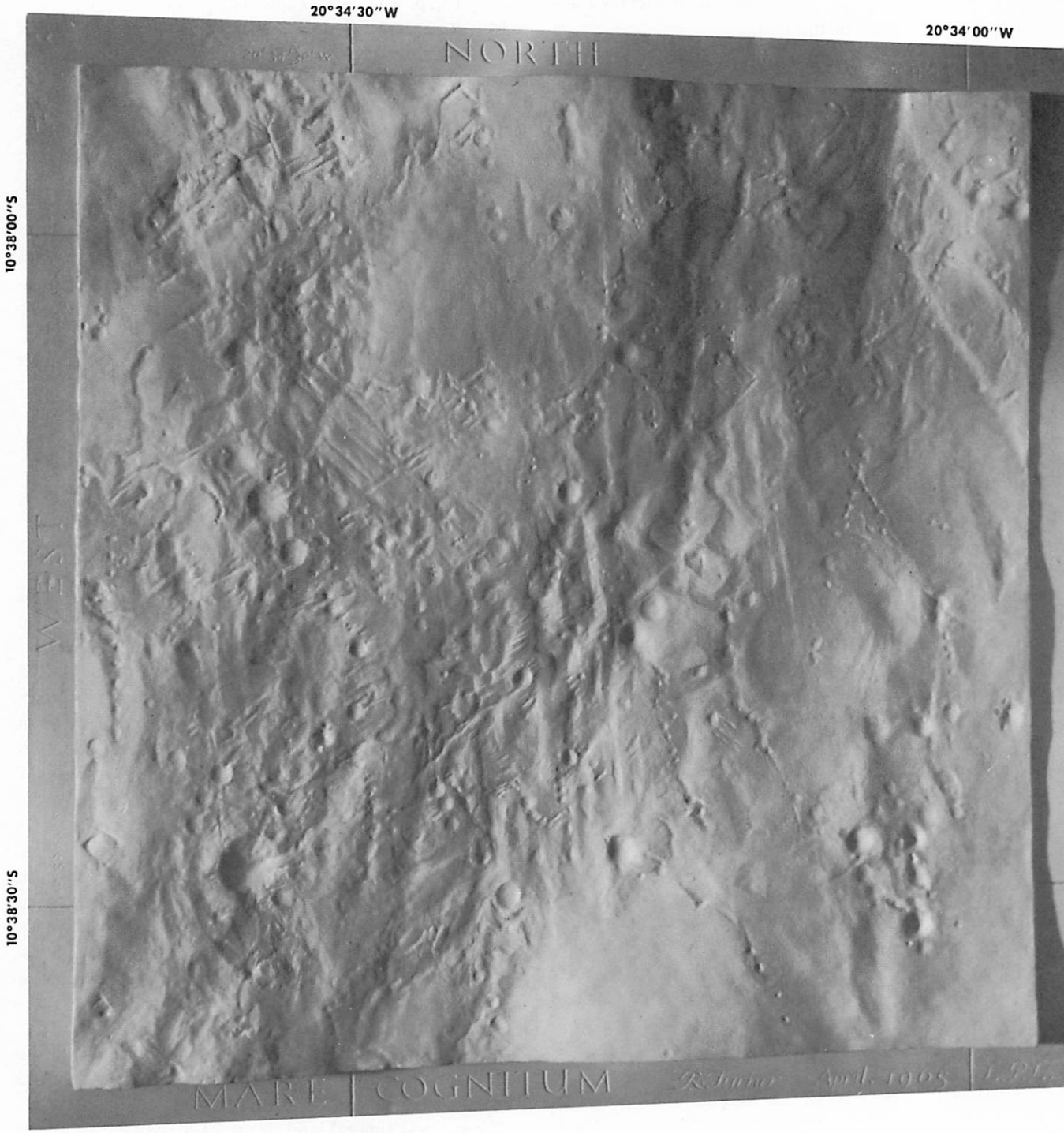

Figs. A-1a and A-1b (loose-leaf insert). Stereo pair of the model of an area in Mare Cognitum near *Ranger VII* impact site. Approximat
scale 1:2600. Western illumination; Sun angle 23°.

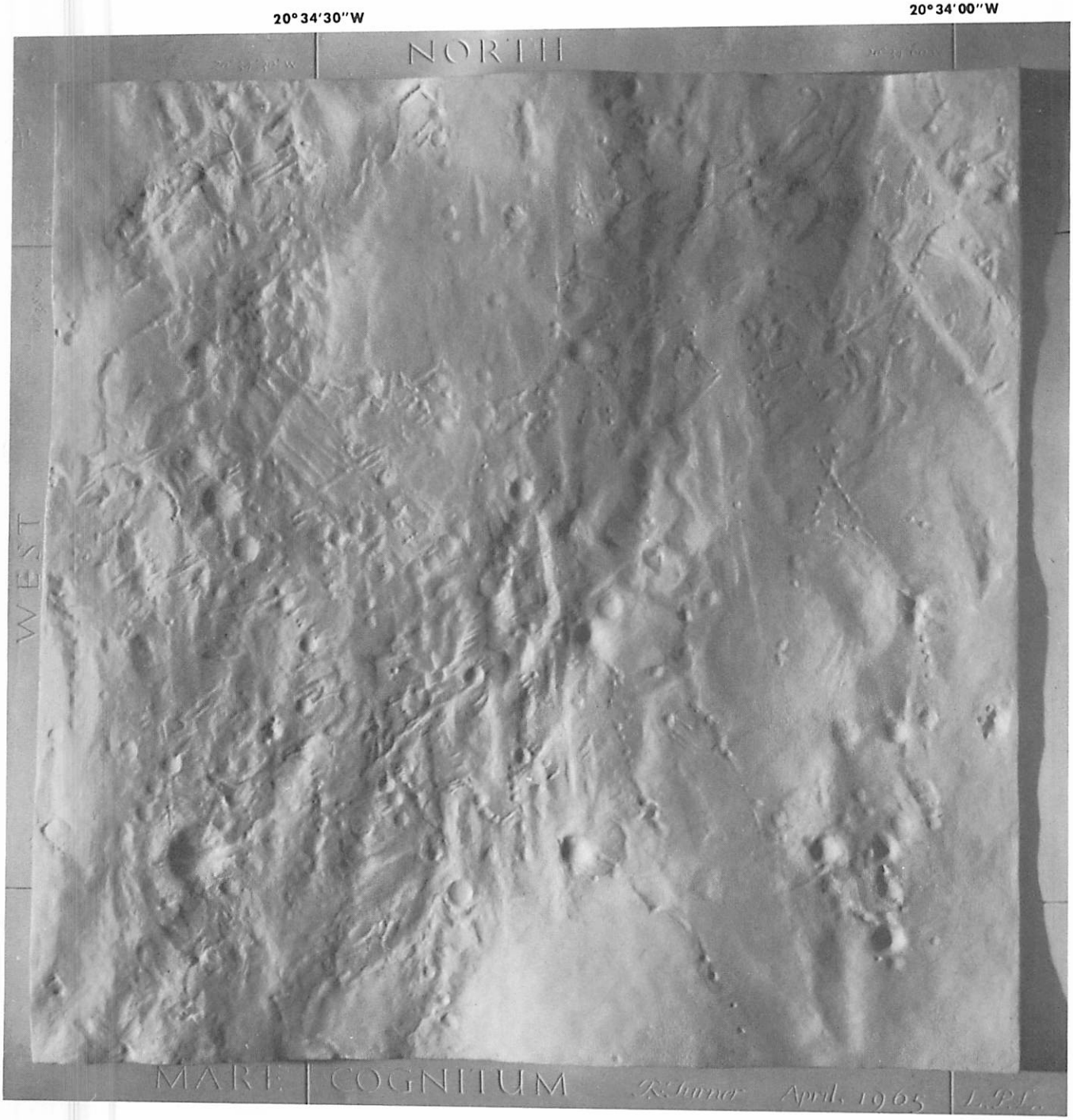
20°34'30"W
20°34'00"W
NORTH
WEST
10°38'00"S
10°38'30"S
MARE COGNITUM
R. Turner April, 1965
L.P.L.

slopes greater than this. In Figures 38 and A-2, it can be seen that very few areas are in full shadow, indicating that only a few short slopes or walls are steeper than 23°. If a scale model of *Surveyor* were placed on the model, the probability of a spacecraft tilt of more than 10° may be estimated. This probability is found to be approximately 10%.

The model shows increased resolution near the center and toward the west; this results from the fact that this area was covered by the last P frames. The smoothness of other areas is largely due to data limitation.

The coordinates used are based on ACIC chart RLC5.

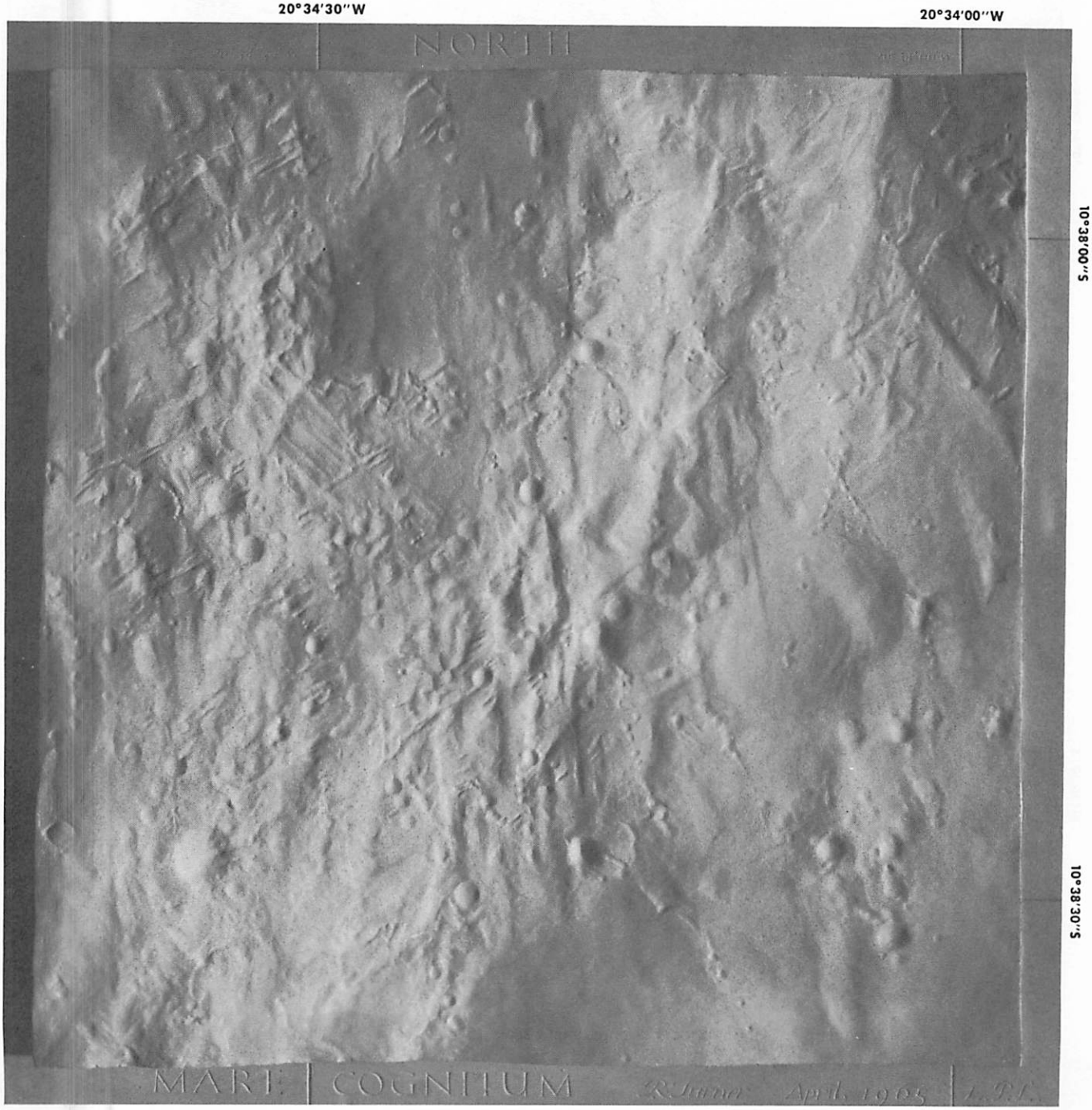

Fig. A-2. Scale model of part of Mare Cognitum near *Ranger VII* impact site. Approximate scale: 1:2600. Eastern illumination; Sun angle 23°.

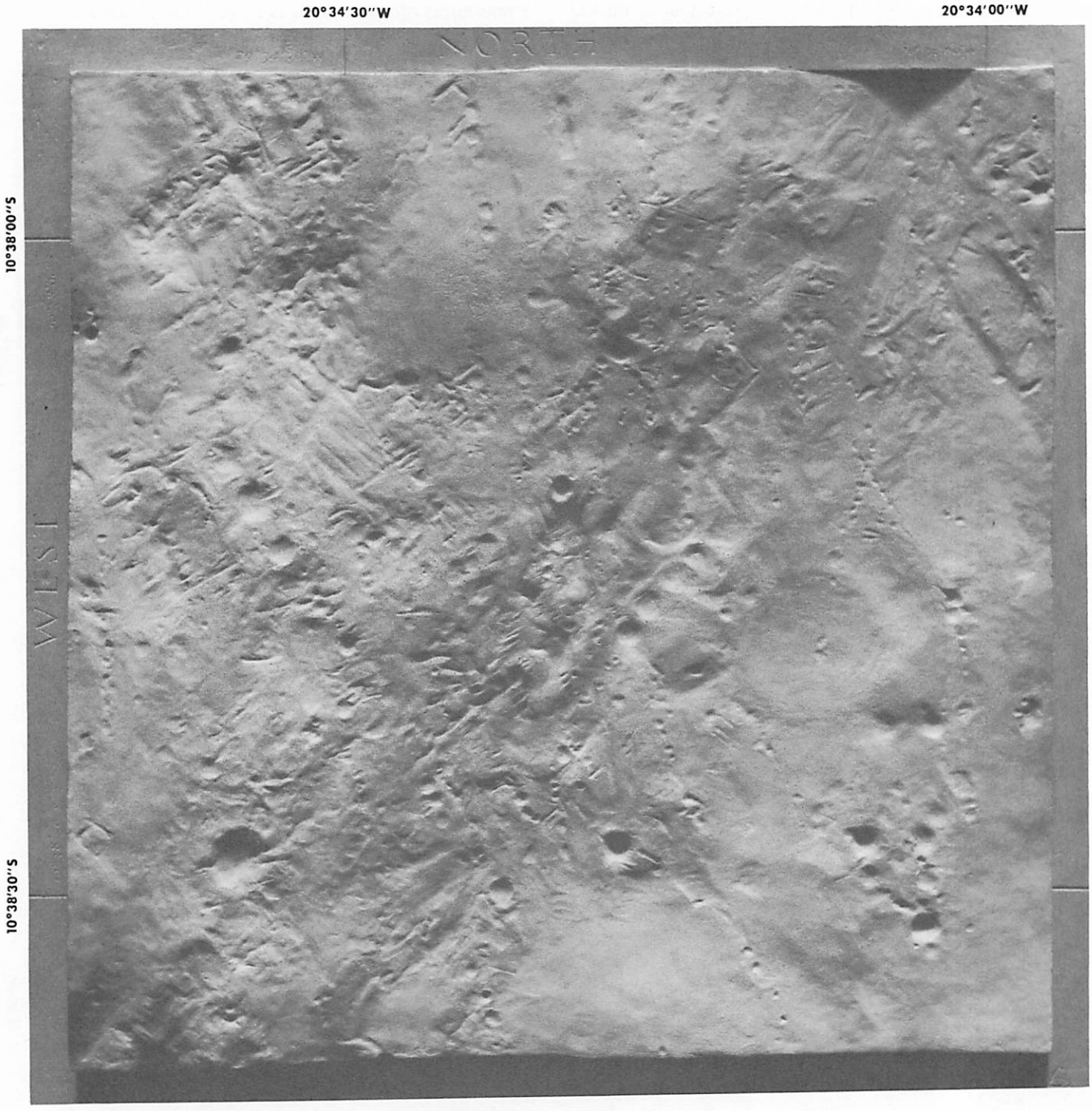

Fig. A-3 Another view of the model. Approximate scale 1:2600. Northern illumination; Sun angle 11°.

APPENDIX B
Last Three Frames Taken by Ranger VII

The last three frames, showing the best resolution attained in the Ranger VII mission, were taken when the spacecraft was less than 2 km from the impact point. The copies reproduced here (Figures B-1 to B-3) were made with two identical printing negatives displaced one-half spacing of the electronic interference lines to suppress these lines without introducing undue blurring of the surface detail. The frame dimensions are given in the legends. Figures B-2 and B-3 have comparable scales but differ in surface texture; B-2 shows broad valleys (lineaments) but no sharp detail (less than 1 m in size), whereas B-3 shows crater rims and other features down to about 30 cm in dimension. The *Ranger VIII-IX* report (Ref. 14), which includes a more general discussion of *Ranger* photographic resolution, points out that the "softness" of lunar detail varies locally, affecting the visibility of small impact craters (meter to submeter range). Figures B-1 and B-2 have resolutions of around 1 m and show detail down to that dimension. Figure B-3 has the highest resolution and shows, in addition to craters, a few rocks each about 1 m in diameter.

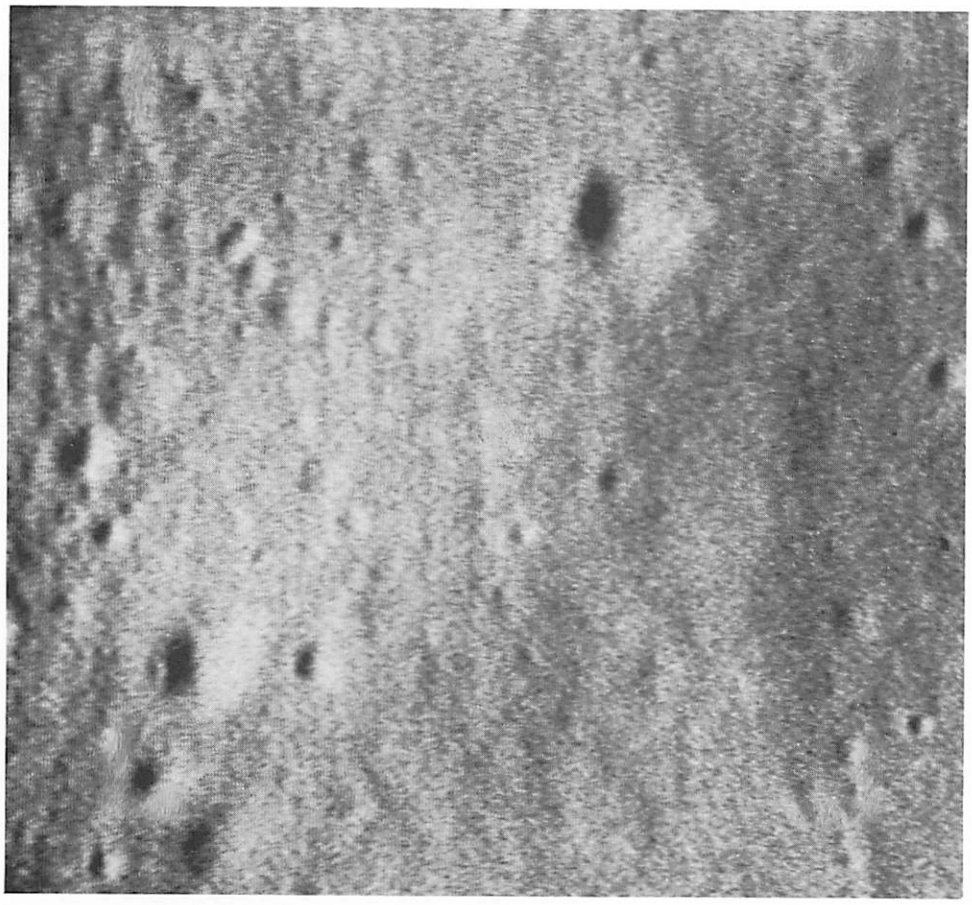

Fig. B-1 Frame 189 P_4, taken 1.74 km from the Moon. Dimensions of area included: 205 (E–W) × 180 (N–S) m.

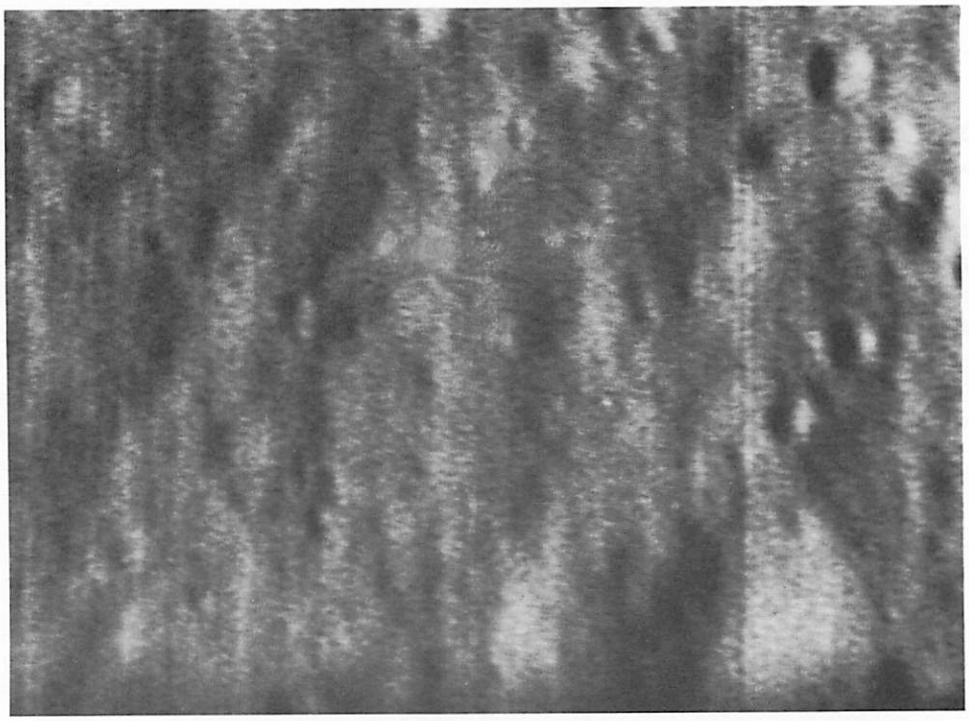

Fig. B-2 Frame 190 P_1, taken 1.07 km from the Moon. Dimensions of area included: 46 × 34 m.

Fig. B-3 Frame 190 P_3, taken 0.52 km from the Moon. Dimensions of area included: 37 × 53 m.